NOTICE

The quality of this microform is heavily dependent upon the quality of the original thesis submitted for microfilming. Every effort has been made to ensure the highest quality of reproduction possible.

If pages are missing, contact the university which granted the degree.

Some pages may have indistinct print especially if the original pages were typed with a poor typewriter ribbon or if the university sent us an inferior photocopy.

Reproduction in full or in part of this microform is governed by the Canadian Copyright Act, R.S.C. 1970, c. C-30, and subsequent amendments.

AVIS

La qualité de cette microforme dépend grandement de la qualité de la thèse soumise au microfilmage. Nous avons tout fait pour assurer une qualité supérieure de reproduction.

S'il manque des pages, veuillez communiquer avec l'université qui a conféré le grade.

La qualité d'impression de certaines pages peut laisser à désirer, surtout si les pages originales ont été dactylographiées à l'aide d'un ruban usé ou si l'université nous a fait parvenir une photocopie de qualité inférieure.

La reproduction, même partielle, de cette microforme est soumise à la Loi canadienne sur le droit d'auteur, SRC 1970, c. C-30, et ses amendements subséquents.

Canada

ZINC/BROMINE BATTERY ELECTROLYTES: ELECTROCHEMICAL, PHYSICO-CHEMICAL AND SPECTROSCOPIC STUDIES

by

Wendy Pell

A Thesis
Submitted to the School of Graduate Studies
in Partial Fulfilment of the Requirements for
the Degree of Doctor of Philosophy
in
The Department of Chemical Engineering
University of Ottawa

ISBN 0-612-00593-3

Canada

UNIVERSITÉ D'OTTAWA
UNIVERSITY OF OTTAWA

Abstract

The zinc/bromine battery is a flowing electrolyte battery operating at ambient temperatures, and having both stationary and mobile applications. It is characterized by a flat voltage discharge profile, can be deeply discharged without adverse effects, and is made from low cost materials which can be recycled at the end of the battery's life. The electrochemically active materials are stored externally to the electrode assembly in two reservoirs, and are pumped to the electrodes during operation. The electrolyte typically includes aqueous zinc bromide and quaternary ammonium salts, such as methyl ethyl pyrrolidinium bromide(MEPBr) and methyl ethyl morpholinium bromide(MEMBr) which complex bromine and reduce self-discharge losses. Modification of the low temperature behaviour of the usual electrolyte, which freezes between -5 and 5 °C, is required if the battery is to perform successfully at low temperatures. This project identified electrochemical and physical chemical techniques to study zinc deposition and bromine production at glassy carbon electrodes as a method to gain quantitative and qualitative information from the electrolyte system. Electrochemical response, chemical species distribution, conductivity and phase change data were obtained for battery electrolytes at low temperatures and used to identify candidate electrolytes for low temperature applications.

The effect of the quaternary ammonium bromide salt on zinc species distribution and zinc deposition has not previously been studied. Spectroscopic and electrochemical studies indicated that the distribution of zinc/bromine complexes in solutions, and zinc deposition at glassy carbon were unaffected by the addition of quaternary ammonium bromides. The distribution of zinc/bromine complexes was significantly affected by temperature and state-of-charge or concentration of the electrolyte. As the temperature was decreased from 25 to -10 °C, zinc species distribution shifted from higher order ($ZnBr_4^{2-}$) to lower order ($ZnBr_2$) species. This result is in agreement with studies of Irish (1963) in aqueous $ZnCl_2$, and Marley and Gaffney (1990) in aqueous $ZnBr_2$ at 25 °C (atmospheric pressure) and 350 °C (2000 psi).

The quaternary ammonium bromide complex was found to act on the free bromine in solution and not on the bromine complexed with zinc. Cyclic voltammograms in dilute (0.05 M) and concentrated (2.25 M) aqueous $ZnBr_2$ solutions indicated that bromide oxidation at glassy carbon was characteristic of a quasi-reversible weak product adsorption process. Addition of the complexing agent was found to facilitate bromine adsorption on glassy carbon, and hence, to increase the reversibility of the reaction.

Several organic compounds, including propan-2-ol, ethylene dichloride, propylene glycol and ethylene glycol, were evaluated as additives to the aqueous electrolyte for low temperature applications using techniques of cyclic voltammetry, chronoamperometry, conductivity, and freezing point determination. The mixed aqueous/organic $ZnBr_2$ electrolytes had lower conductivity and higher nucleation overpotential for zinc deposition than the aqueous $ZnBr_2$ electrolytes, thus, batteries incorporating the mixed aqueous/organic $ZnBr_2$ electrolyte would have lower voltaic and energy efficiencies. Electrochemical studies of bromide oxidation at glassy carbon in propan-2-ol/$ZnBr_2$ solutions identified this reaction to be quasi-reversible, with weak product adsorption. It was found that bromine formed from bromide oxidation underwent an irreversible chemical reaction rather than complexing with the quaternary ammonium bromide salt, and poor battery performance with this electrolyte was predicted. The propan-2-ol electrolytes were evaluated in a 50 Ah single cell $ZnBr_2$ flow battery. The chemical reaction between bromine and propan-2-ol was confirmed in the single cell tests by the absence of bromine phase after charging. The single cell battery incorporating propan-2-ol/$ZnBr_2$ electrolyte was found to have no capacity, and the prediction based on electrochemical and physical chemical analysis was confirmed.

Ethylene glycol was also selected on the basis of electrochemical and physical chemical data, to be tested in the single cell battery. Due to reduced conductivity of the electrolyte (higher solution resistance in the battery), the voltaic and energy efficiencies were expected to be lower than those of a standard electrolyte battery. Electrochemical experiments showed that neither bromide oxidation nor zinc cation reduction reactions were significantly affected by the presence of ethylene glycol. Thus, it was expected that the coulombic efficiency of a battery using ethylene glycol/$ZnBr_2$ electrolyte would be

comparable to that of a battery using the aqueous $ZnBr_2$ electrolyte. Pilot scale testing confirmed these results. The single cell battery, incorporating 25 % by volume ethylene glycol, gave similar coulombic efficiency, with energy and voltaic efficiencies approximately 90 % of the standard electrolyte battery efficiencies. Transport losses, associated with the diffusion of bromine across the separator to the zinc electrode, were higher in the electrolyte with ethylene glycol. It was concluded that ethylene glycol is a suitable electrolyte for zinc/bromine batteries required to operate at low temperatures.

Acknowledgements

I wish to thank my thesis supervisor, Dr. W.A. Adams, for providing me the opportunity to work in this field and at ESTCO.

I would like to thank the Ontario Department of Colleges and Universities, the University of Ottawa, and the Energy Diversification Laboratory, Natural Resources Canada for financial support. Further, I would like to thank Dr. V.S Donepudi for the opportunity to work on practical aspects of battery technology; and Dr. Ian Hill, Ray Doré, John K. Hunt, Steve Tennant and the staff at ESTCO for their support during the course of this project.

Finally, thank you to Keith, Chester, Ollie and our friends for making it possible to keep all things in perspective.

Contents

List of Figures

List of Tables

Nomenclature

Symbols

A	nucleation rate constant(s^{-1})
A	$nF\rho v/M$ (mA/cm^2)
B	$4N_o\pi\mu^2$ (s)
c_1, c_2	coefficients of a linear equation for current density, c_1: $(s^{-0.5}A)/(\Omega^{-0.5}cm^2)$
c_O	surface concentration of the oxidized species ($moles/cm^3$)
c_R	surface concentration of the reduced species ($moles/cm^3$)
c_O^∞	concentration of species O in the bulk ($moles/cm^3$)
c_R^∞	concentration of species R in the bulk ($moles/cm^3$)
D_O	coefficient of diffusivity of species O (cm^2s^{-1})
D_R	coefficient of diffusivity of species R (cm^2s^{-1})
E	electric field experienced by an induced dipole ($V\ m^{-1} = JC^{-1}m^{-1}$)
E	potential (volts)
E_1	initial potential for cyclic voltammetry, or chronoamperometric experiments (volts)
E_2	first vertex potential in cyclic voltammetry, or final potential in chronoamperometric experiments (volts)
E_3	second vertex potential in cyclic voltammetry
E_e	equilibrium reversible potential (volts)
E^θ_e	standard potential of the couple O/R (volts)
E_p	peak potential, sometimes superscripted by A or C to denote anodic or cathodic process respectively (volts)
$E_{p/2}$	half peak potential, superscripts as above (volts)
F	Faraday constant ($C\ mol^{-1}$)
h	height of a cylindrical centre(cm)
i	current (amperes)
I	current density, sometimes superscripted by A or C to denote anodic or

	cathodic process respectively (A cm^{-2})
I_P	peak current density, sometimes superscripted by A or C to denote anodic or cathodic process respectively (A cm^{-2})
$I_\perp$	intensity of light transmitted perpendicular to the plane of maximum polarization
$I_\parallel$	intensity of light transmitted parallel to the plane of maximum polarization
k	rate constant for an electrochemical process (generally s^{-1}) or rate constant of growth parallel to the surface in the right circular conical model(mol/s cm^2)
k'	rate constant for growth perpendicular to the surface in the right circular conical model(mol/s cm^2)
k_1, k_{-1}	forward and reverse rate constants for a chemical reaction (generally s^{-1})
M	molecular weight of the depositing species(g/mole)
n	number of electrons involved in electron transfer reaction or the number of experimental data points
N(t)	number density of centres(cm^{-2})
N_o	number of active sites under particular experimental conditions(cm^{-2})
Q	charge associated with an anodic or cathodic process (Q = i x t) (Q)
r	radius of the growing deposit(cm)
R	gas law constant (J K^{-1} mol^{-1})
R	resistance (ohms)
R^2	the square of the coefficient of correlation
S	surface area of growing nucleus (cm^2)
s_y	standard error of y estimate
t	time (seconds)
T	temperature (K)
x	distance perpendicular from the electrode (cm)
y_i	experimental value
$\bar{y}$	the average value of y_i observations

Greek Letters

α	transfer coefficient, subscripts A and C indicate anodic and cathodic processes respectively (dimensionless)
α	polarizability ($J^{-1}C^2m^2$)
β	amplitude of the polarizability due to a molecular vibration of frequency $\nu_{vib}(J^{-1}C^2m^2)$
ΔE	change in electric field associated with rotational or vibrational transition($V\ m^{-1}$)
ΔE_p	difference between the potential of the anodic and cathodic maximum current in a CV experiment(V)
λ	time of first potential reversal in cyclic voltammetry (seconds)
η	nucleation overpotential (mV)
μ	induced dipole (Cm)
μ	lateral growth rate constant in two rate model for electrochemical phase formation and macrogrowth($cm\ s^{-1}$)
ν	vertical growth rate constant in two rate model for electrochemical phase formation and macrogrowth($cm\ s^{-1}$)
ν	frequency of incident beam radiation(s^{-1})
ν_{vib}	frequency of molecular vibration(s^{-1})
ν	scan rate (Vs^{-1})
ν	degree of polarization(dimensionless)
ρ	density(g/cm^3)

Subscripts

ad	adsorbed species
e	equilibrium
i	refers to the ith experimental value
O	oxidized species
P	peak, or maximum

∥	parallel
⊥	perpendicular
R	reduced species
vib	refers to particular molecular vibration

Superscripts

∞	refers to the bulk phase

Abbreviations

(aq)	aqueous phase
Bu_4NBr	tetrabutylammonium bromide
CPC	carbon plastic composite
CV	cyclic voltammetry
E.R.C.	Energy Research Corporation
ESTCO	Electrochemical Science and Technology Centre, University of Ottawa
Et_4NBr	tetraethylammonium bromide
Exxon	Exxon Research and Engineering Company
J.C.I.	Johnson Controls, Inc.
M	metal
MEMBr	N-ethyl-N-methylmorpholinium bromide
MEPBr	N-ethyl-N-methylpyrrolidinium bromide
O	oxidized species
Pb-acid	lead-acid battery
PN	propionitrile
PVC	polyvinyl chloride
QBr	quaternary ammonium bromide salt, complexing agent for bromine
Quat	quaternary ammonium bromide salt, complexing agent for bromine
R	reduced species
(s)	solid phase

S.E.A.	Studiengesellschaft fur Energiespeicher und Antriebssysteme GMBH
SOC	state-of-charge
SOLA	solution of composition 0.051 M $ZnBr_2$, 1.0 M $AlCl_3$
SOLB	solution of composition 0.051 M ZnBr2, 0.018 M MEPBr, 0.5 M $AlCl_3$
SOLC	solution of composition 2.25 M ZnBr2, 0.5 M $ZnCl_2$, 0.80 M MEPBr
SOLD	solution of composition 2.25 M ZnBr2, 0.5 M $ZnCl_2$, 0.80 M MEPBr, 3.1 M ethylene dichloride
SOLE	solution of composition 2.25 M ZnBr2, 0.5 M $ZnCl_2$, 0.80 M MEPBr, 3.3 M propan-2-ol
SOLF	solution of composition 2.25 M ZnBr2, 0.5 M $ZnCl_2$, 0.80 M MEPBr, 4.5 M ethylene glycol
SOLG	solution of composition 2.25 M ZnBr2, 0.5 M $ZnCl_2$, 0.80 M MEPBr, 2 % by volume propan-2-ol
SOLH	solution of composition 2.25 M ZnBr2, 0.5 M $ZnCl_2$, 0.80 M MEPBr, 2 % by volume ethylene glycol
SLI	starting, lighting and ignition
X	halogen

Chapter 1

Introduction

Currently the world relies almost entirely on non-renewable energy sources. Environmental concerns, including air quality, are forcing scientists and engineers to develop sustainable and renewable energy technologies. Renewable energy from sources such as wind generators or photovoltaic solar energy collectors can be stored in batteries or hydrogen/fuel cell systems. A reliable and durable rechargeable battery is needed to make these systems practical. In vehicular applications, batteries and an electric motor can be used to replace the more common gasoline burning internal combustion engine, thus reducing emissions at the vehicle to zero.

1.1 Batteries

Significant advances have been made over the last several decades in battery and electrochemical device technology. Secondary or rechargeable batteries have been in existence for over 100 years. The rechargeable lead-acid battery developed in 1859 by Planté is still the most widely used battery today. The nickel-iron alkaline battery was introduced by Edison in 1908 as the power source for the early electric automobile; it was used in industrial trucks, underground work vehicles, railway cars, and for stationary applications. The rechargeable nickel-iron battery had the advantages of durability and long-life, but has since lost favour due to its high cost and low specific power. Pocket plate nickel-cadmium batteries have been manufactured since 1909, and were primarily used for heavy duty industrial applications. At the start of World War II, the Leclanche zinc-carbon primary (non-rechargeable) cell, the lead-acid cell and the Edison nickel-iron

secondary battery were predominant. At this time, applications were limited mainly to automotive, signalling and radio. During the 1950's sintered-plate nickel-cadmium batteries were developed with higher power capabilities and higher energy densities, opening markets for aircraft engine starters and communications.

While significant performance improvements have been made with older secondary battery technologies, many new electrochemical systems, including fuel cells and lithium batteries, are being developed in response to the requirements of new applications. Today, batteries find applications in systems ranging from the power source for electric vehicle propulsion, to the power source for memory protection devices in computers, to the power source for implantable medical devices, such as artificial hearts and pacemakers. Applications of secondary (rechargeable) batteries generally fall into two main categories:

1. Applications which require discharge, followed by recharge after use. These applications feature convenience (hand-held calculators, electronic flashes), cost saving (as they can be recharged rather than replaced), and often power drains beyond the capability of primary (non-rechargeable) batteries (electric vehicle, traction industrial truck applications).

2. Applications in which the battery is required to act as an energy storage device in a hybrid system with a prime energy source. The batteries deliver energy to the load on demand, when the prime source is unavailable. Examples of batteries falling into this category are automotive and aircraft starting, emergency no-fail, standby power sources, and hybrid propulsion of electric vehicles.

The interest in batteries and electrochemical technology has been heightened by the need for clean renewable power sources for portable electronics, energy storage and electric vehicles.

1.2 Objectives of This Work

The principal objective of this work is to obtain an understanding of the basic electrochemical behaviour of electrolytes used in the aqueous zinc/bromine battery to

extend the performance of the battery to low temperatures. Vibrational spectroscopic and electrochemical studies in test cells have been used to determine zinc complex species distribution, and kinetic information on zinc cation reduction and bromide oxidation in a range of aqueous and mixed aqueous/organic $ZnBr_2$ electrolytes. A system to identify electrolytes with properties that could improve low temperature operation of the zinc/bromine battery has been developed and the electrolytes have been characterized at low temperatures using electrochemical, spectroscopic and physical chemical techniques.

1.3 Outline of the Thesis

Chapter (2): The basic principles of rechargeable battery operation are introduced. A critical review of zinc/bromine flow battery development is presented.

Chapter (3): The technique of Raman Spectroscopy is discussed, and results of spectroscopic analysis of aqueous zinc/bromide electrolytes are presented. The effects of temperature and quaternary ammonium salt concentration are discussed.

Chapter (4): Physical chemical data are presented for various candidate electrolytes. The potential effects of various physical properties of the electrolytes on battery operation are discussed.

Chapter (5): The results of an electrochemical study of zinc deposition and bromide oxidation at glassy carbon are presented. Selection of potential electrolytes is made based on these and physical chemical results.

Chapter (6): Results of pilot scale testing of alternate electrolytes in a single cell zinc/bromine battery are presented. These results are correlated with the prior electrochemical and physical chemical measurements.

Chapter (7): The results of the thesis are summarized. Conclusions and recommendations for future work are made.

Chapter 2

Theory

2.1 Introduction to Rechargeable Battery Systems

A battery is a device that converts chemical energy, stored in its active materials, directly into electrical energy by means of an electrochemical oxidation reduction (redox) reaction. This type of reaction involves the transfer of electrons through an electrical circuit from one electrode to another. The basic electrochemical unit in a battery is referred to as a cell. Typically, a battery consists of one or more cells connected in series or parallel depending on the desired output voltage and capacity.

Nomenclature to describe different general battery types has been developed. The primary battery is not designed to be rechargeable. Primary batteries generally have high energy per unit volume (energy density) and good shelf-life (i.e. they will not significantly discharge when not in use). They are the most widely used batteries; common examples being zinc-carbon (Leclanché) and alkaline-manganese (zinc/manganese dioxide cells). Reserve batteries are primary batteries which isolate a key component from the rest of the battery. In this condition, chemical deterioration and self-discharge are eliminated, and the battery may be stored for long periods. These batteries are used primarily to deliver high power for relatively short periods of time, often for military applications. Examples of reserve batteries include water activated batteries with magnesium as the anode, and metal halide for the cathode. Secondary batteries are designed to be electrically recharged, and offer a cost saving once the initial outlay for the system has been made. One of the most common applications for rechargeable batteries is for starting, lighting and ignition (SLI) in automobiles. Common examples of rechargeable battery types are lead-acid and nickel-cadmium. Mechanically

rechargeable batteries are recharged by renewing one of the electrodes of the system once it has been discharged, generally the anode. Examples of this type of battery are aluminium-air and zinc-air batteries.

When the electrochemical cell acts as a source of electrical energy, (i.e. a battery during discharge) it is called a galvanic cell. When it is connected to an external source of electric current which drives the chemical reaction (i.e. a battery being charged) it is called an electrolytic cell. The major components of a galvanic cell include:

i) the anode or negative electrode which gives up electrons to the external circuit, and is oxidized or is the site of oxidation during the electrochemical reaction.

ii) the cathode or positive electrode which accepts electrons from the external circuit and is reduced or is the site of reduction during the electrochemical reaction.

The electrodes are usually good electronic conductors and should present little resistance to the flow of electrons. Electrodes are normally constructed of electro-active material alone, or with current collectors. Additives may be in the form of solids, such as metals or carbon, although a wide range of other materials such as conductive polymers and conductive ceramics are also used. A list of physical and electrochemical characteristics of potential electrode materials is presented in Table 2.1. The most advantageous combinations of anode and cathode material are those that result in a light weight, low volume battery which operates at a high cell voltage, and high capacity. In reality, many such combinations are not practical due to reactivity with other cell components, polarization, difficulty in handling, toxicity, or high cost. A practical anode will have the following properties: it will be readily oxidized and efficient as a reducing agent, have good electronic conductivity, stability, ease of fabrication, and low cost. Zinc has been a predominant anode material in both primary and secondary batteries because of its good electrochemical behaviour, high electrochemical equivalence, compatibility with aqueous electrolytes, reasonable shelf-life, low cost, and availability.

A practical cathode will be readily reduced and efficient as an oxidizing agent, stable when in contact with the electrolyte, and have a useful working voltage. In general,

a successful electrode will have the following properties: i) high percentage of active material, ii) high physical stability, iii) high chemical stability, iv) high electrical conductivity, v) ease of fabrication in a suitable form, vi) long useful life-time, vii) non-polluting and non-contaminating, viii) low cost, ix) readily available material, and x) safe operation.

Table 2.2 presents a listing of major battery systems together with the nominal operating voltage of a single cell for each system, and the theoretical capacity based on active anode and cathode materials only.

The third major component of a galvanic cell is the electrolyte which is an ionic conductor and provides the medium for transfer of electrons, as ions, inside the cell between the positive and negative electrodes.

The electrolyte is typically a liquid containing dissolved salts, acids or alkalis to maintain conductivity. The electrolyte can also be a molten salt, an ionically conducting polymer, or a conducting ceramic. The electrolyte must not be electronically conductive as this would cause internal short-circuiting, and should not be parasitically reactive with the electrode materials. Note that sulphuric acid (electrolyte) reacts with both lead and lead oxide to form lead sulphate in the lead-acid battery. Practical electrolytes must also be stable with changing temperature, relatively safe to handle, and of low cost.

A galvanic cell which acts as a battery typically includes a separator. The separator physically isolates the negative and positive electrodes. It is permeable to the electrolyte in order to maintain the desired ionic conductivity. Technical requirements for separators include mechanical strength to withstand handling during assembly and operation of the battery and chemical resistivity in acid and/or oxidizing environments. The separator material must also be both physically and chemically stable over a wide temperature range. The electrical resistivity of the separator must be minimized to maximize the battery voltage at high rates of discharge. A summary of a range of separators and their specific properties is given in Table 2.3. New research on ion selective separator/electrolyte materials is likely to lead to battery technology which is restricted by cathode/anode interference. An example would be in the alkaline Zn/MnO_2 system where zincate ions ($[Zn(OH)_4]^{2-}$) reduce the rechargeablity of the MnO_2 cathode.

Table 2.1: Characteristics of Electrode Materials (adapted from Linden, 1984)

Material	Atomic or molecular weight, g	Standard Potential 25 °C, V	Valence change	Melting Point, °C	Density, g/cm^3	Electrochemical equivalents		
						Ah/g	g/Ah	Ah/cm^{3*}
Anode materials								
H_2	2.01	0	2	...	...	26.59	0.037	
Li	6.94	-3.01	1	180	0.54	3.86	0.259	2.06
Na	23.0	-2.71	1	98	0.97	1.16	0.858	1.14
Mg	24.3	-2.38	2	650	1.74	2.20	0.454	3.8
Al	26.9	-1.66	3	659	2.69	2.98	0.335	8.1
Ca	40.1	-2.84	2	851	1.54	1.34	0.748	2.06
Fe	55.8	-0.44	2	1528	7.85	0.96	1.04	7.5
Zn	65.4	-0.76 -1.25**	2	419	7.14	0.82	1.22	5.8
Cd	112.4	-0.40	2	321	8.65	0.48	2.10	4.1
Pb	207.2	-0.13	2	327	11.34	0.26	3.87	2.9
Cathode materials								
O_2	32.0	1.23	4	...	...	3.35	0.30	
Cl_2	71.0	1.36	2	...	...	0.755	1.32	
Br_2	159.8	1.07	2	-7.2	3.12	0.340	2.98	0.98
SO_2	64.0	...	1	...	...	0.419	2.38	
MnO_2	86.9	1.23	1	...	5.0	0.308	3.24	1.54
NiOOH	91.7	0.49*	1	...	7.4	0.292	3.42	2.16
CuCl	99.0	0.14	1	...	3.5	0.270	3.69	0.95
AgO	123.8	0.57*	2	...	7.4	0.432	2.31	3.20
HgO	216.6	0.10*	2	...	11.1	0.247	4.05	2.74
Ag_2O	231.7	0.35*	2	...	7.1	0.231	4.33	1.64
PbO_2	239.2	1.69	2	...	9.4	0.224	4.45	2.11

* Based on density values shown

** Basic electrolyte; all others, aqueous acid electrolyte

Table 2.2: Theoretical voltage and capacity of major battery systems (adapted from Linden, 1984).

Battery System	Anode	Cathode	Reaction mechanism	V	Theoretical Capacity	
					g/Ah	Ah/kg
Primary						
Leclanché	Zn	MnO_2	$Zn+2MnO_2 \rightarrow ZnO \cdot Mn_2O_3$	1.6	4.46	224
Magnesium	Mg	MnO_2	$Mg+2MnO_2+H_2O \rightarrow Mn_2O_3+Mg(OH)_2$	2.8	3.69	271
Alkaline MnO_2	Zn	MnO_2	$Zn+2MnO_2 \rightarrow ZnO+Mn_2O_3$	1.5	4.46	224
Mercad	Cd	HgO	$Cd+HgO+H_2O \rightarrow Cd(OH)_2+Hg$	0.91	6.15	163
Silver oxide	Zn	AgO	$Zn+Ag_2O+H_2O \rightarrow Zn(OH)_2+2Ag$	1.6	5.55	180
Zinc/air	Zn	O_2 (air)	$Zn+1/2O_2 \rightarrow ZnO$	1.65	1.55	800
Li/SO_2	Li	SO_2	$2Li+2SO_2 \rightarrow Li_2S_2O_4$	3.1	2.64	379
Li/MnO_2	Li	MnO_2	$Li+Mn^{IV}O_2 \rightarrow Mn^{III}O_2(Li^+)$	3.5	3.50	286
Reserve						
Cuprous chloride	Mg	CuCl	$Mg+Cu_2Cl_2 \rightarrow MgCl_2+2Cu$	1.6	4.14	241
Zinc/silver oxide	Zn	AgO	$Zn+AgO+H_2O \rightarrow Zn(OH)_2+Ag$	1.81	3.53	283
Secondary						
Lead-acid	Pb	PbO_2	$Pb+PbO_2+2H_2SO_4 \rightarrow 2PbSO_4+2H_2O$	2.1	8.32	120
Edison	Fe	Ni oxide	$Fe+2NiOOH+2H_2O \rightarrow 2Ni(OH)_2 + Fe(OH)_2$	1.4	4.46	224
Nickel-cadmium	Cd	Ni oxide	$Cd+2NiOOH+2H_2O \rightarrow 2Ni(OH)_2 + Cd(OH)_2$	1.35	5.52	181
Silver-zinc	Zn	AgO	$Zn+AgO+H_2O \rightarrow Zn(OH)_2+Ag$	1.85	3.53	283
Nickel-zinc	Zn	Ni oxide	$Zn+2NiOOH+2H_2O \rightarrow 2Ni(OH)_2 + Zn(OH)_2$	1.73	4.64	215
Silver-Cadmium	Cd	AgO	$Cd+AgO+H_2O \rightarrow Cd(OH)_2+Ag$	1.4	4.41	227
Zinc/bromine	Zn	Br_2	$Zn+Br_2 \rightarrow ZnBr_2$	1.85	4.2	238
Zinc/chlorine	Zn	Cl_2	$Zn+Cl_2 \rightarrow ZnCl_2$	2.12	2.54	394
High temperature	Li(Al) Na	FeS S	$2Li(Al)+FeS \rightarrow Li_2S+Fe+2Al$ $2Na+3S \rightarrow Na_2S_3$	1.33 2.1	2.99 2.65	345 377
Fuel cell						
H_2/O_2	H_2	O_2	$H_2+1/2O_2 \rightarrow H_2O$	1.23	0.336	2975

Table 2.3: Specific properties of selected separator materials (adapted from Linden, 1984).

Separator material	Resistivity, $m\Omega/cm^2$	Chemical stability	Battery systems
Cellophane	2.3 - 2.8	poor	Zn/AgO, Ni/Zn, Pb-acid
Polyvinyl acetate	5.4	poor	Ni/Zn
Celgard	6.2	good	Ni/Zn
Microporous plastic	19	good	Ni/Zn, Pb-acid, Zn/Br_2, Li/FeS_2
	5.4	good	
Nylon	6.2	good	Ni/Zn, Zn/AgO
Polypropylene	2.8	good	Zn/AgO, Pb-acid, Ni/Zn
Polyvinyl chloride	3.7	fair	Pb-acid

A galvanic cell is shown schematically in Figure 2.1 below. When a cell is connected to a load during discharge, electrons flow from the negative electrode, through the external load to the positive electrode, where the electrons are accepted and the cathode material is reduced. The electrical circuit is completed by ions in the electrolyte. In the electrolyte, current flows through two-way migration of anions toward the negative electrode, and cations toward the positive electrode. During recharge of a rechargeable or secondary battery, the current flow is reversed, and the external load replaced by a power supply. Oxidation takes place at the positive electrode and reduction at the negative electrode.

A cell can be constructed in many shapes, including cylindrical, button, flat and prismatic, and the cell components can be engineered to accommodate these shapes.

An ideal rechargeable battery is one that is inexpensive, has adequate energy for the application, has an infinite cycle life, can handle any power level, operates within a full range of temperature and environmental requirements, is light in weight, has unlimited shelf-life, and is completely safe and consumer proof. Batteries are typically evaluated on the basis of:

i) energy density, the ratio of the energy available from a cell or battery to its

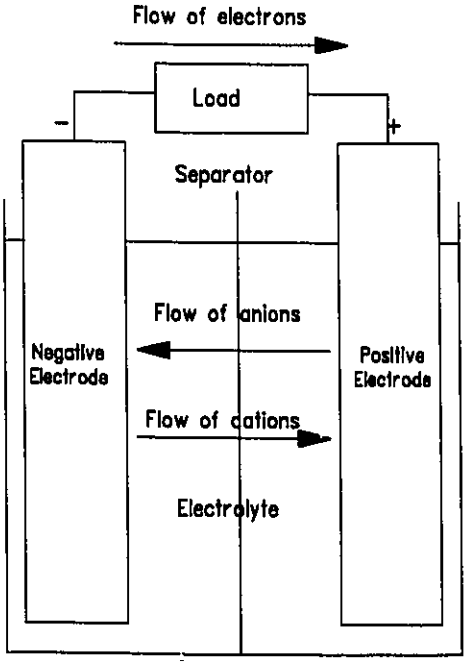

Figure 2.1: Schematic diagram of a galvanic cell (discharging electrochemical cell).

volume (Wh/l) or its weight (Wh/kg). Theoretical energy density assumes that 100 % of the battery weight or volume is due to active material. Practical energy density includes the weight or volume of electrochemically inactive components such as electrolyte, separators, electrode grid supports, current collectors, and outer casings, and is measured at a specific rate.

ii) power density, the ratio of the power available from a cell or battery to its volume (W/l) or its weight (W/kg) at a specific state-of-charge.

iii) capacity, the total number of ampere-hours or watthours that can be withdrawn from a fully charged cell or battery under specific conditions of discharge.

iv) shelf life, the duration of storage under specified conditions at the end of which a cell or battery still retains the ability to give specified performance.

v) cycle life, the number of cycles under specified conditions which are available from a secondary battery before it fails to meet specified performance criteria.

vi) self-discharge, the extent of capacity deterioration as a result of chemical action occurring during storage or rest periods.

vii) coulombic efficiency, the ratio of the output of a secondary cell or battery, measured in ampere-hours, to the input required to restore the initial state of charge, under specified conditions.

$$\textit{Coulombic Efficiency} = \left(\frac{\textit{Amp hours delivered}}{\textit{Amp hours input}}\right) x\ 100 \qquad (2.1)$$

viii) energy efficiency, the ratio of the watthours delivered on discharge of a battery to the watthours needed to restore it to its original state under specified conditions of charge and discharge.

$$\textit{Energy Efficiency} = \left(\frac{\textit{Watt hours delivered}}{\textit{Watt hours input}}\right) x\ 100 \qquad (2.2)$$

ix) voltaic efficiency, the ratio of average voltage during discharge to average voltage during recharge under specified conditions of charge and discharge.

$$Voltaic\ Efficiency = \left(\frac{Energy\ Efficiency}{Coulombic\ Efficiency}\right) x\ 100 \qquad (2.3)$$

2.2 General Introduction to the Zinc/Bromine Battery

2.2.1 The Zinc/Bromine Battery System

The secondary zinc/bromine flow battery has been proposed for use in energy storage and vehicular propulsion applications due to its high theoretical and practical energy densities, 430 Wh/kg and 70 to 80 Wh/kg respectively(Leo and Bharvani, 1984; Leo and Charkey, 1985; Kanazashi *et al.*, 1985; Fujii *et al.*, 1986; Fujii *et al.*, 1988). A standard lead-acid battery has a theoretical energy density of 170 Wh/kg and typically operates at 30 to 35 Wh/kg (Linden, 1984). The zinc/bromine (Zn/Br_2) battery also has relatively high specific power, 100 to 120 W/kg for 30 to 50 kWh systems (Eidler and Yaccarino, 1989; Bellows et al., 1985; Lex and Mathews, 1991), and high coulombic efficiency, 86 to 91 %. The specific power of a zinc/bromine battery is dependent on the size and design. Depending on the composition of the electrolyte, the choice of separator, and the electrode spacing, a battery can be designed to maximize energy or power output. The practical advantages of this system include low cost of materials which can be recycled at the end of the battery's life, operation under ambient conditions (it does not require high temperature for operation), and a flat voltage discharge profile. The selling price for zinc/bromine batteries is projected to range between \$20 and \$100/kWh, and is dependent upon the application (Putt, 1979; Seitz, 1987). In comparison, low rate nickel/cadmium batteries are priced at \$400 to \$1000/kWh, while high rate nickel/cadmium batteries range from \$600 to \$1000/kWh (Adams, 1994; Donepudi and Pell, 1992). Minimal hydrogen gas is produced during charging and any such gas is readily swept away in the electrolyte stream. Zn/Br_2 batteries can also be completely discharged without any negative effects.

Disadvantages of the system include the complexity of the circulation system, the propensity of zinc to form dendrites, the relatively high rate of self-discharge, and the

relatively small temperature window for operation, 20 °C to 60 °C. System engineering constraints due to material compatibility and stability at high temperatures limit the upper value further, to 45 °C.

A zinc/bromine flow battery includes two electrolyte reservoirs, a separate electrode assembly termed the stack, a circulation system of pumps and valves to conduct the electrolyte from the reservoirs to the stack, and a thermal management system usually consisting of a heat exchanger or cooler to maintain operating temperature between 20 °C and 45 °C. A simplified schematic diagram of a zinc/bromine single cell is shown in Figure 2.2.

2.2.2 Zinc/Bromine Battery Electrodes

The electrode assembly of a multi-cell battery consists of carbon plastic bipolar electrodes connected in series to the next cell in the stack. Each electrode assembly has two monopolar electrodes, one positive and the other, negative, at either end of the stack. A bipolar electrode is constructed with positive and negative active materials on opposite sides of an electronically conductive plate. Bipolar design requires only two external electrical contacts to the two monopolar end electrodes. In addition to the simplicity of electrical connections within the battery, bipolar cells have the advantage of more uniform distribution of current density and voltage across the electrode surfaces. The bipolar arrangement is also favoured in this system due to the lower weight and cost of composite bipolar materials compared to metal current collectors used in monopolar cells. Metal current collectors would also be prone to corrosion from the bromine reactant in the electrolyte. Figure 2.3 shows a schematic diagram of a flow frame bipolar cell sub-assembly.

The carbon plastic composite (CPC) electrodes are typically made from 20% (by weight) carbon black, 70% polyolefin copolymer, and approximately 4% each of carbon and glass fibres. The fabrication technique for CPC electrodes results in a smooth surface with low surface area. This provides a suitable substrate for zinc deposition, but the bromine electrodes require activation in the form of high surface area carbon (>

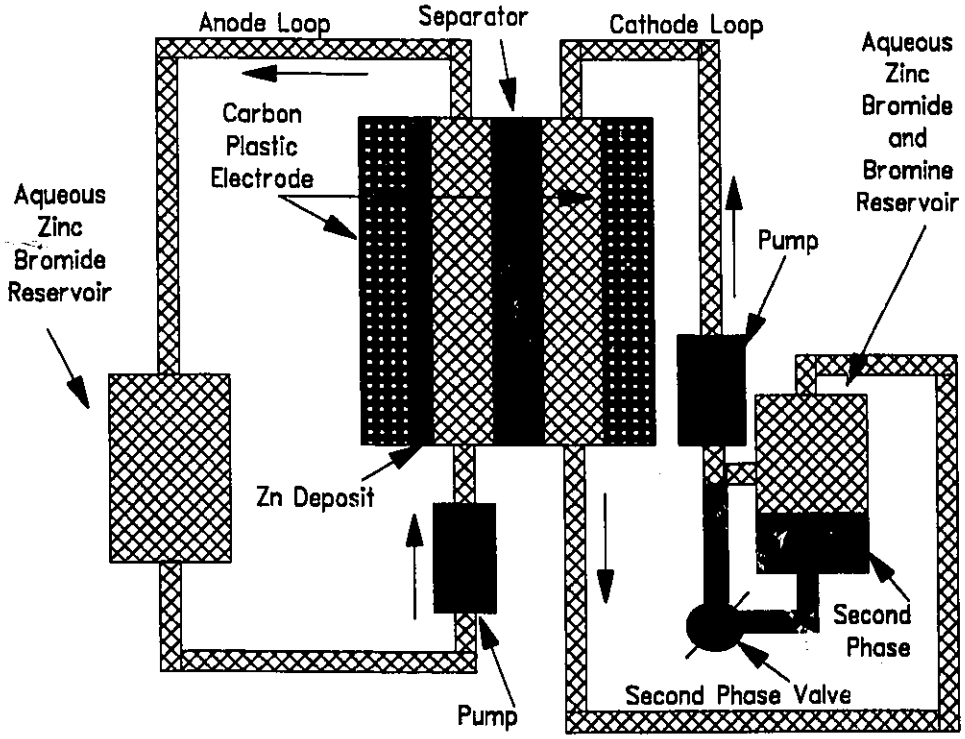

Figure 2.2: Schematic diagram of a zinc/bromine flow cell. The operating voltage ranges from 1.7 to 1.0 V during discharge, and 1.7 to 2.1 V during charge.

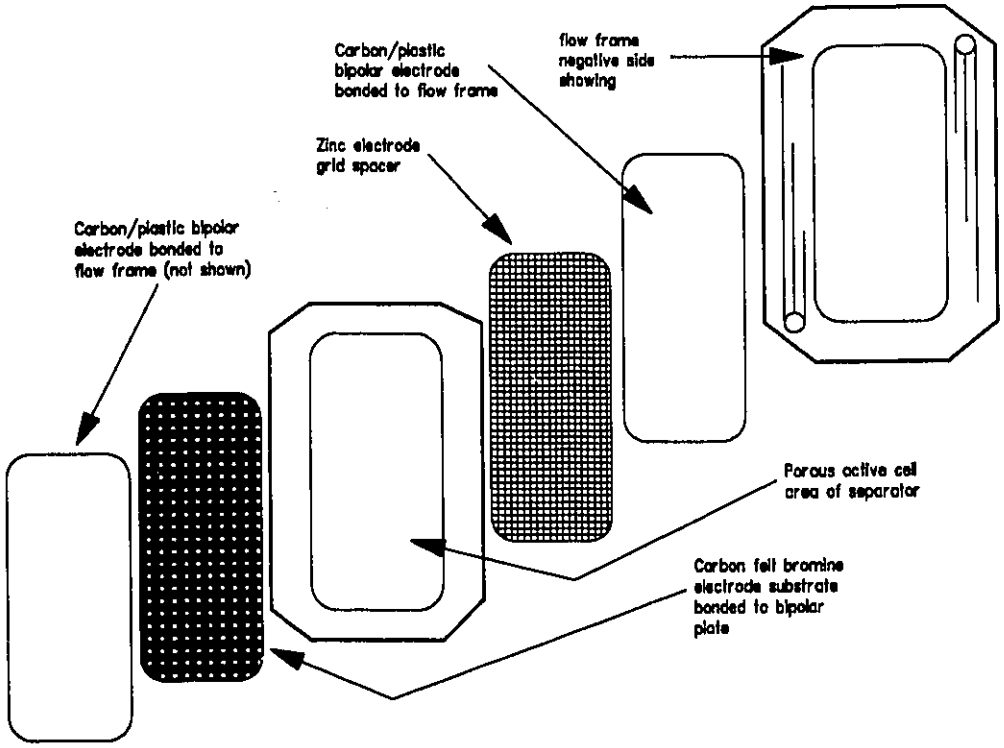

Figure 2.3: Flow frame bipolar cell sub-assembly

1500cm^2/cm^2). Exxon Research and Engineering Company (Exxon) bonded a high surface area carbon black (greater than 1500 cm^2/cm^2 electrode) to the bromine CPC electrode. Energy Research Corporation (E.R.C.) bonded carbon felt to CPC, and Meidensha used a highly porous carbon cloth as described by Kinoshita (1988).

The carbon plastic composite active electrode is generally supported in high density polyethylene flow frames as shown in Figure 2.3. The flow frames are injection moulded components with manifolds and flow channels to direct the positive and negative electrolytes over the electrodes(Leo, 1991). The flow channels ensure uniform flow over the electrodes.

2.2.3 Reservoirs and Circulation Dynamics

One reservoir contains anolyte fluid, which is pumped to the negative electrodes of the stack, and the other, catholyte, which is pumped to the positive electrodes of the stack. These electrolytes contain the active material, zinc cations and bromide anions; the electrode assembly is inert and is a site for the reactions to occur. These solutions serve as both the electrolyte and the active material. Typically, the catholyte enters the top of the stack and exits from the bottom, while the anolyte enters the bottom and exits from the top of the stack. This counter current flow promotes thermal exchange between the actively cooled anolyte and the catholyte.

2.2.4 System Considerations

The separator is generally made of porous high density polyethylene/silica material, and is the subject of much proprietary development. Zinc/bromine batteries have been designed as flow batteries for a number of reasons. As the active material is contained in the reservoirs, design of a battery with large reservoirs relative to the stack size results in systems having high capacity and high energy density. In fact, the size of the reservoirs, along with the electrode spacing, determines the battery capacity. Secondly, storing the active material external to the electrode assembly when the system is not in operation, results in low self-discharge and a long storage life for the system.

2.2.5 Battery Chemistry

A standard electrolyte contains 2 to 3 M aqueous $ZnBr_2$, and 1 M polybromide complexing agent, QBr. Often supporting salts such as $ZnCl_2$ and NH_4Cl (McBreen and Gannon, 1983; Cathro, Cedzynska and Constable, 1985), and KCl and NaCl (Lim *et al.*, 1977) are used to increase electrolyte conductivity. For convenience, the battery electrodes are named for the discharge reactions; thus the zinc reaction occurs at the anode, and the bromine reaction at the cathode. On charge, zinc cations, Zn^{2+}, are reduced to zinc metal which forms a solid layer on the surface of the anode. Bromide anions, Br^-, are oxidized to Br_2 at the cathode, and the bromine is subsequently complexed with the organic polybromide in solution. The complexed polybromide is initially soluble in the aqueous solution, but as it absorbs bromine, it forms a heavy black second phase in the catholyte reservoir. During discharge, zinc solid is oxidized and bromine is reduced. The charge reactions are shown below:

	$E_e^0(25°C)$	$E_e^0(50°C)$	
$Zn^{2+}(aq) + 2e^- \rightarrow Zn(s)$	-0.763 V	-0.760 V	
$2Br^-(aq) \rightarrow Br_2 + 2e^-$	1.085 V	1.056 V	(2.4)
$Zn^{2+}(aq) + 2Br^-(aq) \rightarrow Zn(s) + Br_2$	1.848 V	1.816 V	

$$n(Br_2) + QBr(aq) \rightarrow Q(Br_2)_n \cdot Br$$

where QBr is an unsymmetrically substituted quaternary ammonium salt such as N-ethyl-N-methylmorpholinium bromide, or N-ethyl-N-methylpyrrolidinium bromide. In the above reaction scheme n is the number of moles of bromine that can react with 1 mole of quaternary ammonium salt. For the salts listed above n can assume a value between 1 and 7.

The structures of the N-ethyl-N-methylmorpholinium bromide and N-ethyl-N-methylpyrrolidinium bromide are shown in Figure 2.4. The selection and optimization of QBr species has been the subject of many studies, and is dependent on the particular application(Eustace, 1980; Gibbard, 1983; Cathro *et al.*, 1986; Cedzynska, 1989).

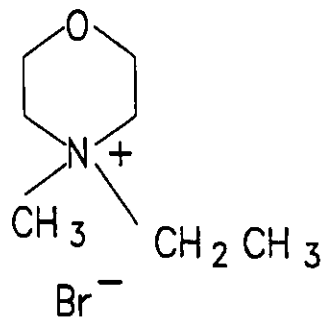

N-ethyl-N-methylmorpholinium bromide

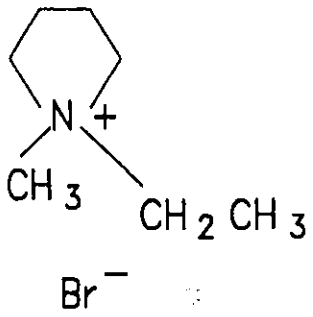

N-ethyl-N-methylpyrrolidinium bromide

Figure 2.4: Structure of unsymmetrically substituted quaternary ammonium salts used in zinc/bromine battery to complex bromine.

As the zinc/bromine battery can be completely discharged, two additional characteristics of the battery performance can be calculated. The residual capacity is the ratio of the capacity, in ampere-hours, that can only be recovered at low current to the input capacity required to restore a completely discharged battery to its fully charged state. The residual capacity corresponds to the zinc remaining on the anode, and to the bromine remaining in the catholyte chamber. Choosing a lower cut-off voltage or lower discharge rate reduces the residual capacity. High residual capacity could be an indication of electrode fouling or degradation of the high surface area positive electrodes. Residual capacity is defined in Equation 2.5 below.

$$\textit{Residual Capacity} = \left(\frac{\textit{Amp hours delivered strip cycle}}{\textit{Amp hours input}}\right) x\ 100 \qquad (2.5)$$

Transport losses are determined as the ratio of capacity not attributed to either residual or useful capacity to the capacity required to restore a discharged battery to its fully charged state and are defined in Equation 2.6. Efficiencies and losses are calculated to 1.0 V/cell for zinc/bromine batteries. Transport losses are attributed to the diffusion and migration of bromine species across the separator and to shunt current losses through the flow channels between cells in the bipolar stack. Battery failure, due to separator puncture or warpage, would result in high transport losses.

$$\textit{Transport Losses} = 100 - \textit{Coulombic Efficiency} - \textit{Residual Capacity} \qquad (2.6)$$

Much developmental work has been conducted on this system to improve the ambient temperature performance. If the Zn/Br_2 battery is to function well over a wide range of temperatures, the low temperature behaviour and performance must be improved. Furthermore, fundamental studies to determine the effects of electrolyte additives on the kinetics and reversibility of the reactions occurring at each of the zinc and bromine electrodes have not been reported. A fundamental understanding of the effects of electrolyte additives could lead to new approaches for improvements in battery capacity

and efficiency. This work has not been previously undertaken and is the subject of this thesis.

2.3 Milestones in Zinc/Bromine Battery Development

2.3.1 Aqueous Flowing Electrolyte

Two different flowing electrolyte systems have been described. The first, an aqueous zinc bromide system, was initially developed by Exxon (Bellows *et al.*, 1971). The aqueous system has been the system of choice by industrial developers, Studiengesellschaft fur Energiespeicher und Antriebssysteme GMBH (S.E.A.) in Austria (Tomazic, 1989; Kordesh *et al.*, 1992), Johnson Controls, Inc. (J.C.I.) in the USA (Bolstad and Miles, 1989), and Meidensha (Jinnai, 1990) and Toyota (Tange, 1989) in Japan. This is the system that was described above in the general introduction to zinc/bromine batteries, and a schematic diagram of the aqueous flow cell is shown in Figure 2.2.

2.3.2 The Flowing Aqueous/Propionitrile Electrolyte Zinc/Bromine Battery

A system using a propionitrile solution as the catholyte and aqueous zinc bromide solution as the anolyte (Singh, White and Parker, 1983; Avraamides, 1987) has also undergone development. A schematic diagram of a zinc/bromine cell employing propionitrile electrolyte is presented in Figure 2.5.

The aqueous and organic phases are prevented from mixing by a microporous plastic separator (Cathro, 1988). The propionitrile electrolyte was used to limit self-discharge of the battery, by making anolyte and catholyte fluids immiscible. Propionitrile is immiscible with water, inert towards bromine, and a good solvent for the Br_3^- ion. As a method to control self-discharge has been developed for the totally aqueous phase electrolyte system, the organic electrolyte has not gained prominence. Furthermore, the propionitrile system has the disadvantages of toxicity and flammability of the solvent, and low conductivity which results in poor power performance.

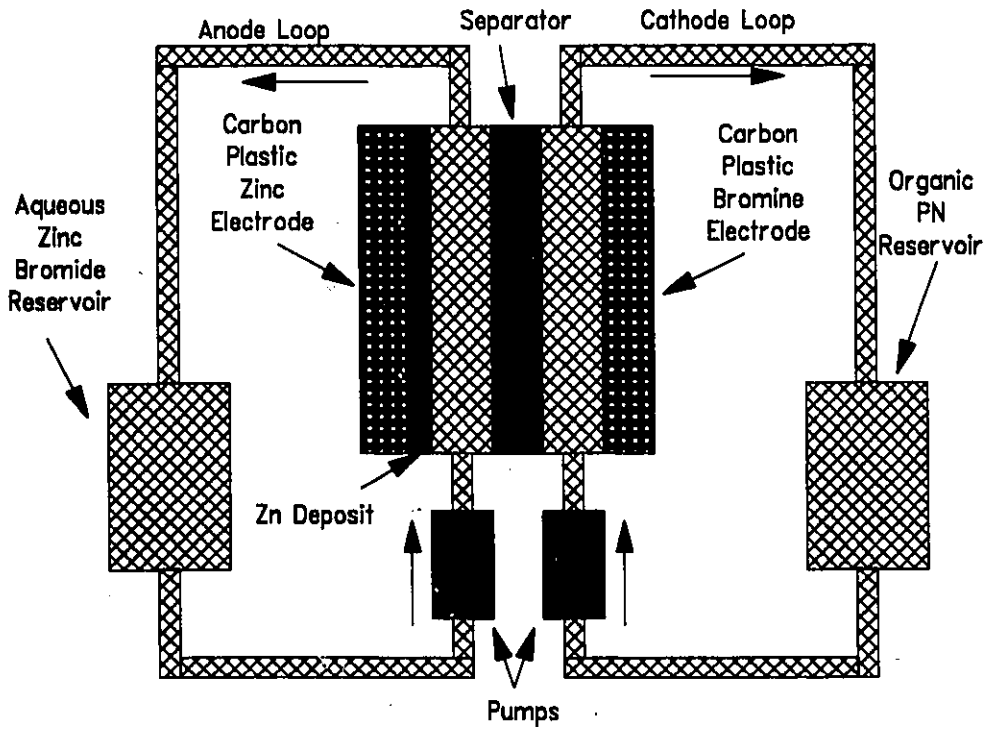

Figure 2.5: Diagram of zinc/bromine cell with a propionitrile (PN) electrolyte.

2.3.3 Non flow zinc/bromine battery development

A third technology based on a non-flow zinc/bromine battery is in early stages of development by Manassen and Cabasso (1990). This battery incorporates an activated carbon anode and cathode wetted with zinc chloride, zinc iodide or potassium chloride electrolyte. Bromine is adsorbed on the activated carbon cathode and separated from the zinc by a patented acrylamide membrane. Limitations of the non-flow system include limitations to battery size and total storage capacity, as well as the need to build higher voltage units composed of multiple bipolar cells (Gross, 1991). Due to these limitations, the zinc/bromine flow battery is generally seen to have greater commercial potential.

2.3.4 Areas of Active Research

Areas requiring development in zinc/bromine flow batteries include self-discharge control, zinc dendrite suppression, electrode design, and extreme temperature operation. Many aspects of the design and optimization of this battery, including electrolyte composition (Singh and White, 1983; Mastragostino and Valcher, 1983; Cathro *et al.*, 1985; 1986; 1988), electrode construction (Cathro *et al.*, 1987; Biserni *et al.*, 1986), separator composition and construction (Cathro *et al.*, 1988), thermal management (Ito, 1990), and system engineering (Bellows *et al.*,1971; Will, 1971: Grimes, 1986) have been considered to address these problems.

2.3.4.1 Self-discharge

Self-discharge occurs when bromine diffuses across the separator or through the flow channels to the zinc electrode; this can occur both during operation and during periods of rest. It results in reduced usable battery capacity and possible thermal runaway (Adams *et al.*, 1990). Early solutions to the self-discharge problem included the use of activated charcoal as a bromine absorber (Barnartt and Forejt, 1964), bromine extraction by organic solvents (Kinoshita, 1988), the use of electrolyte circulation systems having ion exchange membranes as separators (Lim *et al.*, 1977), and finally, complexation of bromine to depress bromine activity in the aqueous solution (Rallo and

Silvestroni, 1972; Eustace, 1980). The early work at Exxon to identify complexing agents greatly reduced the self-discharge losses. More recently, the problem of self-discharge has been addressed by the development of novel separators (Cathro *et al.*, 1988; Assink and Arnold, 1991), and by modification of the electrolyte. Several researchers have considered the addition of alternate zinc salts in attempts to decrease self-discharge (Tange, 1989). Tange (1989) suggests that the replacement of $ZnBr_2$ by $Zn(NO_3)_2$, $ZnSO_4$, $ZnSiF_6$, $Zn(CN)_2$, $Zn(BF_4)_2$, and $ZnCl_2$ and ZnF_2 decreases the concentration of free bromine in the aqueous solution, and thus decreases self-discharge. Bellows and Kantner (1987) proposed the use of surfactants to decrease the wettability of the microporous separator by water immiscible bromine complexes. This limits bromine transport to the zinc anode and also prevents self-discharge. This work has resulted in significant reductions in self-discharge losses, and as a result the technology is suitable for more widespread applications.

Shunt currents result from the fact that the cells in the bipolar stack are fed electrolyte from a common manifold system, large ports at the top and bottom of the electrode frame. Voltage differences between cells in the stack can drive parasitic currents through the conductive electrolyte in the flow channels and manifolds. Flow channels leading from the manifold to the active cell area are designed to be long and thin, to increase electrical resistance in the path of the shunt current, and therefore, limit the current drain. These channels increase the pumping power needed to circulate the electrolyte, so battery design must optimize for low shunt currents, while minimizing pumping power losses. Shunt currents can provide two additional problems. If the shunt currents are high enough, zinc deposition at the negative end of the circuit can result in zinc growing into the flow channels. This problem was observed in early stack tests, and has been eliminated through optimization of the flow channel design. The second problem caused by shunt currents is stack capacity redistribution. Cells near the centre of the stack can lose more capacity than cells near the ends of the stack because of the current distribution. This capacity redistribution can eventually lead to short circuiting of the cells at the end of the stack where the zinc deposit builds up. Deep discharge cycles are recommended to remove the excess zinc build up in the stack (Grimes, 1987;

Leo, 1991). A shunt current protection system was developed by Exxon (Leo, 1991). A bias current is applied through the manifold creating a voltage gradient which matches the voltage gradient in the active cells. There is still a coulombic loss associated with the bias current, but the capacity redistribution is eliminated. Periodic deep discharge cycles are still required as small differences in zinc deposit quality within each cell will be magnified by multiple partial discharge cycles.

2.3.4.2 Zinc Electrode Behaviour

Zinc electrode failure is generally due to one of the following processes, i) dendrite formation, ii) shape change and slumping. The effects of each of these failure mechanisms on the zinc electrode morphology is shown if Figure 2.6.

Zinc electrodes are subject to dendrite growth. At critical current densities, and concentrations, zinc redeposited on charge can grow into needlelike dendrites. The dendrites tend to grow toward the counter electrode, and can penetrate the separator causing cell shorting. The suppression of zinc dendrite formation has also been studied by several workers. Addition of lead, indium, and thallium at low concentrations (10^{-5} to 10^{-3}M) (Meidensha, 1984), of tin (Jinnai, 1988, Jinnai *et al.* 1986b), and of organic surfactants (Jinnai, 1986a; 1988; Grimes, 1987) at concentrations ranging from 10^{-5} to 0.1 weight percent have been proposed. Zinc plating has also been controlled through system engineering including maintaining a minimum flow rate, flow direction reversal and counter current flow of anolyte and catholyte through the stack (Iacovangelo and Will, 1986; Jorne *et al.*, 1987; Chen, 1990). Periodically the battery should be discharged at progressively lower current to a 20 mV open circuit voltage, to maintain a clean uniform surface for plating. This discharge cycle is referred to as "stripping the battery". One manufacturer (J.C.I.) has been able to maintain over 25 charge cycles between stripping cycles with negligible performance degradation in unmodified electrolyte (Lex and Mathews, 1991). This work has been critical to the development of the technology, as dendrite formation has been a major failure mechanism at room temperature.

On continuous cycling zinc electrodes can experience relocation of the zinc from the outside edges to the centre of the electrode. The tendency to agglomerate at the plate

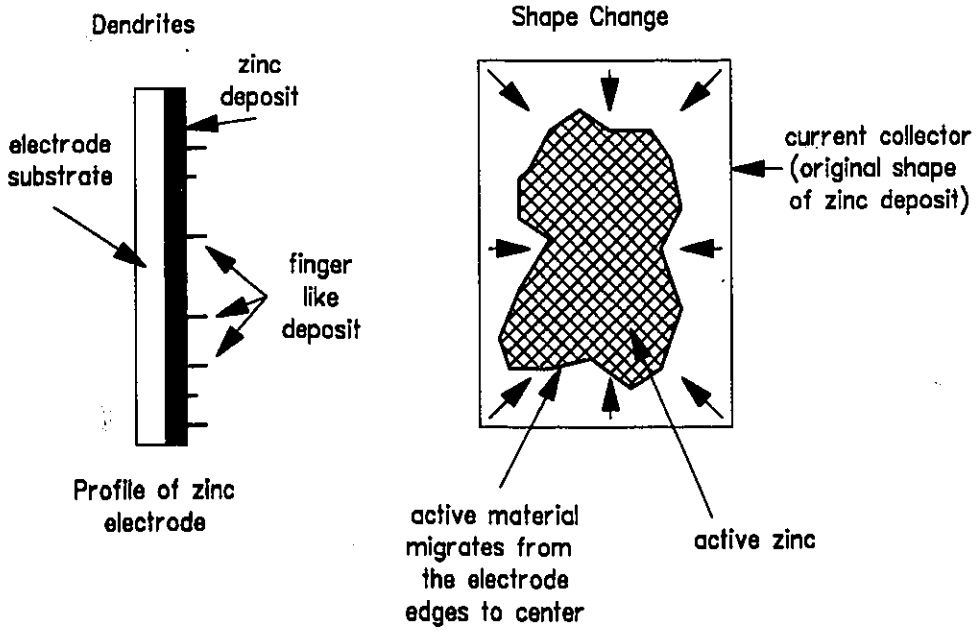

Figure 2.6: Zinc electrode failure mechanisms: dendrite formation and shape change.

centre is also called densification (Duffield, 1991). On discharge, metallic zinc is oxidized to ionic Zn^{2+}, which dissolves in solution. During charge zinc is redeposited back onto the current collector substrate. Due to a number of effects (thermal and concentration gradients, current density distribution, gravitational effects) dissolution and redeposition is not uniform. As a result, the active material is moved from the electrode edges toward the electrode centre as shown in Figure 2.6. If the zinc deposit is centred toward the bottom of the electrode, slumping is said to occur. A mechanism for shape change has been proposed based on gravitational effects by Boden *et al.* (1969). This mechanism is not consistent with the fact that sometimes zinc also moves away from the plate bottom and it is now believed that gravity does not influence shape change (Gunther, *et al.*, 1987). McBreen (1972) suggested that differences in current distribution during charging and discharging result in shape change of the zinc electrode. A second theory assumes the shape change is due to forced convection coupled with variations in electrolyte composition and flow direction across the face of the electrode surface (Choi, *et al.*, 1976a, 1976b). At present, the shape change mechanism has not been irrefutably confirmed (Duffield, 1991). Generally, shape change is not a problem with zinc/bromine batteries as the zinc is deposited on an inert carbon surface(Lim *et al.*, 1977). Furthermore, periodic stripping of the battery ensures that the surface for deposition is uniform.

Kinetics at the zinc electrode in aqueous $ZnBr_2$ are complicated by the presence of zinc bromine complexes. Zinc ions can react with bromide ions in the electrolyte to form several different complexes as shown below (Evans and White, 1987).

$$Zn^{2+} + Br^- \rightleftharpoons ZnBr^+ \tag{2.7}$$

$$ZnBr^+ + Br^- \rightleftharpoons ZnBr_2 \tag{2.8}$$

$$ZnBr_2 + Br^- \rightleftharpoons ZnBr_3^- \tag{2.9}$$

$$ZnBr_3^- + Br^- \rightleftharpoons ZnBr_4^{2-} \quad (2.10)$$

Studies in aqueous $ZnCl_2$ and $ZnBr_2$ electrolytes indicate that the complexing ion has a major effect on the kinetics of zinc deposition. The kinetics in $ZnBr_2$ electrolytes are faster than in $ZnCl_2$ electrolytes (McBreen and Gannon, 1983; McBreen, 1993). Addition of bromide salts of potassium and aluminum to aqueous $ZnBr_2$ inhibit the deposition kinetics. EXAFS studies indicated the bromide salts act as bromide anion donors and result in the formation of the higher order complexes such as $ZnBr_4^{2-}$ (McBreen, 1993). Stability constants in zinc chloride complexes are higher than those for zinc bromide complexes (Short and Morris, 1961). The decreasing order of stability of zinc halide complexes in ethylene glycol and methanol was also found to be Cl > Br > I (Kumagai, 1984). Higher order zinc chloride complexes are more stable than the corresponding zinc bromide complexes, thus, explaining the lower nucleation overvoltage and faster kinetics in $ZnBr_2$ electrolytes(Leo *et al.*. 1986).

2.3.4.3 The positive electrode and material stability

The bromine electrode must be inexpensive, of high performance, and durable. Furthermore, this electrode must be compatible with the electrolyte, and must be fabricated in the bipolar battery design that has gained acceptance as the most practical for this system (Bellows *et al.*, 1979; Kanazashi *et al.*, 1985). Titanium electrodes, coated with a catalyst were used in some early systems, but this material is expensive and subject to severe corrosion under cell reversal conditions (Cathro, Cedzynska and Constable, 1987). Porous, vitreous carbon bonded to a graphite substrate has been used to produce an electrode of sufficient activity, but the electrode was found to be brittle and difficult to bond to the plastic electrode frames (Cathro, Cedzynska, and Constable, 1987). The purpose of the porous vitreous carbon in this design is to protect the graphite material from bromine intercalation (Kinoshita, 1988). Bromine is known to form intercalation compounds with graphite, and these materials have been reported by Putt (1979) to lead to the destructive failure of the electrode. The most common solid electrode used for the positive in the zinc/bromine battery is the carbon plastic composite (CPC) electrode

(Kinoshita, 1988). It is possible to produce these electrodes in high volume and low cost using co-extrusion and injection moulding techniques. CPC bromine electrodes show overpotentials of 0.2 to 0.3 V under typical charge/discharge conditions (Kinoshita, 1988). Researchers at Exxon Research and Engineering Company have reported that addition of a high surface-area carbon to the CPC electrode surface reduces the overpotential to near zero (Grimes, 1984). This carbon layer should have a minimum surface area of 1500 cm^2/cm^2 to minimize the overpotential.

Chemical stability of some carbons in aqueous bromine solutions has been a problem. Bellows (1983) estimated the carbon corrosion rate for CPC at 1.7 V, and 30 °C to be 0.015%/year or 336 years for a total carbon consumption of 5 %. This work indicates that carbon stability is not the cause of battery failure in CPC electrode systems, and the lifetime of CPC electrodes is in excess of 500 to 1000 cycles. In another study, accelerated aging tests have estimated the lifetime of a CPC electrode to be 96 months(Arnold, 1991). Studies by Kanazashi (1985) have shown that plastic swelling, resulting in increases in electrode and separator thickness, occurs in ambient temperature catholyte. Swelling is likely the result of absorption of bromine by the plastic components, and can lead to failure due to internal shorting of the battery.

2.3.4.4 Thermal Management

As has been previously discussed, the operating temperature of the zinc bromine battery falls between 20 and 45 °C. At lower temperatures the coulombic efficiency improves due to reduced Br_2 diffusion, while voltaic efficiency declines due to increased electrolyte resistance. Higher operating temperatures have the reverse effect on coulombic and voltaic efficiencies. Also, the quality of the zinc deposit gets poorer with increasing temperature (Leo and Charkey, 1985). Further, at higher temperatures, negative effects are noticed in the deformation of the separator, warping and tearing causing increased self-discharge and decreased current collecting area. This results in lower overall system efficiency. Another factor to be considered is the effect of elevated temperature on stack construction. Currently the techniques of vibration and infrared welding are used in stack construction; elevated temperatures can lead to stack rupturing (Nash, 1990). Stacks

designed with bolted construction are capable of operating at slightly higher temperatures, the limit being 45 °C (Tomazic, 1990). Upon heating, the plastic casing expands, but is held secure by the screws and bolts, and acts as a gasket for the battery stack. The pumps also contribute to the thermal management problem due to inefficiencies and viscous heating effects of the fluid passing by the pump head (Nash, 1990). Extreme temperature can result in bromine gassing. A 75% energy efficient battery will evolve 0.2 kWh waste heat for every kWh of energy stored and delivered in a 12 hour cycle (Leo and Bharvani, 1984).

Several different directions have been studied to thermally manage the zinc/bromine battery. Zinc electrodes are being designed to improve deposition technology to allow higher operating temperatures of 35 to 45 °C. The higher operating temperature would allow the use of lower cost thermal management systems (cooling tower versus refrigeration) in areas with warm climates(Leo and Charkey, 1985). Researchers (Eustace, 1980; Gibbard, 1983; Cedzynska, 1989; Eidler, 1992) are identifying complexing agents that do not decompose, and maintain their complexing ability at elevated temperatures, to control bromine gassing. Successful high temperature complexing agents have yet to be identified and this work is progressing elsewhere (Eidler, 1992).

The heat exchanger, therefore, is a key component in the battery system. It is generally used to remove excess heat generated in battery operation as a by-product of inefficiencies of operation, and maintains the battery at a constant operating temperature, between 20 and 35 °C. As the electrolyte can be used to carry heat from the stack, the exchanger is generally placed on the anolyte (less viscous fluid) loop. As the battery itself is an excellent heat exchanger, only one electrolyte stream needs to be cooled, and it will in turn cool the other stream as they pass through the battery (Bolstad and Miles, 1989). There are several restrictions placed on the development of the heat exchanger. The nature of the aqueous electrolyte introduces design problems. The electrolyte is corrosive, and would corrode many commonly used heat exchanger materials including aluminum and copper. Even slight corrosion is undesirable, as metal impurities can significantly alter the zinc plating morphology. Researchers have proposed the use of a

titanium plate heat exchanger (Leo and Bharvani, 1984). Other researchers have considered radiative, evaporative cooling, and several other heat transfer devices(Nash, 1990). Selection of the heat exchanger is dependent on the capacity of the battery, the application, and weight and volume restrictions. With suitable insulation, the internally generated heat can be used to stave off freezing during cold weather (Eskra, *et al.* 1991).

2.4 Low Temperature Development

For many applications, low temperature performance is important. Reduced temperatures result in viscosity increase, conductivity decrease and eventually, electrolyte freezing. Addition of a thermal management system, including a heater, can be used so that the battery can operate in low temperature environments. A second approach, as used in this study, is to modify the battery electrolyte so that it remains liquid at low temperatures. Workers at Johnson Controls, Inc. (J.C.I.) (Eidler, 1992) have identified solid formation of standard zinc bromide electrolytes at 5 °C. Preliminary differential scanning calorimetry experiments were performed on limited concentrations of several chloride salts. These results indicated freezing point depressions of over 25 °C for 0.5 M concentration of salt. It is likely that these measurements do not take into account super cooling effects, and actual freezing temperatures are much higher. Room temperature resistivity measurements were also performed. However, due to the preliminary nature of J.C.I.'s low temperature experiments, potential candidates for low temperature operation were not identified. Researchers (Eidler, 1992) also considered the freezing of the organic polybromide liquid phase (the second phase). Long before this phase solidifies, it becomes very viscous. At 40 °C the viscosity of the organic phase is approximately 17 mPa·s; this value increases to 25 mPa·s at 20 °C, and increases even further at lower temperatures. The viscosity of the aqueous phase is of the order of 7 to 14 mPa·s between 50 and 20 °C. Addition of organic chlorides prevents freezing and limits viscosity increase down to -20 °C (Eidler, 1992). However, the use of this additive has several detrimental effects, including materials restrictions (polyvinyl chloride plastic is not resistant), and it is not miscible with the aqueous phase. Furthermore, it has lower

voltaic efficiency (as a result of lower conductivity), and reduced energy efficiency.

2.5 General Chemistry of $ZnBr_2$ in Water

The species distribution of zinc bromide salt alone in aqueous solutions has been studied by numerous workers in the absence of polybromide complexing agents. In 1983, Kalman *et al.* identified Zn^{2+}, $ZnBr_2$, $ZnBr_3^-$, and $ZnBr_4^{2-}$ species in aqueous solutions using techniques of x-ray diffraction and Raman spectroscopy. In 1984, P.L. Goggin *et al.* further identified the structure of the above species; pyramidal for $ZnBr_3^-$, bent for $ZnBr_2$, and tetrahedral for $ZnBr_4^{2-}$. This work is important as it identifies complexed zinc ions as the species undergoing reduction during zinc charging. Zinc/bromine battery electrolytes incorporate quaternary ammonium salts (e.g., N-ethyl-N-methylmorpholinium bromide (MEMBr), N-chloromethyl-N-methylpyrrolidinium bromide, N-methoxymethyl-N-methylpiperidinium bromide, N-ethyl-N-methylpyrrolidinium bromide (MEPBr)) into the catholyte, as well as additives such as NaBr, LiCl and NH_4Cl. The complex bromide salts are referred to in the literature as "Quats" (QBr) or as the polybromide phase. The distribution of zinc bromide species in these more complex systems has not been identified but would provide a deeper understanding for further battery engineering development of the Zn/Br_2 system.

Physical chemical studies of the aqueous - polybromide system have been conducted by numerous groups. Gibbard, in 1981, determined the activity coefficients of aqueous zinc bromide solutions over the concentration range 0.1 to 4 M and the temperature range, 0 to 36 °C. He found significant variation with both temperature and concentration, indicating each of these factors should be critical to the battery performance. Furthermore, as electrolyte activity is highly dependent on temperature and concentration, this work identifies the need to conduct experiments using actual battery electrolytes at temperatures of interest. He also noted a change in open circuit potential at room temperature, in cells which had been thermally cycled above 36 °C.

Cathro *et al.* (1985; 1986) determined the diffusion coefficient of bromine in aqueous solutions containing quaternary ammonium salts, and KCl at room temperature.

Density and viscosity of the solutions were also determined. Bromine transport was dependent on the complexing agent and was 6% higher in MEPBr than in MEMBr. To prevent self-discharge losses, the bromine transport should be minimized; therefore MEMBr is a better complexing agent. Bajpal (1981) also identified MEMBr as a good complexing agent from results of a vapour pressure study of bromine in quaternary ammonium salt complexes. MEMBr resulted in the lowest vapour pressures of the quaternary salts considered. The stability of the polybromide phase was considered by Hoobin *et al.* (1989) and the concentration of QBr in the polybromide phase was found to remain unchanged with aging, as was the Br^- concentration in the aqueous phase. The diffusion coefficient for bromine in aqueous electrolyte in the presence of Et_4NBr and Bu_4NBr was found by Cedzynska (1989). At higher concentrations (>0.3M), these compounds, while significantly reducing the bromine concentration in the aqueous phase, formed a solid brown phase. The variety and number of bromine complexing agents used in these studies is quite large. The bromine species distribution is highly dependent on the selection of the complexing agent, and thus, it is important that a basic understanding of potential commercial electrolyte systems be achieved. Studies have identified MEPBr and MEMBr as the best quaternary salts for room temperature complexation, and as a result these materials have been used in this project.

There have been few electrochemical studies of Zn/Br_2 battery electrolytes at practical battery concentrations (> 2 M $ZnBr_2$). Cyclic voltammetry for zinc deposition from 3M $ZnCl_2$ on glassy carbon was performed (McBreen and Gannon, 1983) at pH 2.8, with a sweep rate of 50 mV/sec. The voltammogram exhibited a nucleation loop in the cathodic current. McBreen and Gannon (1983) reported qualitatively similar results in zinc bromide solution. They identified an instantaneous nucleation, kinetic growth control mechanism for deposition of zinc on glassy carbon from $ZnCl_2$ and $ZnBr_2$ solutions. This work has practical significance as it shows electrochemical results in the high concentration aqueous solutions used in actual batteries.

The Br_2/Br^- reaction was studied electrochemically on vitreous (glassy) carbon discs. The electrolytes used in the study of Vogel and Mobius (1991) included 0.25 M $ZnBr_2$, NaBr or NH_4Br. Results indicate that bromine oxidation/reduction is irreversible.

Vogel and Mobius (1991) identified NH_4Br as a complexing salt which binds Br_2 in the aqueous phase, and can contribute to self-discharge, and concluded that ammonium salts should not be used as the supporting agents. Mastragostino and Gramellini (1985) propose that both anodic and cathodic processes in electrolytes containing 0.5 M $NaClO_4$ involve two consecutive steps:

$$Br_2 + e^- \rightarrow Br_{ad} + Br^- \quad 1$$
$$Br_{ad} + e^- \rightarrow Br^- \quad 2 \qquad (2.11)$$

They identified reaction 2.11-1 to be rate determining for the cathodic reaction (bromine reduction), and reaction 2.11-2 to be rate determining for the anodic reaction (bromide oxidation). Bromine adsorption has been identified as the critical step leading to bromide/bromine oxidation/reduction. The effect of the polybromide complexing agent on bromine adsorption is, therefore, important. In subsequent work, Vogel and Mobius (1991) found limiting currents, in pure polybromide solutions, were not reproducible as the surface of the carbon electrodes became coated by solid polybromides during cycling.

Electrochemistry experiments have not been performed in solutions containing active material at actual battery concentrations, or in solutions containing quaternary ammonium bromide complexing agents. The results of Vogel and Mobius(1991) and Mastragostino and Gramellini (1985) indicate that additives affecting bromine radical adsorption should be visible in electrochemical experiments conducted in solutions approximating operating battery electrolytes. Therefore, we have conducted electrochemical experiments in solutions approximating operating battery electrolytes with the expectation of observing the effects of quaternary ammonium salt concentration and electrolyte composition on bromine radical adsorption.

Chapter 3

Raman Spectroscopy of Aqueous Zinc Bromide Electrolytes

3.1 Raman Theory

Raman spectroscopy, discovered over sixty years ago by Sir C.V. Raman (Raman and Krishnan, 1928; Stencel, 1990), is a technique which studies the energy levels of molecules by examining the light scattered by them. The incident beam of light is a stream of photons, all of the same energy (i.e., frequency). When the beam passes through the sample, some of the photons collide with sample molecules. If the collision is elastic, then the photon is scattered with the same energy and frequency as the photons in the incident beam. These photons are said to undergo Rayleigh scattering. If the collision is inelastic, then an incident photon can lose energy to the sample molecule, and emerge at lower frequency, or it can gain energy from the sample molecule and emerge at higher frequency. Photons scattered at lower frequency than the incident radiation give rise to the Stokes lines, while those scattered at higher frequency give rise to the anti-Stokes lines. In a Raman experiment, the frequencies of scattered light are analyzed and interpreted in terms of the molecular energy levels.

The change in the photon's energy, ΔE, is the difference in energy between two allowed energy states of the sample molecule. That is, ΔE represents a change in vibrational and/or rotational energy of the molecule. The Stokes lines are generally more intense than the anti-Stokes lines, as the former are accompanied by an increase in molecular energy (which can always occur subject to selection rules), and the latter result

in a decrease in molecular energy (which can only occur if the molecule is initially in an excited state). In either case, the total radiation scattered at frequencies other than the incident is very small, on the order of 10^7 or 10^8 times less intense than Rayleigh scattering, and a sensitive apparatus is needed.

3.1.1 The Concept of Polarizability in the Classical Theory of the Raman Effect (Banwell, 1983)

A molecule placed in a static electric field will undergo distortion, the positive nuclei will be attracted toward the negative pole of the field, and the electrons to the positive pole. This separation of charge leads to an induced electric dipole moment and the molecule is said to be polarized. The induced dipole moment depends both on the electric field and the ease at which the molecule can be distorted or the polarizability, α. The induced dipole moment is written:

$$\mu = \alpha E \tag{3.1}$$

When a sample of diatomic or linear polyatomic molecules is subjected to a beam of incident radiation, each molecule experiences an electric field:

$$E = E_o \sin 2\pi \nu t \tag{3.2}$$

where ν is the frequency of the electric field. The induced dipole is, therefore,

$$\mu = \alpha E = \alpha E_o \sin 2\pi \nu t \tag{3.3}$$

An oscillating dipole will emit radiation of its own oscillating frequency, ν, and Equation 3.3 is the classical explanation of Rayleigh scattering.

When a molecule undergoes a rotation or vibration which changes the polarizability, then the oscillating dipole in Equation 3.3 will have the changing polarizability superimposed on it. For a vibration of frequency ν_{vib} the changing polarizability can be written as:

As a result the oscillating dipole can be written as:

$$\alpha = \alpha_o + \beta \sin 2\pi \nu_{vib} t \tag{3.4}$$

$$\mu = \alpha E = (\alpha_o + \beta \sin 2\pi \nu_{vib} t) E_o \sin 2\pi \nu t \tag{3.5}$$

which reduces to:

$$\mu = \alpha_o E_o \sin 2\pi \nu t + \frac{1}{2} \beta E_o (\cos 2\pi (\nu - \nu_{vib}) t - \cos 2\pi (\nu + \nu_{vib}) t) \tag{3.6}$$

Classical theory predicts, therefore, that the oscillating dipole will emit radiation at the incident frequency, ν, and also at frequencies ν-ν_{vib} and ν+ν_{vib}, provided that β is not zero. β is zero for vibrations that do not alter the polarizability of the molecule.

The general rule for Raman spectroscopy is a molecular rotation or vibration is Raman active if it causes some change in a component of the molecular polarizability. The Rule of Mutual Exclusion further applies to the vibrational Raman spectra: if a molecule has a centre of symmetry, then Raman active vibrations are IR inactive, and vice versa. If the molecule has no centre of symmetry, the vibrations can be both IR and Raman active.

3.1.2 Polarization of Light and the Raman Effect (Banwell, 1983)

The only light that will pass through a polaroid filter or a Nicol prism has its electric (magnetic) vector confined to a particular plane. The light which passes through such a filter is plane polarized light. When the polarized light falls on a second filter or analyzer, it will pass with undiminished intensity provided the second filter is oriented parallel to the first. At other orientations, the intensity passed will decrease until the filters are perpendicular, and no light passes.

If the light incident on the analyzer is only partially polarized (only some of the rays have electric vectors parallel to a given plane), some light will always pass through the analyzer. The intensity will go through a minimum, when the analyzer is perpendicular to the plane of maximum polarization. The degree of polarization is the ratio of intensities of light transmitted perpendicular (minimum) to light transmitted

parallel (maximum) to this plane:

$$\rho = \frac{I_{\perp}}{I_{\parallel}} \tag{3.7}$$

Some lines found in Raman spectra are plane polarized to different extents, even if the incident light is depolarized. In general, symmetric vibrations result in polarized or partially polarized Raman lines, while non-symmetric vibrations give depolarized lines. For $\rho \leq 3/4$, the Raman line is polarized, and the vibration symmetric. For $\rho \geq 3/4$, the line is depolarized and the vibration is not symmetric. Further, the higher the molecular symmetry of the sample molecule, the smaller will be the degree of depolarization of the Raman line for a particular vibration.

3.1.3 The Raman Instrument

Raman spectroscopy is essentially an emission technique, with the bulk of the instrument a visible region spectrometer. It is the monochromatic excitation source which results in the observable Raman spectra. A block diagram of a typical laser Raman spectrometer is shown in Figure 3.1. Elements of this system include the laser source, collimating lenses or mirrors, the sample cell and positioner, input optics, monochromator, detector, amplification electronics, computer interface and computer, and spectral display system.

The choice of laser source depends on the experimental requirements. Laser frequencies range from near infrared to near UV, and are tuned to maximize the Raman signal for a minimal amount of material and excitation power. The He-Ne laser typically operates at 632.8 nm and the argon laser at 514.5 and 488.0 nm. Rayleigh scattering is diminished with a confined laser beam and the Raman spectra can be recorded to within 20 cm^{-1} of the incident frequency. The monochromator contains dispersive elements, generally holographic gratings whose number depends on the amount of discrimination required.

Photomultipliers and photodiodes of silicon and/or germanium are used as detectors. Photomultiplier tubes have very low background noise as compared to Ge and

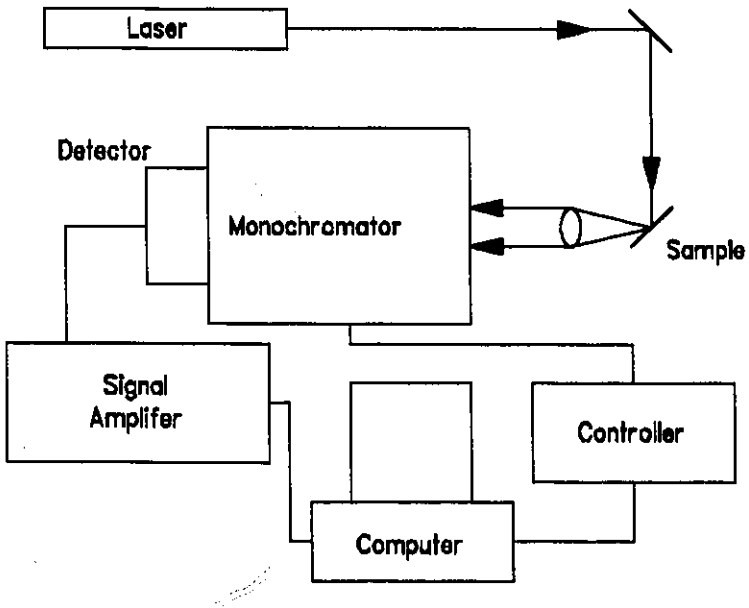

Figure 3.1: Block diagram of a Raman spectrometer.

Si photodiodes. Multichannel analyzers using photodiodes have become popular because of the increased speed of acquisition of a spectrum as compared with photomultipliers. Photomultipliers do, however, provide superior spectral resolution due to their greater sensitivity.

3.2 Experimental

3.2.1 The Raman Spectrometer

Raman spectra were collected using a Spectra Physics Series 2000, 5 W Argon ion laser tuned to the 514.5 nm line, and a Ramanor HG.2S spectrophotometer. The power level at the sample was 200 mW, except for spectra recorded for the black polybromide phase, where the power at the sample was reduced to 10 mW. Slit width was set between 600 and 800 μm, and scan speed ranged from 6 to 60 cm^{-1}. Spectra were obtained over the range of 50 to 3800 cm^{-1}. The detector used in these studies was a Spex Photometer holder and a Hamamatsu photomultiplier tube. The Raman spectrometer was calibrated using a Neon light source. The temperature of the sample was held constant by placing sample tubes in an insulated aluminum block through which isopropanol was circulated from a temperature controlled Neslab constant temperature bath to maintain constant temperature to ±2 °C (Preston and Adams, 1979). Data were collected digitally using an IBM AT compatible computer, and were analyzed using Spectra Calc curve resolution software (Copyright 1987,1988, Galactic Industries Corporation).

3.2.2 Solution Preparation

A solution containing 3 M $ZnBr_2$ was prepared volumetrically from 7.64 M stock $ZnBr_2$ solution (Johnson Controls, Inc.). A series of solutions were obtained from the electrolyte of a $ZnBr_2$ 2 kWh battery at various stages of charge operated during this research. State-of-charge (SOC) of 0 % represents the discharged battery, and SOC of 100 % is the fully charged battery. The electrolyte at 0 % SOC (uncharged) contained 3 M $ZnBr_2$ and a proprietary mixture of quaternary ammonium bromide complexing agent.

Liquid bromine, (99.5 %, laboratory reagent grade) was obtained from BDH Chemicals, Inc.

3.3 Results and Discussion of Raman Spectra Collected in Aqueous Zinc Bromide Electrolytes

The Raman spectra of the 3 M $ZnBr_2$ and battery electrolyte solutions were measured between 50 and 3800 cm^{-1} as a function of temperature between 0 and 25 °C. Aqueous zinc bromide species, previously identified in the region 150 to 250 cm^{-1} (Macklin and Plane, 1970), were found in the present study as shown in Figures 3.2, 3.3 and 3.4 for catholyte at 20 °C, anolyte at 20 °C, and 3 M $ZnBr_2$ as a function of temperature. Raman band locations for various zinc/bromine complexes are shown in Table 3.1 (Yellin and Plane, 1961; Macklin and Plane, 1970; Goggin *et al.*, 1985; Yang *et al.*, 1988).

Table 3.1: Raman band locations for aqueous zinc/bromine complexes.

Complex	Approximate Raman Band Location
$ZnBr^+$	240 cm^{-1}
$ZnBr_2$	205 cm^{-1}
$ZnBr_3^-$	183 cm^{-1}
$ZnBr_4^{2-}$	170 cm^{-1}

All Raman spectra collected between 150 and 250 cm^{-1} were analyzed using Spectra Calc software routines (Galactic Industries, Inc.). It was assumed that the Raman bands were Lorentzian in nature for curve fitting calculations, as the dominant influence in the liquid phase is collision broadening, which gives rise to Lorentzian band shapes rather than Gaussian band shapes (Marley and Gaffney, 1990). The CURVEFIT routine in the Spectra Calc software package optimizes peak height, position, and width through an iterative technique. Three peaks, those associated with the $ZnBr_2$, $ZnBr_3^-$, and $ZnBr_4^{2-}$

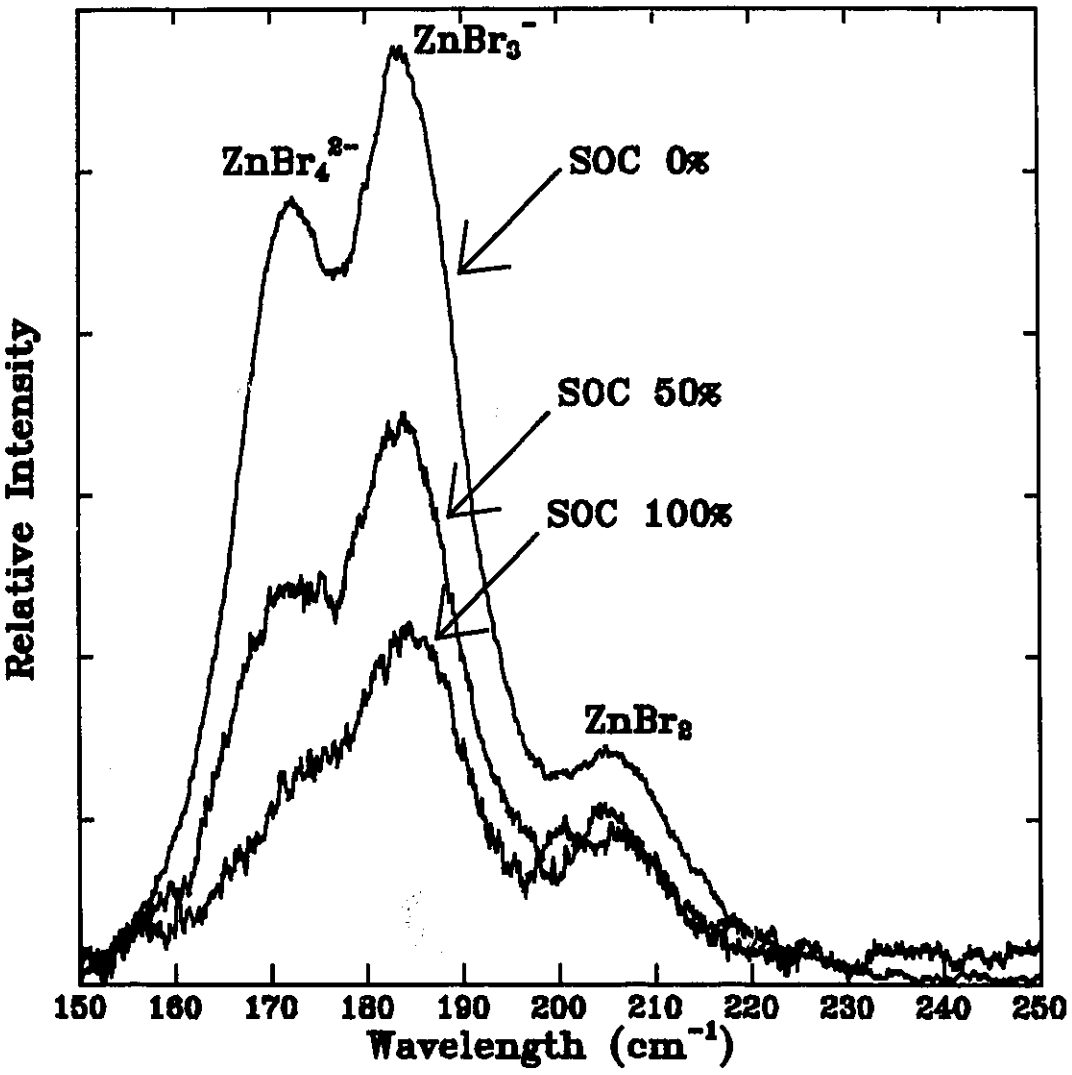

Figure 3.2: Raman spectra of aqueous zinc bromide anolyte at 25 °C, as a function of the state-of-charge of the battery.

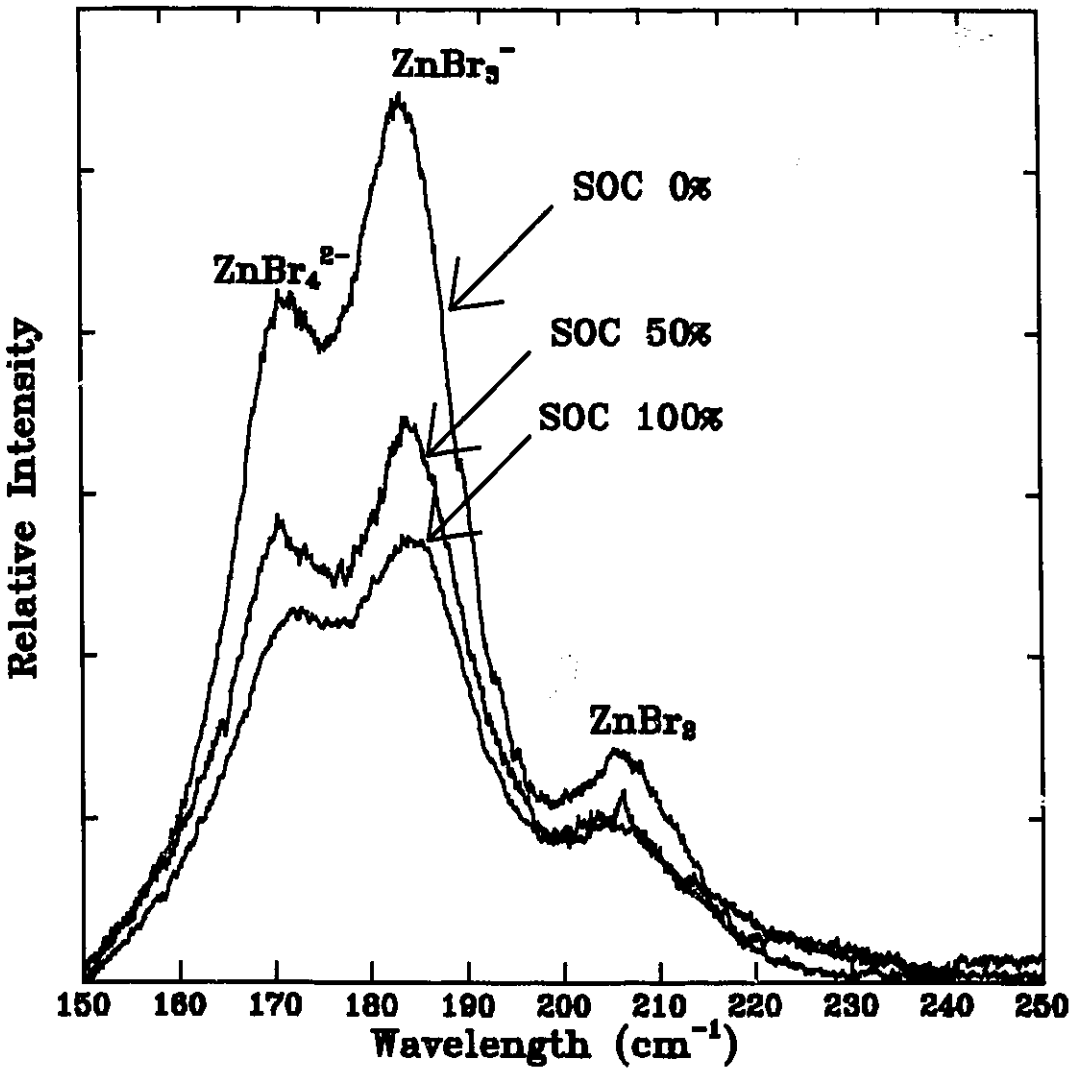

Figure 3.3: Raman spectra of aqueous zinc bromide catholyte at 25 °C as a function of state-of-charge of the battery.

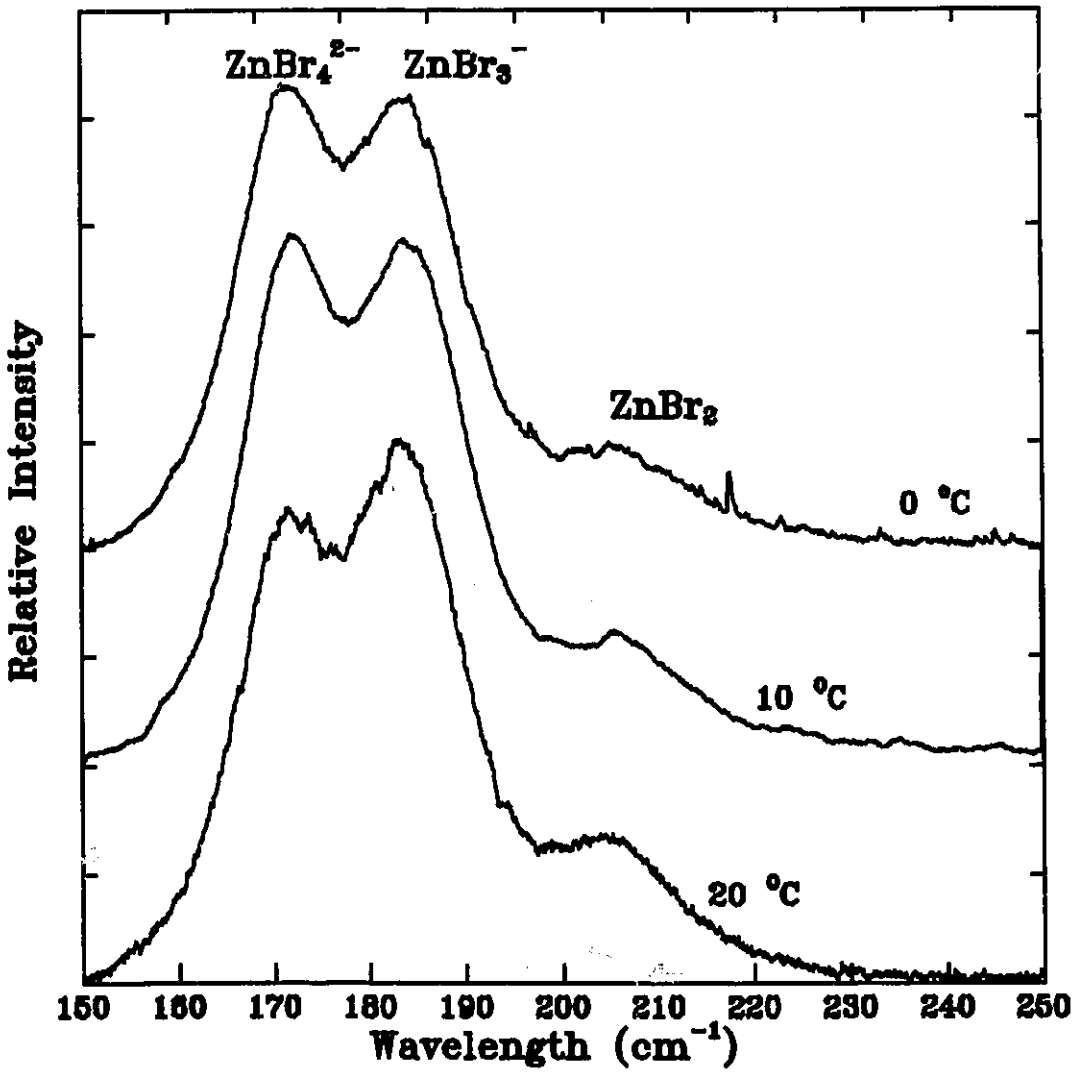

Figure 3.4: Raman spectra for aqueous 3M $ZnBr_2$ as a function of solution temperature.

species, were readily identified in the experimental spectra obtained. The fourth complexed species, $ZnBr^+$, centred at 240 cm^{-1}, was not evident in these spectra. As a result, the synthetic spectra were calculated based on only three Lorentzian bands centred around 170, 183, and 205 cm^{-1}. Results of curve resolution analysis for room temperature anolyte at 0 % state-of-charge are presented in Figure 3.5. Integrated Raman band intensities were calculated and are presented in Tables 3.2-3.4.

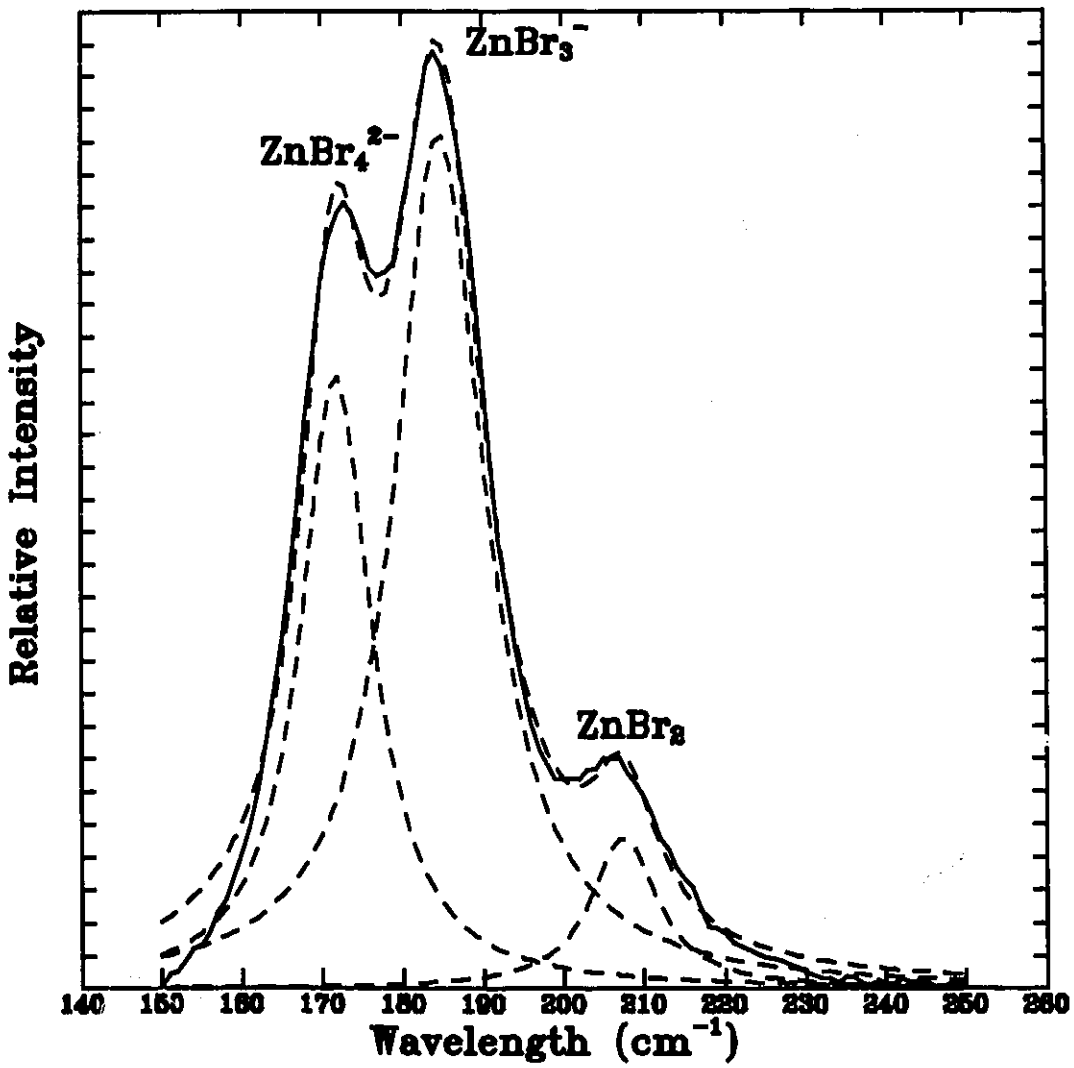

Figure 3.5: Raman spectrum of aqueous zinc bromide anolyte (3M $ZnBr_2$, 1M QBr), at 0 % SOC. The dashed curves correspond to each of the Lorentzian bands representing the complexed zinc/bromine species and the synthesized spectrum.

Table 3.2: Raman intensities of zinc bromide electrolytes as a function of state - of - charge, at 25 °C.

Raman Peak Centre (cm^{-1})	Solution	Relative Peak Height	Peak Width (cm^{-1})	Relative Integrated Intensity
ANOLYTE				
172	SOC 0 %	1.811	10.5	28.0
	SOC 50 %	0.879	11.2	13.9
	SOC 100 %	0.419	16.2	9.0
184	SOC 0 %	2.621	13.5	50.5
	SOC 50 %	1.586	13.6	30.7
	SOC 100 %	0.939	12.6	16.6
206	SOC 0 %	0.458	10.0	6.7
	SOC 50 %	0.332	12.5	6.0
	SOC 100 %	0.367	11.5	5.8
CATHOLYTE				
172	SOC 0 %	3.537	10.9	54.6
	SOC 50 %	0.863	13.0	15.5
	SOC 100 %	4.235	13.5	77.4
184	SOC 0 %	4.958	12.2	87.0
	SOC 50 %	1.183	13.7	23.0
	SOC 100 %	5.903	14.8	119.9
207	SOC 0 %	0.990	11.7	16.9
	SOC 50 %	0.266	14.6	5.5
	SOC 100 %	1.668	12.7	28.6
3 M $ZnBr_2$				
172	3 M $ZnBr_2$	1.890	10.4	26.9
184	3 M $ZnBr_2$	2.371	13.8	46.5
205	3 M $ZnBr_2$	0.455	11.4	7.6

Table 3.3: Raman intensities of zinc bromide electrolytes as a function of state - of - charge, at 10 °C.

Raman Peak (cm^{-1})	Solution	Relative Peak Height	Peak Width (cm^{-1})	Relative Integrated Intensity
ANOLYTE				
172	0 %	2.667	10.8	40.9
	50 %	1.134	10.1	16.3
	100 %	0.389	18.4	9.3
184	0 %	3.237	13.3	61.3
	50 %	1.469	13.2	27.7
	100 %	0.736	13.8	14.1
206	0 %	0.516	10.2	7.7
	50 %	0.225	9.8	3.3
	100 %	0.248	10.3	3.6
CATHOLYTE				
172	0 %	1.637	10.8	25.2
	50 %	2.516	11.0	38.9
	100 %	5.478	15.8	114.5
184	0 %	2.193	13.2	41.3
	50 %	2.993	13.4	57.2
	100 %	6.365	14.9	130.3
207	0 %	0.359	11.5	6.0
	50 %	0.482	9.9	5.5
	100 %	1.793	13.4	32.0
3 M $ZnBr_2$				
172	3 M $ZnBr_2$	10.09	10.3	147.7
184	3 M $ZnBr_2$	10.85	13.9	213.9
205	3 M $ZnBr_2$	1.765	12.9	32.7

Table 3.4: Raman intensities of zinc bromide electrolytes as a function of state - of - charge, at 0 °C.

Raman Peak (cm^{-1})	Solution	Relative Peak Height	Peak Width (cm^{-1})	Relative Integrated Intensity
ANOLYTE				
172	0 %	2.921	10.5	43.4
	50 %	1.383	10.6	20.6
	100 %	0.547	13.1	9.8
184	0 %	3.164	13.3	59.9
	50 %	1.631	13.0	30.3
	100 %	1.097	16.3	24.2
206	0 %	0.439	10.3	6.6
	50 %	0.229	9.3	3.1
	100 %	0.282	10.4	4.1
CATHOLYTE				
172	0 %	3.251	10.3	47.7
	50 %	2.596	10.9	40.0
	100 %	4.584	14.7	90.1
184	0 %	4.061	12.8	74.5
	50 %	2.666	13.2	50.3
	100 %	4.519	13.4	84.5
207	0 %	0.555	10.7	8.7
	50 %	0.375	9.6	5.3
	100 %	1.059	11.2	16.3
3 M $ZnBr_2$				
172	3 M $ZnBr_2$	1.788	10.4	26.3
184	3 M $ZnBr_2$	1.857	14.0	36.8
205	3 M $ZnBr_2$	0.269	11.8	4.6

The above studies were performed without the addition of an internal standard: therefore, it is not possible to calculate absolute molar concentrations. The experimental data were analyzed for relative molar concentrations of species. In order to convert the measured Raman intensities to species concentration, the molar intensities of Macklin and Plane (1970) were applied. Accepted values of molar intensity are given in Table 3.5 below (Macklin and Plane, 1970).

Table 3.5: Values of molar intensity for aqueous $ZnBr_4^{2-}$, $ZnBr_3^-$, $ZnBr_2$, and $ZnBr^+$, as determined by Macklin and Plane (1970).

Complex	$ZnBr^+$	$ZnBr_2$	$ZnBr_3^-$	$ZnBr_4^{2-}$
Molar Intensity	0.40 ± 0.08	0.85 ± 0.08	1.8 ± 0.3	1.75 ± 0.10

This work assumed that the molar intensities for the aqueous zinc/bromide species were independent of temperature. Based on the corrected intensities, the percents of complexed species were calculated, and are shown in Tables 3.6 and 3.7. The ratio of relative integrated intensities for the $[ZnBr_4^{2-}]/[ZnBr_2]$ and $[ZnBr_3^-]/[ZnBr_2]$ species are shown in Table 3.8. These data, which have not been corrected for molar intensity, do not give a true indication of relative concentrations of complexed species. The data do, however, emphasize changes in species distribution with temperature and state of charge.

Table 3.6: Relative concentration of complexed species as a function of temperature for 3 M $ZnBr_2$ solutions.

Temperature (°C)	% of total complexed species (±3 %)		
	$ZnBr_4^{2-}$	$ZnBr_3^-$	$ZnBr_2$
25	31	51	18
10	35	49	16
0	37	50	13
-7	48	41	11

Table 3.7: Relative concentration of complexed species as a function of state-of-charge and temperature for 3 M $ZnBr_2$ zinc/bromine battery electrolytes including 1 M quaternary ammonium complexing agent.

State-of-charge	Anolyte % of total complexed species (±3 %)			Catholyte % of total complexed species (±3 %)		
	$ZnBr_4^{2-}$	$ZnBr_3^-$	$ZnBr_2$	$ZnBr_4^{2-}$	$ZnBr_3^-$	$ZnBr_2$
Temperature 25 °C						
0 %	32	54	14	30	51	19
50 %	25	53	22	32	45	23
100 %	24	43	32	31	46	23
Temperature 10 °C						
0 %	35	51	14	32	52	16
50 %	33	54	14	36	51	13
100 %	31	45	24	37	41	22
Temperature 0 °C						
0 %	38	50	12	35	52	13
50 %	36	52	11	40	49	11
100 %	24	56	20	44	40	16

Results of this study indicated that the species distribution was dependent on both temperature and state-of-charge (or concentration). The $ZnBr^+$ species was not observed in the experimental spectra obtained in aqueous 3 M $ZnBr_2$, or 3 M $ZnBr_2$ and 1 M QBr solutions. As temperature decreased from 25 to 0 °C, species distribution shifted from lower to higher order complexes (from $ZnBr_2$ to $ZnBr_4^{2-}$complexes). This result is supported by the work of Yang *et al.*, (1988) who found the 240 cm^{-1} band at temperature greater than 100 °C and low bromine to zinc concentration ratios and also by Irish *et al.*, (1963), who found the concentration of $ZnCl_2$ in aqueous solutions to be larger at 70 °C than at 25 °C. Similar results for zinc bromine species at 25 °C, atmospheric pressure and 350 °C, 2000 psi have been reported by Marley and Gaffney(1990).

Table 3.8: The ratio of the relative integrated intensites shown in Tables 3.2 to 3.4 as a function of state-of-charge and temperature for 3 M $ZnBr_2$ zinc/bromine battery electrolytes including 1 M quaternary ammonium complexing agent.

Temp. (°C)	Anolyte Ratio of Relative Integrated Intesity of Species X:$ZnBr_2$			Catholyte Ratio of Relative Integrated Intensity of Species X:$ZnBr_2$		
	Species X			Species X		
	$X=ZnBr_4^{2-}$	$ZnBr_3^-$	$ZnBr_2$	$ZnBr_4^{2-}$	$ZnBr_3^-$	$ZnBr_2$
0 % State - of - Charge						
25	4.2	7.5	1	3.2	5.1	1
10	5.3	8.0	1	4.2	6.9	1
0	6.6	9.1	1	5.5	8.6	1
50 % State - of - Charge						
25	2.3	5.1	1	2.8	4.2	1
10	4.9	8.4	1	7.1	10.4	1
0	6.6	9.8	1	7.5	9.5	1
100 % State - of - Charge						
25	1.6	2.9	1	2.7	4.2	1
10	2.6	3.9	1	3.6	1.8	1
0	2.4	5.9	1	5.5	5.2	1
3 M $ZnBr_2$						
25	3.5	6.1	1			
10	4.5	6.5	1			
0	5.7	8.0	1			
-7	8.9	7.9	1			

As state-of-charge increased the concentration of Zn^{2+} and Br^- ions in solution decreased as metallic zinc was plated at the negative electrode, and bromide ions formed bromine at the positive electrode. It was found that species distribution did change with

state-of-charge, but that clear trends were not observed. Generally, anolyte species distribution shifted to lower order species. Results for catholyte solutions were not clear. At room temperature, species distribution shifted to lower order species, but at lower temperature, the relative concentration of both $ZnBr_4^{2-}$ and $ZnBr_2$ species increased as state-of charge increased. This result was due to competing effects of temperature, which shifted the species distribution to higher order species, and the lowering of zinc cation and bromide anion concentration, which shifted the species distribution to lower order species.

Table 3.9 relates the percentage of total complexed species for electrolytes containing quaternary ammonium salt to that for 3 M $ZnBr_2$. The ratio of the percentage of the total complexed species at 0 % SOC to the percentage of total complexed species in 3 M $ZnBr_2$ for both anolyte and catholyte solutions was approximately 1 for 0, 10 and 25 °C. It can be concluded that relative concentrations of zinc bromide complexes are not affected by the addition of 1 M quaternary ammonium bromide complexing agent.

Table 3.9: Ratio of relative concentration of zinc bromide complexes for anolyte and catholyte solutions of 3 M $ZnBr_2$ and 1 M QBr to 3 M $ZnBr_2$ as a function of temperature.

Temperature (°C)	[% of total complexed species, Anolyte at 0% SOC] / [% of total complexed species, 3 M $ZnBr_2$]			[% of total complexed species, Catholyte at 0% SOC] / [% of total complexed species, 3 M $ZnBr_2$]		
	$ZnBr_4^{2-}$	$ZnBr_3^-$	$ZnBr_2$	$ZnBr_4^{2-}$	$ZnBr_3^-$	$ZnBr_2$
25	1.0	1.1	0.8	1.0	1.0	1.1
10	1.0	1.0	0.9	0.9	1.1	1.0
0	1.0	1.0	0.9	0.9	1.0	1.0

The distribution of zinc bromide complexed species in aqueous zinc bromide solutions was found to be a function of both concentration of reacting species, and temperature. In conclusion, Raman spectroscopic analysis of $ZnBr_2$ solutions as a function of temperature indicated that the addition of complexing agent had no effect on species distribution. Further, decreasing the solution temperature shifted the species

distribution toward higher order complexes. Electrolytes at high state-of-charge tended to have more lower order species ($ZnBr_2$) than electrolytes at low state-of-charge.

The effect of quaternary ammonium bromide salt on zinc complexed and free bromine in aqueous zinc bromide electrolytes was also studied using Raman spectroscopy. Figure 3.6 shows the Raman spectra collected in 3 M $ZnBr_2$ and in 3 M $ZnBr_2$, 1 M QBr at 25 °C. This figure shows that the relative species distributions of the zinc bromine complexes are unchanged by the addition of quaternary ammonium complexing agent.

The spectra of pure liquid bromine, and bromine in water are shown in Figure 3.7. Figure 3.8 shows the Raman spectra of 3 M $ZnBr_2$ with excess bromine, and 3 M $ZnBr_2$, 1 M QBr, with excess bromine. The Raman spectrum of 3 M $ZnBr_2$ with excess bromine shows a single broad peak which includes contributions from $ZnBr_4^{2-}$, $ZnBr_3^-$, $ZnBr_2$, and Br_2(aq) species. Due to the broad undefined nature of this peak, it is not possible to determine relative concentrations of species. In the presence of QBr, the Br_2(aq) forms an insoluble black oil, $Q(Br)_nBr$. The spectrum shown in Figure 3.8 for solutions including QBr was obtained by limiting the laser power to 10 mW, and focusing the laser on the black oil. Clearly, the peak from bromine has shifted from 310 cm^{-1} for Br_2 in water, to 270 cm^{-1} for quaternary ammonium complexed bromine. A response for zinc complexed bromine between 170 and 205 cm^{-1} is absent from this spectrum as these species are aqueous, and are insoluble in the organic phase. Raman results indicated that the addition of quaternary ammonium salts affects the nature of the free bromine only.

3.4 Conclusions Based on Raman Spectroscopy

The complexed $ZnBr_4^{2-}$, $ZnBr_3^-$, and $ZnBr_2$ species were identified in Raman spectra as a function of temperature and state-of-charge of the battery. It was found that zinc species distribution shifted to higher order species ($ZnBr_4^{2-}$) as temperature decreased. Species distribution was also dependent on state-of-charge, but clear trends were not evident. It was found, however, that the addition of MEPBr to the electrolyte did not effect the distribution of zinc/bromine complexes. MEPBr acted only on the free bromine in solution.

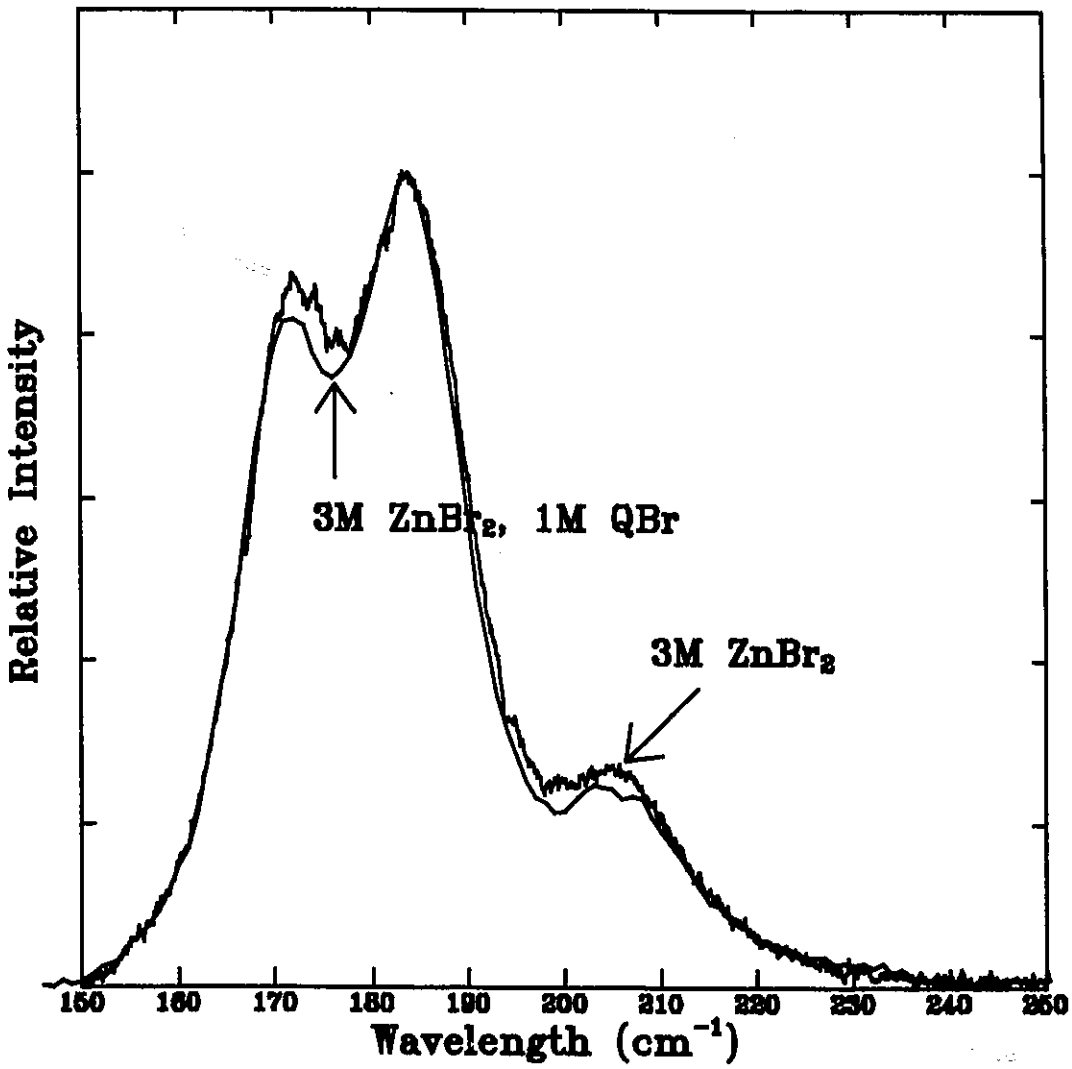

Figure 3.6: Raman spectra of 3 M aqueous zinc bromide and 3 M aqueous zinc bromide, 1 M QBr.

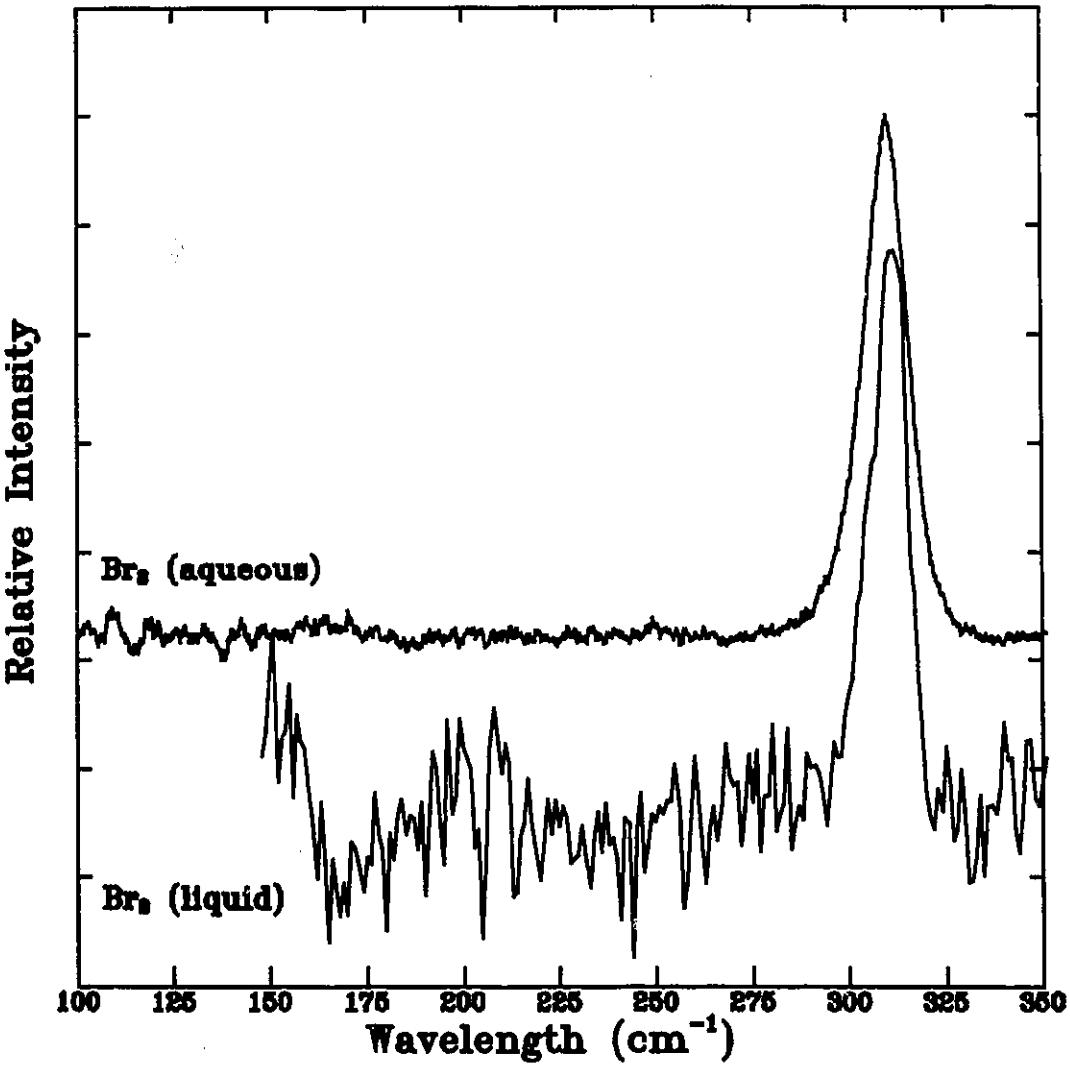

Figure 3.7: Raman spectra of liquid bromine and bromine in water.

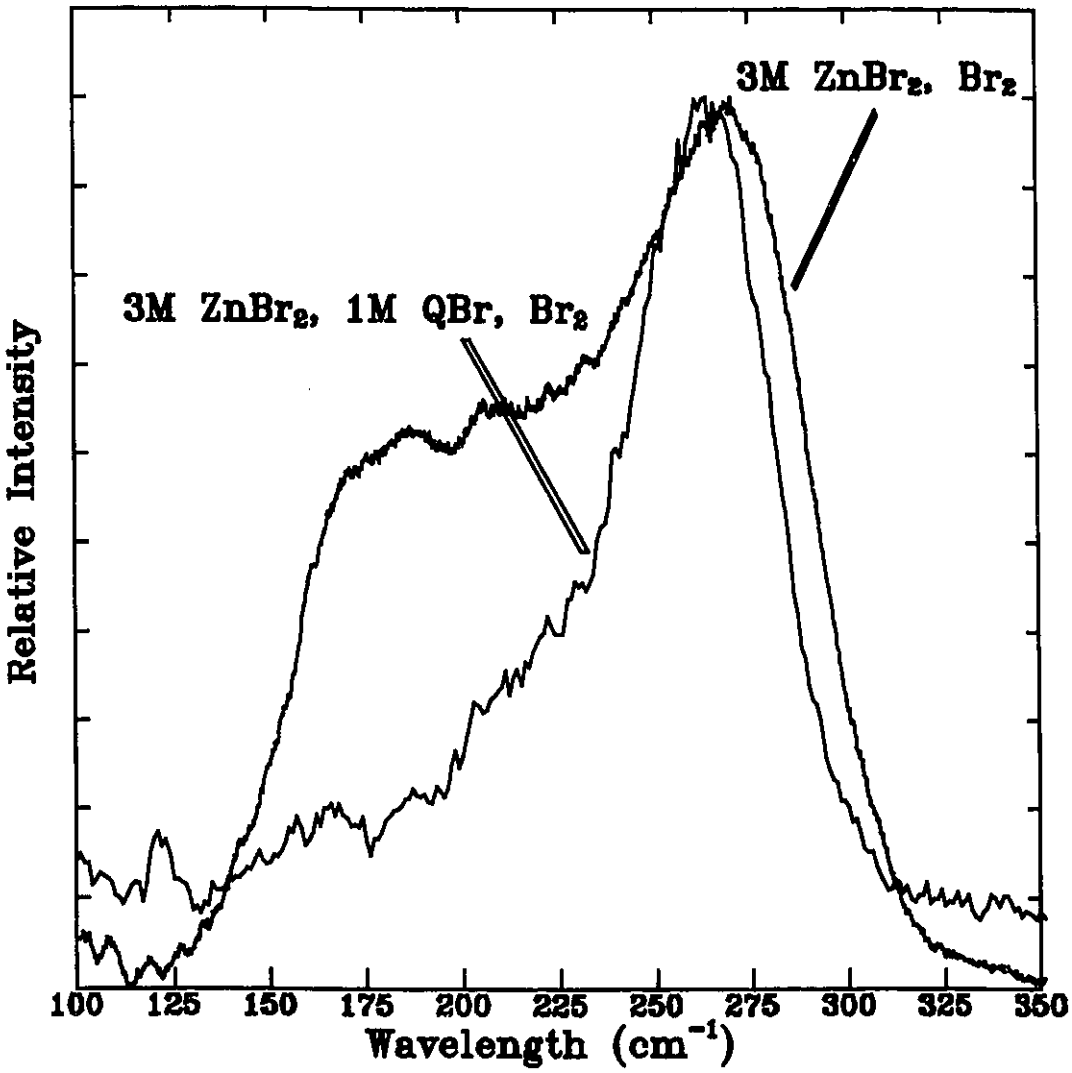

Figure 3.8: Raman spectra of 3 M $ZnBr_2$ with excess Br_2, and 3 M $ZnBr_2$, 1 M QBr and excess Br_2.

Chapter 4

Physical Properties of Zinc/Bromine Battery Electrolytes

In all batteries the electrolyte is an important component. A practical electrolyte must be ionically conductive, electronically insulating, stable with respect to other battery cell components and with changing temperature, safe to handle and of low cost. Ideally, the electrolyte should also have a low density (to maximize specific energy). As viscosity is integrally linked to electrolyte conductivity, it should be minimized so as to maximize electrolyte conductivity. Viscosity is very important in the zinc/bromine battery as it significantly affects the pumping demands for this flow battery. Since the pumps must draw power from the battery itself, it is important to minimize losses, and therefore, the electrolyte should have as low a viscosity as possible. Finally, because this is a flow battery, freezing of the electrolyte will cause the battery to stop functioning. As a result, the freezing temperature of the electrolyte is very important in determining the low temperature limit of operation. The viscosity, conductivity and freezing temperature of potential electrolytes for zinc/bromine batteries were evaluated, and their possible effects on battery operation are discussed in this chapter.

4.1 Experimental

4.1.1 Conductivity Measurements

Electrolyte conductivity was measured in a constant temperature bath between -25 and 25 °C (±1 °C). The bath included an insulated chamber containing ethylene glycol,

and a circulating bath containing a heating knife and an immersion cooler. Temperature was controlled using an OMEGA CN9000A thermocouple sensor temperature controller. Electrolyte conductivity was measured with a YSI Conductance-Resistance Meter, Model 34, and a YSI conductivity probe, Model 3403, Cell constant 1.0/cm. The conductivity probe was an immersion type, using platinized platinum black electrodes. Conductivity was measured as a function of temperature for several different electrolytes. Measurements were performed on electrolytes prepared volumetrically, as well as on electrolytes recovered from cycling zinc/bromine batteries. Each experiment (at each temperature and concentration) was repeated three times.

4.1.2 Freezing Temperature Determination

Cooling curves were obtained by placing approximately 7 ml of electrolyte into a vacuum jacketed glass vessel. A temperature well was located in the centre of the vessel and a type T thermocouple, coated with heat transfer paste, was inserted in the well. The space between the inner and outer walls of the vessel was evacuated, and the vessel was then placed in an insulated dewar containing a small volume of liquid nitrogen. The bath temperature was measured at the external wall of the vessel adjacent to the sample. Room, bath and sample temperatures were monitored using a Fluke Hydra Data Logger, Model 2625A, Hydra Starter Software and an IBM compatible computer.

4.1.3 Solution Preparation

Solution preparation was described previously in section 3.2.2.

4.2 Discussion of Physical Properties

The temperature range within which battery electrolytes remained liquid was determined, and is presented in Tables 4.1 and 4.2 below, for standard battery electrolytes and electrolytes with high concentrations of organic additives. Figure 4.1 shows freezing point depression plotted as a function of solute concentration in solutions of water and

Table 4.1: Freezing temperatures for various aqueous zinc/bromide electrolytes

Electrolyte	Freezing Temperature Range (°C) (±2 °C)
3 M $ZnBr_2$	0
2.25 M $ZnBr_2$, 0.5 M $ZnCl_2$, 0.8 M MEPBr	-10
2.25 M $ZnBr_2$, 0.5 M $ZnCl_2$, 0.8 M MEPBr, Catholyte 0% State of Charge	-10 to -15
2.25 M $ZnBr_2$, 0.5 M $ZnCl_2$, 0.8 M MEPBr, Anolyte 0% State of Charge	-10
2.25 M $ZnBr_2$, 0.5 M $ZnCl_2$, 0.8 M MEPBr, Catholyte 100 % State of Charge	-10
2.25 M $ZnBr_2$, 0.5 M $ZnCl_2$, 0.8 M MEPBr, Anolyte 100% State of Charge	-5

Table 4.2: Freezing temperatures for various aqueous and mixed aqueous/organic zinc/bromide electrolytes

Electrolyte	Freezing Temperature (°C) (±2 °C)	Freezing point depression (± °C)
2.25 M $ZnBr_2$, 0.5 M $ZnCl_2$, 0.8 M MEPBr	-10	-
2.25 M $ZnBr_2$, 0.5 M $ZnCl_2$, 0.8 M MEPBr, 25 % propan-2-ol(3.3 M)	-20	10
2.25 M $ZnBr_2$, 0.5 M $ZnCl_2$, 0.8 M MEPBr, 25 % ethylene dichloride (3.1 M)	-10	-
2.25 M $ZnBr_2$, 0.5 M $ZnCl_2$, 0.8 M MEPBr, 50 % propylene glycol (6.8 M)	-15	5
2.25 M $ZnBr_2$, 0.5 M $ZnCl_2$, 0.8 M MEPBr, 25 % ethylene glycol (4.5 M)	-15, slushy	>5
2.25 M $ZnBr_2$, 0.5 M $ZnCl_2$, 0.8 M MEPBr, 50 % ethylene glycol (8.9 M)	>-15	>5

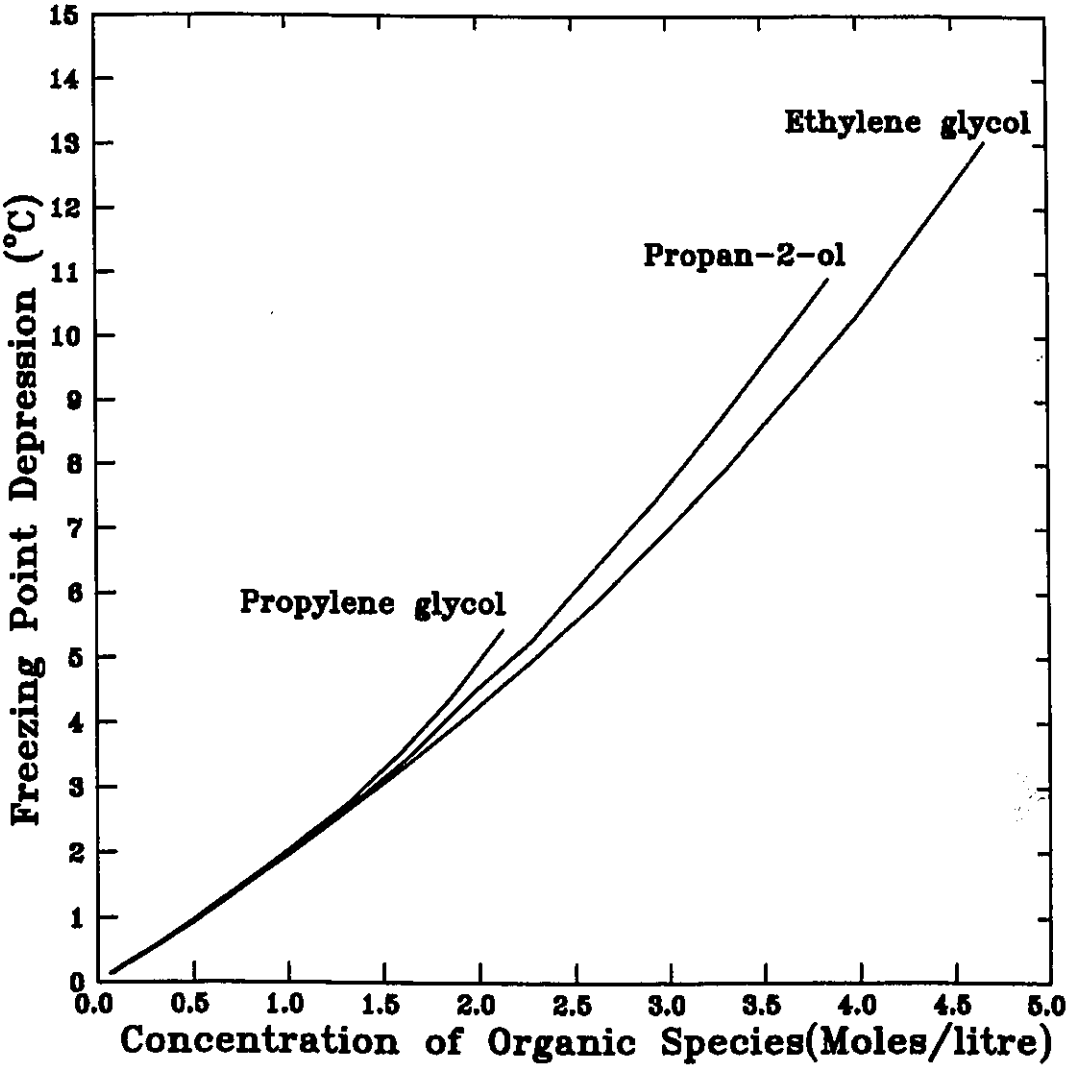

Figure 4.1: Freezing point depression of water/alcohol and water/diol solutions at 25 °C, data from CRC, (1985d).

propylene glycol, ethylene glycol, or propan-2-ol(CRC, 1985d).

A concentration of 25 % by volume of organic corresponds to a molarity of 3 to 5 M. In this concentration range, solutions of water and propan-2-ol, ethylene glycol or propylene glycol freeze in the same temperature range. Mixed aqueous/organic and mixed aqueous $ZnBr_2$/organic solutions experienced a freezing point depression of the same order of magnitude (compare results in Table 4.2 and Figure 4.1). Therefore, any of these electrolytes, at high concentration of organic, would have significantly reduced freezing points.

Relative viscosity of propan-2-ol, ethylene glycol, and propylene glycol/water solutions at 25 °C, are plotted in Figure 4.2 based on data from CRC (1985d). An optimal electrolyte will have a low relative viscosity to reduce pumping energy and power requirements. Over the concentration range of 3 to 9 M, solutions of ethylene glycol and water exhibited the lowest relative viscosity, and those of propylene glycol and water, the highest relative viscosity. Based on these data, solutions of ethylene glycol would have the lowest pumping losses and be the preferred choice.

The specific gravity of aqueous solutions of propan-2-ol, ethylene glycol or propylene glycol are plotted in Figure 4.3. As the organic materials are added to depress the freezing point, and are not considered to be "active", it is desirable to minimize the specific gravity of the solutions, thus maximizing the specific energy of the battery. Electrolytes containing significant concentrations of propan-2-ol have considerably lower specific gravity than those containing ethylene glycol or propylene glycol. If battery weight is of key importance, then these data indicate that solutions of propan-2-ol are preferred.

It was not possible to look at the effect of ethylene dichloride concentration on solution relative viscosity, specific gravity and freezing point depression as ethylene dichloride is insoluble in aqueous zinc bromide electrolyte.

Electrolyte conductivity was determined experimentally for two different series of electrolytes. The first were electrolytes extracted from cycling $ZnBr_2$ batteries as a function of state - of - charge. The experimental conductivities obtained are plotted in Figures 4.4 and 4.5 for anolyte and aqueous phase catholyte electrolytes respectively.

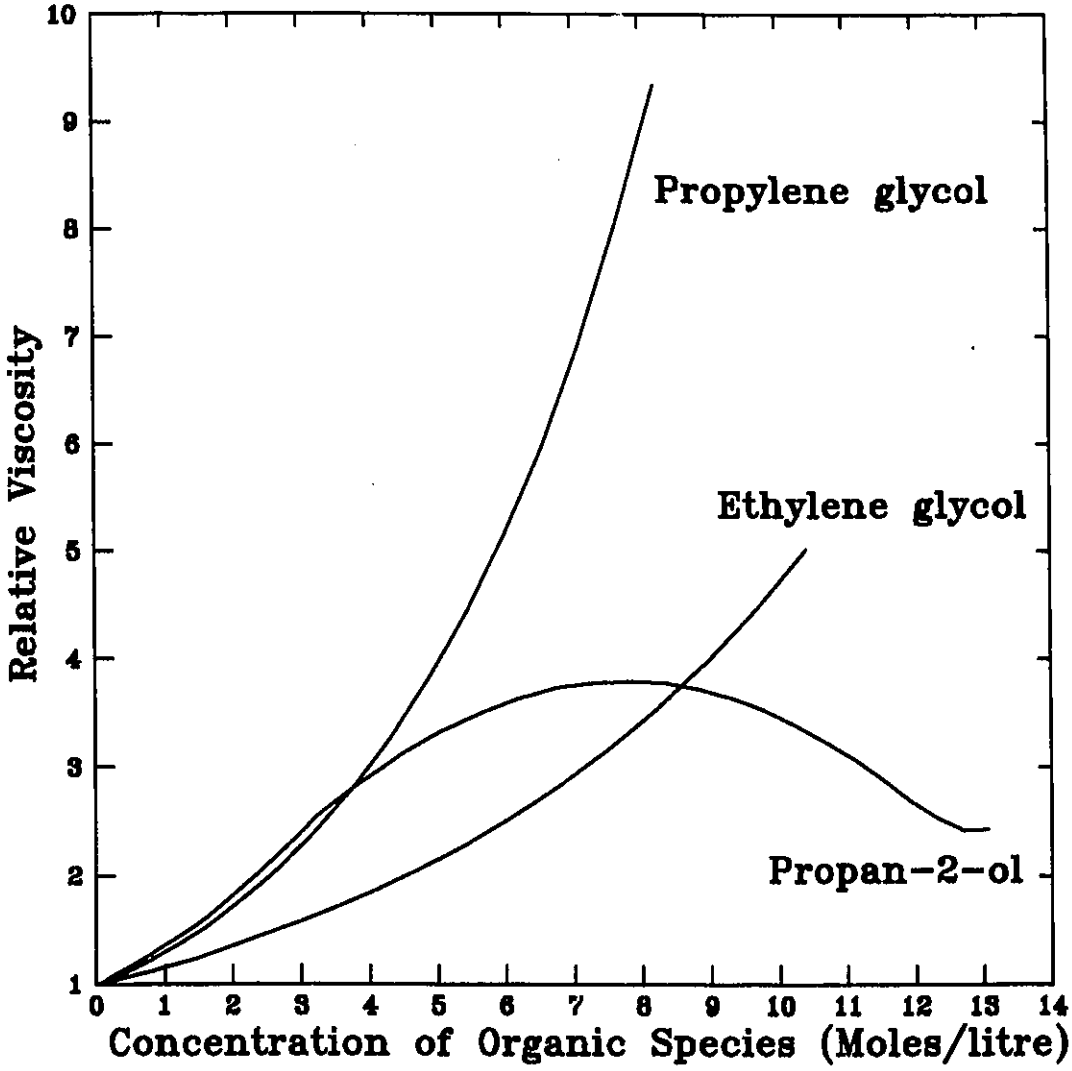

Figure 4.2: Relative viscosity of aqueous solutions of alcohol or diol, as a function of alcohol or diol concentration at 25 °C, data from CRC, (1985d).

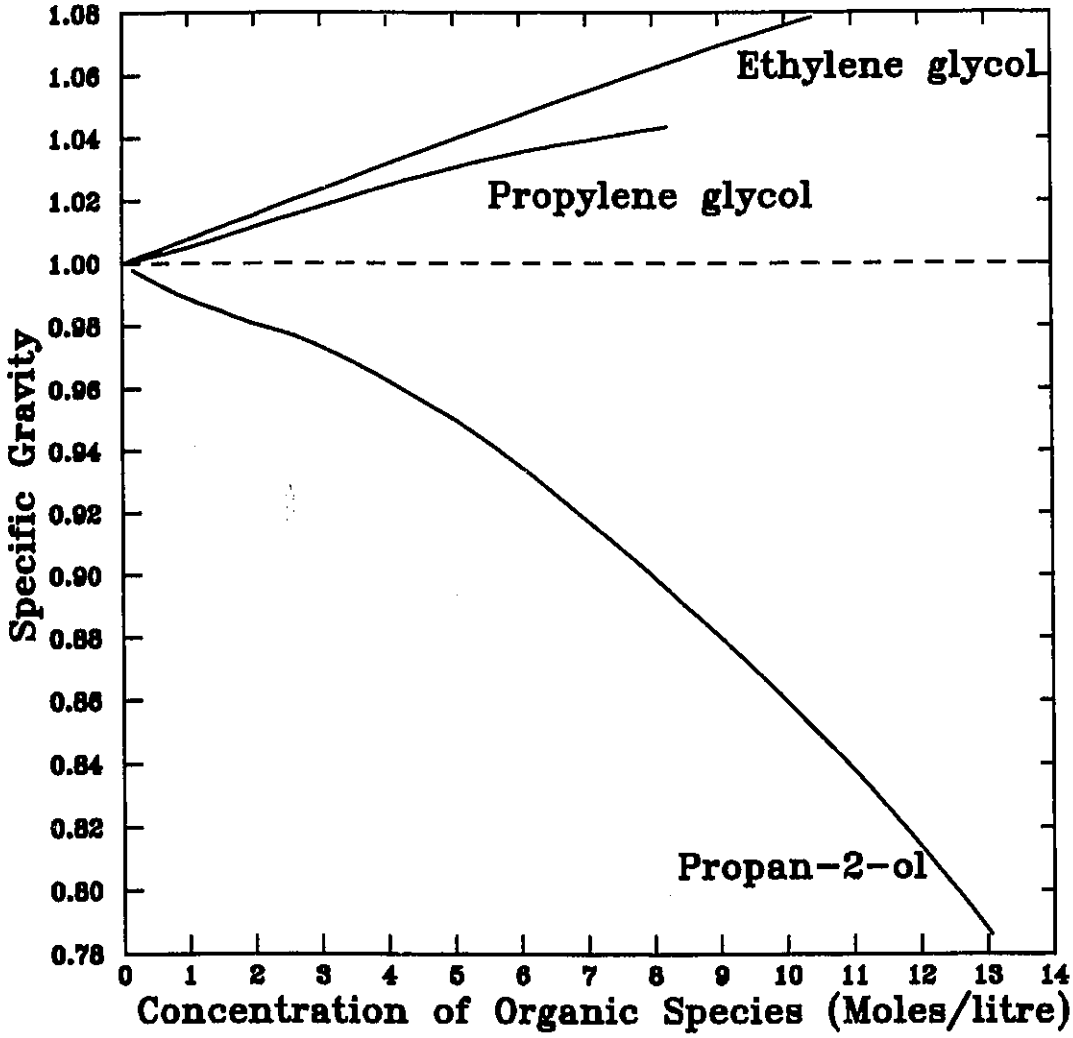

Figure 4.3: Specific gravity plotted as a function of alcohol or diol concentration at 25 °C, data from CRC (1985d).

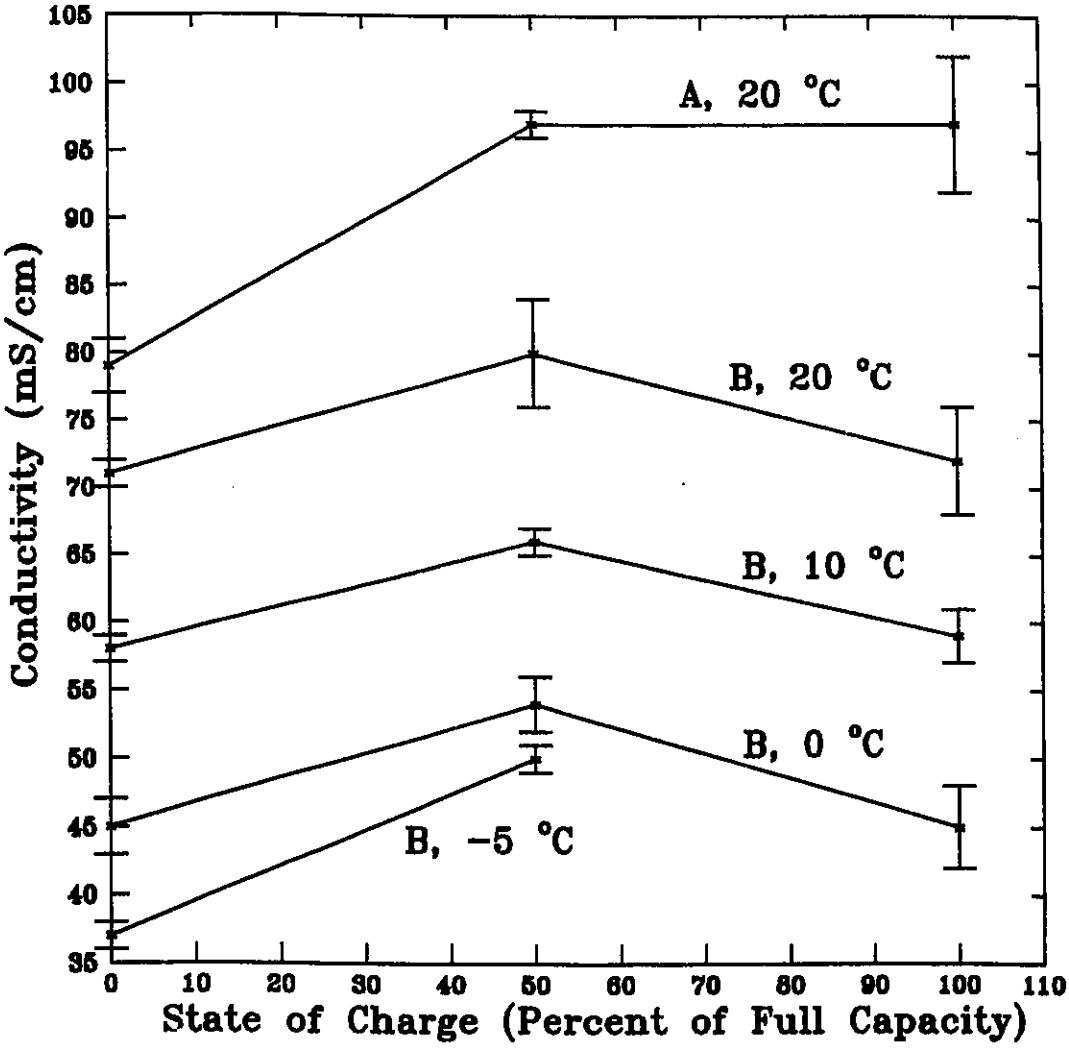

Figure 4.4: Anolyte conductivity as a function of SOC for samples recovered from cycling $ZnBr_2$ batteries, A) 2.25 M $ZnBr_2$, 0.5 M $ZnCl_2$, 1.0M MEPBr; B) 3 M $ZnBr_2$, 0.25 M MEMBr, 0.75 M MEPBr.

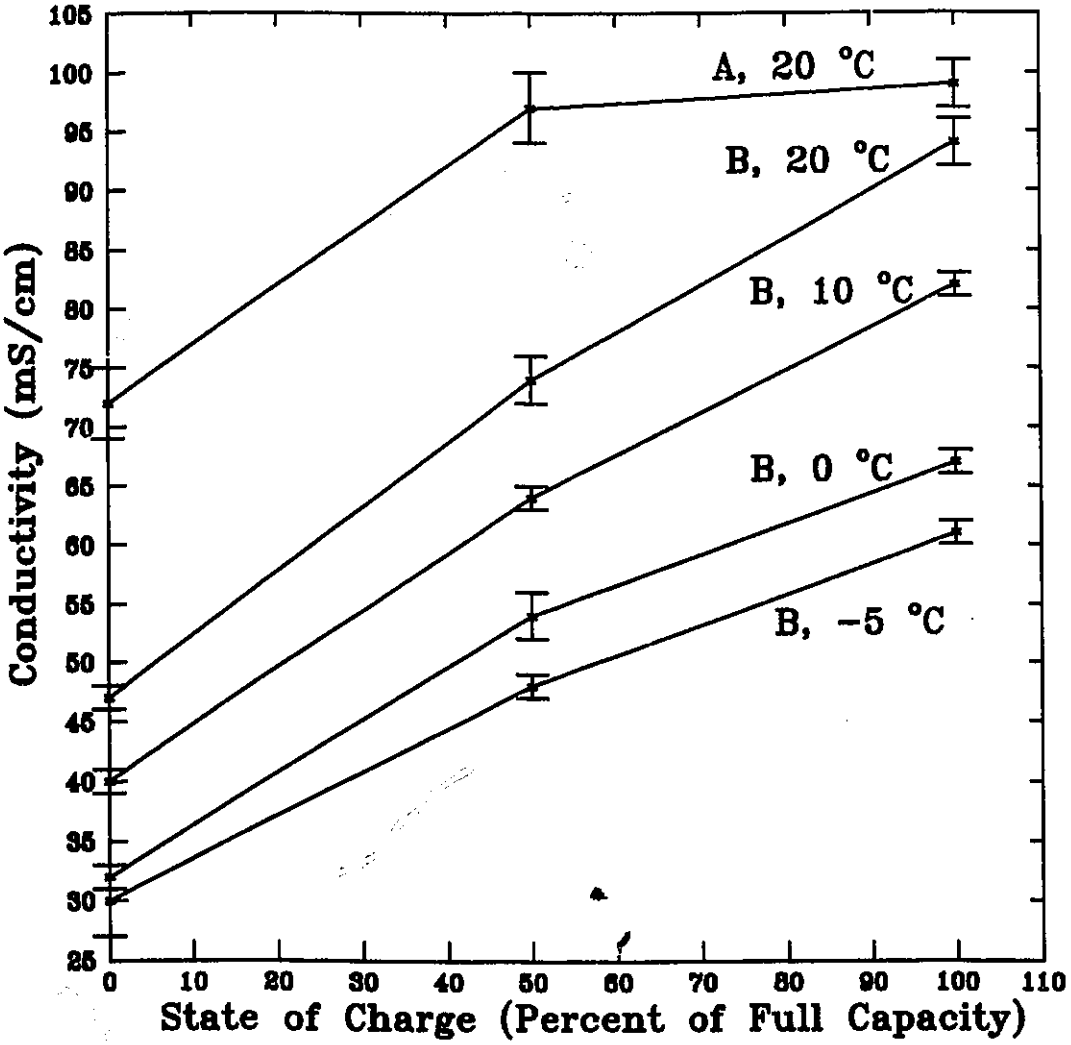

Figure 4.5: Catholyte conductivity as a function of SOC for samples recovered from cycling $ZnBr_2$ batteries, A) 2.25 M $ZnBr_2$, 0.5 M $ZnCl_2$, 1.0M MEPBr; B) 3 M $ZnBr_2$, 0.25 M MEMBr, 0.75 M MEPBr.

Electrolyte conductivity is a complex function of the concentration and mobility of ions in solution. In the anolyte solution, conductivity initially increased as the state-of-charge increased, and then levelled off or decreased slightly. In the uncharged state, SOC 0%, the concentration of ions (Zn^{2+}, Br^-) was highest, but due to the high viscosity of the electrolyte the mobility of these ions was restricted. As the battery charged, the concentration of Zn^{2+} ions decreased as metallic zinc plated at the anode, and the concentration of free Br^- decreased as Br_2 formed at the cathode. Initially, the decrease in ionic concentration was compensated by the increased mobility of ions in solutions. Above 50 % SOC, the increasing mobility of ions was insufficient to counteract the decreasing ionic concentration, and the conductivity stabilized. The distribution of ionic species was further complicated by the presence of complex species such as $ZnBr^+$, $ZnBr_2$, $ZnBr_3^-$, $ZnBr_4^{2-}$ in aqueous solution and by the presence of quaternary ammonium complexing agent. As the battery charged, the species distribution in the anolyte shifted to lower order zinc/bromine species ($ZnBr_2$ and $ZnBr_3^-$ from $ZnBr_4^{2-}$). The lower order species are believed to have lower ionic diffusivity(Hsie and Selman, 1985). Therefore, the ionic mobility was decreased due to the increased number of lower order species.

Conductivity of the aqueous phase of catholyte solutions increased as a function of state-of-charge. As the battery charged, bromide ions were oxidized to bromine which complexed with the quaternary ammonium salts and settled to the bottom of the catholyte reservoir as a more viscous second phase. Thus, as the battery charged, the concentration of Zn^{2+}, Br^-, and QBr in the aqueous catholyte phase decreased. Furthermore, zinc bromide species distribution was found to shift from lower order to higher order species (Chapter 3). As a result, the ionic diffusivity and mobility increased as state-of-charge increased.

Conductivity of all electrolytes decreased with decreasing temperature. Increased solution resistance with temperature should result in low voltaic and energy efficiencies in batteries operated at reduced temperatures. Low temperature experimental studies of a zinc/bromine battery used for energy storage in a photovoltaic system resulted in low voltaic and energy efficiencies as predicted (Cournoyer, 1992; Pell et al., 1992).

The conductivity of alternate electrolytes for low temperature operation of a

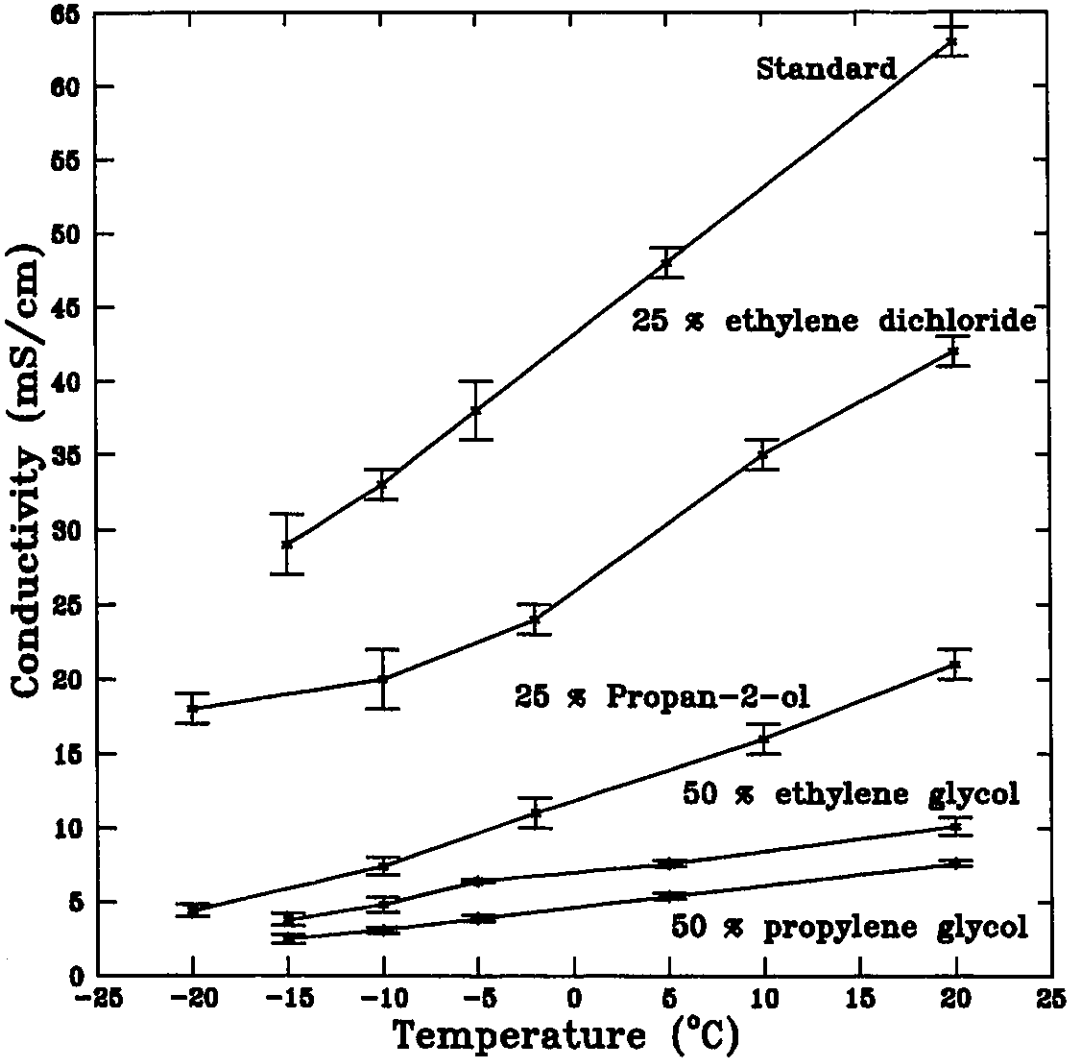

Figure 4.6: Electrolyte conductivity as a function of temperature for several different electrolytes (see Table 4.2).

zinc/bromine battery was also evaluated, and the results of this study are presented in Figure 4.6. In all cases, electrolyte conductivity decreased with decreasing temperature, due to increased solution viscosity (and reduced mobility of ions). Addition of organic to the aqueous electrolyte decreased the solution's conductivity, and would likely result in decreased voltaic and energy efficiencies in a battery. The electrolyte containing 25 % by volume of ethylene dichloride showed the smallest decrease in conductivity. This is because conductivity was determined in the aqueous phase, and ethylene dichloride is insoluble in water. At all temperatures considered, the 50 % (8.9 M) ethylene glycol/$ZnBr_2$ solution had higher conductivity than the 50 % (6.8 M) propylene glycol/$ZnBr_2$ solution. For applications where power capabilities are important, electrolyte conductivity should be high, and ethylene glycol/water electrolytes would, therefore, be better than propylene/glycol electrolytes for use in a zinc/bromine battery. The 25 % by volume solution of propan-2-ol had conductivity twice that of the glycols. As a result of the conductivity study, electrolytes containing propan-2-ol and ethylene glycol were evaluated as potential candidates for low temperature electrolytes.

4.3 Conclusions Based on Physical Properties of Zinc/Bromine Battery Electrolytes

Based on the experimental data, and information from the literature, several conclusions can be drawn. Ethylene dichloride did not reduce the freezing temperature of the aqueous phase of the electrolyte. Propan-2-ol had the lowest density of any of the electrolytes considered, and therefore, should add the least amount of inactive weight to the electrolyte. Ethylene glycol, had the lowest viscosity, and therefore, would have the lowest pumping losses. Conductivity was reduced in all electrolytes containing organics, but was least affected in ethylene dichloride electrolyte. Conductivity in propylene glycol was lower than in ethylene glycol, indicating that batteries employing propylene glycol electrolytes would have lower voltaic and energy efficiencies. Ethylene glycol, propan-2-ol and ethylene dichloride electrolytes will be subject to further study in the next chapter as it appears possible to design a flowing electrolyte system for low temperature applications employing these additives.

Ethylene dichloride was included in further studies even though it is insoluble in aqueous solutions. It is however, soluble in the organic bromine phase that forms during charging; and can significantly reduce the viscosity of this phase at low temperatures (Eidler, 1992). During discharge, approximately 30 % by volume of the circulating electrolyte is comprised of the organic phase (Eidler, 1992). As this viscous phase contributes significantly to pump requirements (i.e., parasitic power drains on the battery), a reduction in the organic solution viscosity can improve the low temperature performance of the battery.

Chapter 5

Electrochemical Investigation of Zinc Deposition and Bromide Oxidation in Aqueous and Mixed Aqueous/Organic Zinc Bromide Electrolytes

5.1 Theory

5.1.1 Introduction to Cyclic Voltammetry (Pletcher, 1991; Southampton Electrochemistry Group, 1990a)

In the preliminary investigation of new electrochemical systems, cyclic voltammetry is very useful. An electrochemical spectrum (current versus potential) can be readily obtained indicating the potentials at which electrochemical processes occur at the working electrode. From the dependence of peak amplitude on potential scan rate, the involvement of coupled homogeneous reactions, adsorption and diffusion are readily identified. The difference between the first and subsequent cyclic voltammograms provides useful mechanistic information. Many experiments can be performed in a short time, and the data are presented in a manner which allows for rapid qualitative interpretation without detailed calculation. Kinetic parameters can be determined from quantitative analysis of the first potential scan of cyclic voltammograms for specific reaction schemes.

The potential time waveform used in cyclic voltammetry is shown in Figure 5.1.

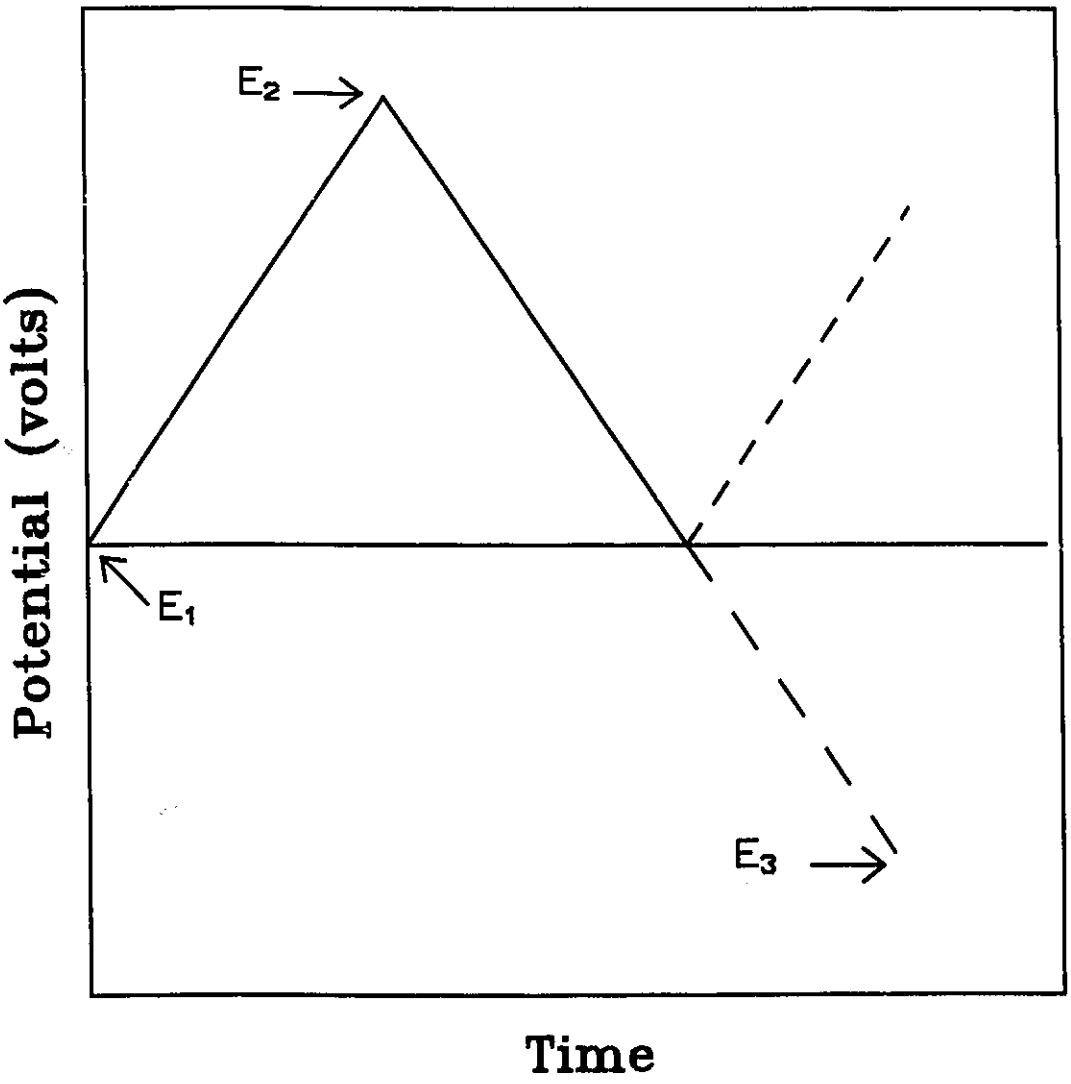

Figure 5.1: The potential time waveform used in cyclic voltammetry experiments.

The current (I) response to this changing potential is recorded and displayed as a function of potential (E). Briefiy, the working electrode potential is swept through a potential range where a reaction occurs (E_1 to E_2), the direction of the scan is then reversed (at E_2) in order to determine if the products of electron transfer are stable, and if reaction intermediates and final products are electroactive. Once the potential reaches the initial potential (E_1) there are several options. The scan can be halted, again reversed, or can continue to a further value. Potential scan rates for conventional experiments range from a few mVs^{-1} to a few hundred Vs^{-1}.

The simplest reaction scheme to consider is the reversible reduction of species O, where O is the only electroactive species initially present in the solution. The reaction being studied is:

$$O + ne^- \rightarrow R \tag{5.1}$$

If a slow linear potential is applied to such a system, the voltammogram will appear as a steady state I vs E curve. Under steady state conditions, concentrations above a certain distance from the electrode are maintained uniform by natural convection. In the region near the electrode, (Nernst diffusion layer) the concentration profile is nearly linear. At the electrode surface the ratio of the concentration of the oxidized and reduced species, c_O/c_R is given by the Nernst equation.

$$E_e = E_e^\theta + \frac{RT}{nF}\ln\frac{c_O}{c_R} \tag{5.2}$$

where the equilibrium (reversible) potential, E_e, is related to the standard potential of the couple O/R, E_e^θ, and the surface concentrations of O and R, c_O and c_R. The activity coefficients of O and R are assumed unity so that concentrations are used in the Nernst equation.

As the potential is made more negative, the concentration of O at the electrode surface must decrease. As a result, the concentration gradient increases, and the current also increases. Eventually the surface concentration of reactant O approaches zero, the steady state concentration profile results, and the reaction is diffusion controlled. Subsequent

reduction in the applied voltage results in a current plateau.

At higher potential scan rates, the diffusion layer does not have sufficient time to relax to its equilibrium state, and the concentration profile is not linear. As soon as a potential is reached where reduction of O can occur, the concentration of species O decreases to satisfy the Nernst equation, and a concentration gradient is established. Current proportional to the concentration gradient flows through the external circuit. The gradient, once established, begins to relax, owing to diffusion of species O from the bulk. At the same time the electrode potential is still changing, initially growing larger, and the surface concentration continues to decrease, until it effectively reaches zero. In this case, the concentration gradient is always greater than for the steady state case as the diffusion layer is thinner, and therefore, the current corresponding to these conditions will be larger than the steady state current. Once the surface concentration reaches zero, the concentration gradient begins to decrease due to relaxation effects. At this time the current also begins to decrease. This overall behaviour results in a peak shaped current - potential response.

The current response corresponding to a reversal in potential at steady state (slow potential scan rate) should directly track the forward response. When the scan direction is reversed at higher potential scan rates, there is a considerable amount of R present at the electrode surface. R continues to form until the potential reaches E_e^θ. Once the potential approaches E_e^θ, R begins to be re-oxidized to O, and a reverse current flows. The surface concentration of R eventually reaches zero, and a concentration gradient as described above develops. Using a similar argument as above, a peaked response develops. Generally, the charge associated with the reverse process will be lower than that of the forward process. During most of the experiment the concentration gradient is driving R away from the electrode; therefore some of the product R diffuses away from the electrode and cannot be re-oxidized on the timescale of the cyclic voltammogram.

In the above case, electron transfer rates at all potentials are much greater than the rate of mass transport. When the rate of mass transfer is similar to the rate of electron transfer (i.e., a slow electron transfer reaction), the surface concentration will not be at equilibrium, and the Nernst equation will not be satisfied. Slow electron reactions are

driven by the application of an overpotential. As the potential scan rate increases, the rate of mass transfer becomes comparable to the rate of electron transfer and the separation between anodic and cathodic peaks increases. The shape of the peaks also becomes broader as overpotential increases with current density. The irreversible peak current density is lower than that for the reversible case under the same conditions due to the shape of the current vs voltage curve. The peak for an irreversible reaction is broader than for a reversible reaction, as the surface concentration of O changes more slowly with potential, and once the surface concentration of O reaches zero, the concentration profile is less steep and the flux to the surface lower than for the reversible case. Absence of a reverse peak is the most remarkable difference. This characteristic could also be due to the occurrence of a fast chemical reaction following the reduction process.

It is also quite possible for a processes to be reversible at low potential scan rates and irreversible at higher rates. The intermediate state is referred to as quasi-reversible. A quasi-reversible system will have a reverse peak, and will have peak current density, I_p, increasing with the square root of the potential scan rate but not dependent on it.

Cyclic voltammetry can be used to study surface processes, i.e., when product and reactant are not suspended in electrolyte. The simplest case to consider is adsorption where only the adsorbed species of O and R are electroactive in the potential range being considered. The analysis of such a system is straight forward as mass transfer effects can be ignored as the reacting species is adsorbed on the electrode. For a reversible reaction, the resulting CV is characterized by two symmetric peaks, with current rising from zero to a maximum and falling to zero again. There is essentially little or no peak separation, and the charges associated with the cathodic and anodic processes are equal. The symmetry results as the fixed amount of reactant (O adsorbed on the surface) can be reduced. The values of I_p, E_p (the potential at which I_p occurs), and the shape of the peak are dependent on the nature of the adsorption isotherm. If adsorption can be described via a Langmuir isotherm, it can be shown that peak current is proportional to the potential scan rate, and not to the square root of the potential scan rate.

For the irreversible reduction of adsorbed O, the shape of the forward peak is no longer symmetric, and the reverse peak is absent. For a quasi-reversible system, there will

be a reverse peak, but neither peak will be symmetric, and the peak potentials will not be coincident.

The more general case occurs when both the adsorbed and solution species are electroactive. For strongly adsorbed species, two anodic and two cathodic peaks are realized for a reversible system. Symmetrically shaped peaks correspond to the adsorbed species, and conventionally shaped peaks to the solution species. A strongly adsorbed reactant is stabilized at the surface with respect to the electrode reaction, and results in reduction at a higher potential. A strongly adsorbed product favours the reaction, and results in a peak at a potential lower than the solution peak. The maximum current associated with the solution peaks is found to increase with the square root of the potential scan rate, and the maximum current associated with the adsorbed species increases with potential scan rate. Further, these peaks exhibit different dependence on concentration, the solution peak maximum increases linearly with concentration, while the adsorbed species peak maximum increases with concentration (not necessarily linearly) until it reaches a limiting value associated with complete coverage. The separation between the adsorption and solution peaks indicates the relative strength of the adsorption, increasing with increasing peak separation. For very weakly adsorbed species, two separate peaks are generally not found, although the CV will be distorted. For a weakly adsorbed reactant, the maximum forward peak current will be higher than for a simple reversible system, and the reverse peak will be slightly enhanced. For weak product adsorption, the forward peak will be slightly higher, and the reverse peak will be considerably higher than for the simple reversible case. The forward peak is also shifted to more positive potential. In the event that the adsorption reaction is followed by a chemical reaction, the oxidation peak is smaller than the reduction peak, and the peak potential of the reductant peak is smaller than the reduction in the absence of adsorption.

The cyclic voltammogram characteristic of metal deposition onto a foreign substrate is readily recognizable. The forward (deposition) peak is similar to that for a process involving only solution soluble species. It is identifiable by a very steep leading edge. The reverse scan is very different from that for a solution soluble species. There is a potential range over which the cathodic current density of the reverse scan is higher

than on the forward scan. The current trace crosses over the forward scan, and the reverse peak is sharp and symmetrical. The unusual cathodic peak results from nucleation of the metal phase, M, on the electrode surface. A prerequisite for growth of the metal species on the foreign electrode is the formation of thermodynamically stable nuclei on the surface. The formation of these nuclei requires a potential more negative than that to reduce the metal cations, and leads to nucleation overpotential. Thus, on the forward scan a potential significantly more negative than the equilibrium potential for the M/M^{n+} couple in the test solution is required before deposition commences. On the reverse scan, the deposition is occurring at the metal surface and continues while the reaction, $ne^- + M^{n+} \rightarrow M$, is thermodynamically and kinetically favourable, until the equilibrium potential is reached. The second cross-over on the cyclic voltammogram corresponds to the equilibrium potential, and the difference between this potential, and the potential at which deposition began on the forward scan is the nucleation overpotential. Generally nucleation overpotential will be greater on the first scan than on subsequent cycles.

The symmetric reverse peak is explained since the reacting material is deposited on the electrode, and therefore, does not need to diffuse there in order to react. It is thus symmetrical, and very like that for an adsorbed species. The peak current density can be high as the metal is on the surface and diffusion will not limit the supply of reactants. The area under this reverse peak, often called the stripping peak, corresponds to the amount of metal deposited on the electrode at cathodic potentials. If the reactions, $ne^- + M^{n+} \rightleftharpoons M$, are the only electrode processes occurring, the anodic charge and the total cathodic charge (area under both the forward and reverse scans at cathodic potential) must be equal as all the metal deposited onto the electrode surface will be redissolved in the anodic process. For a rapid M^{n+}/M couple, the response on the reverse scan will pass directly through the zero current axis; this crossover point occurs close to E_e.

5.1.2 Chronoamperometry (Southampton Electrochemistry Group, 1990b)

The most powerful technique to study the early stage of metal deposition is step potential chronoamperometry. In chronoamperometry, the current-time response of an

instantaneous change in potential at the working electrode is recorded to study reaction kinetics. The initial potential E_1 is selected, such that no reaction occurs at the working electrode. Then, at time t=0, the potential is very rapidly changed to a new value, E_2, where reduction or oxidation occurs. The potential-time profile for a single potential step chronoamperometric experiment is shown if Figure 5.2.

For a general case, current response will be given by one of the curves shown in Figure 5.3. If the rate of the reaction is slow, or E_2 corresponds to a low over-potential, a current-time transient known as kinetic control results (see curve 'a', Figure 5.3). This is because the surface concentration of the reactant does not change significantly due to the imposition of the pulse, and diffusion is not significant. The measurement is steady state. If the reaction is diffusion controlled, Fick's Second Law can be solved with appropriate boundary conditions. The Cottrell equation, for the oxidation of species O, results for a planar electrode, and is given below:

$$|I| = \frac{nFD^{1/2}c_o^{\infty}}{\pi^{1/2}t^{1/2}} \tag{5.3}$$

where n is the number of electrons involved in the electron transfer, F is the Faraday constant, D is the coefficient of diffusivity of species O, C_o^{∞} is the bulk concentration of species O and t is the time.

Thus for a diffusion controlled reaction occurring at a planar electrode, the current density falls as $t^{-1/2}$ as shown in curve c) of Figure 5.3. For an intermediate situation, where the rates of diffusion and electron transfer are comparable, the I vs t transient has the form of curve b); the current density falls with time but less steeply than for the diffusion controlled case. Under these conditions the system exhibits mixed control.

The growth of crystals on electrodes can occur in a number of different situations including 1) the new phase forms on the surface of an inert electrode by electrodeposition from species in solution, 2) the new phase forms on the surface of an electrode of the same material as the depositing species by electrodeposition from species in solution, 3) the new phase can form from electro-dissolution of the electrode, followed by subsequent precipitation from reaction in solution, or the ions can pass from the electrode

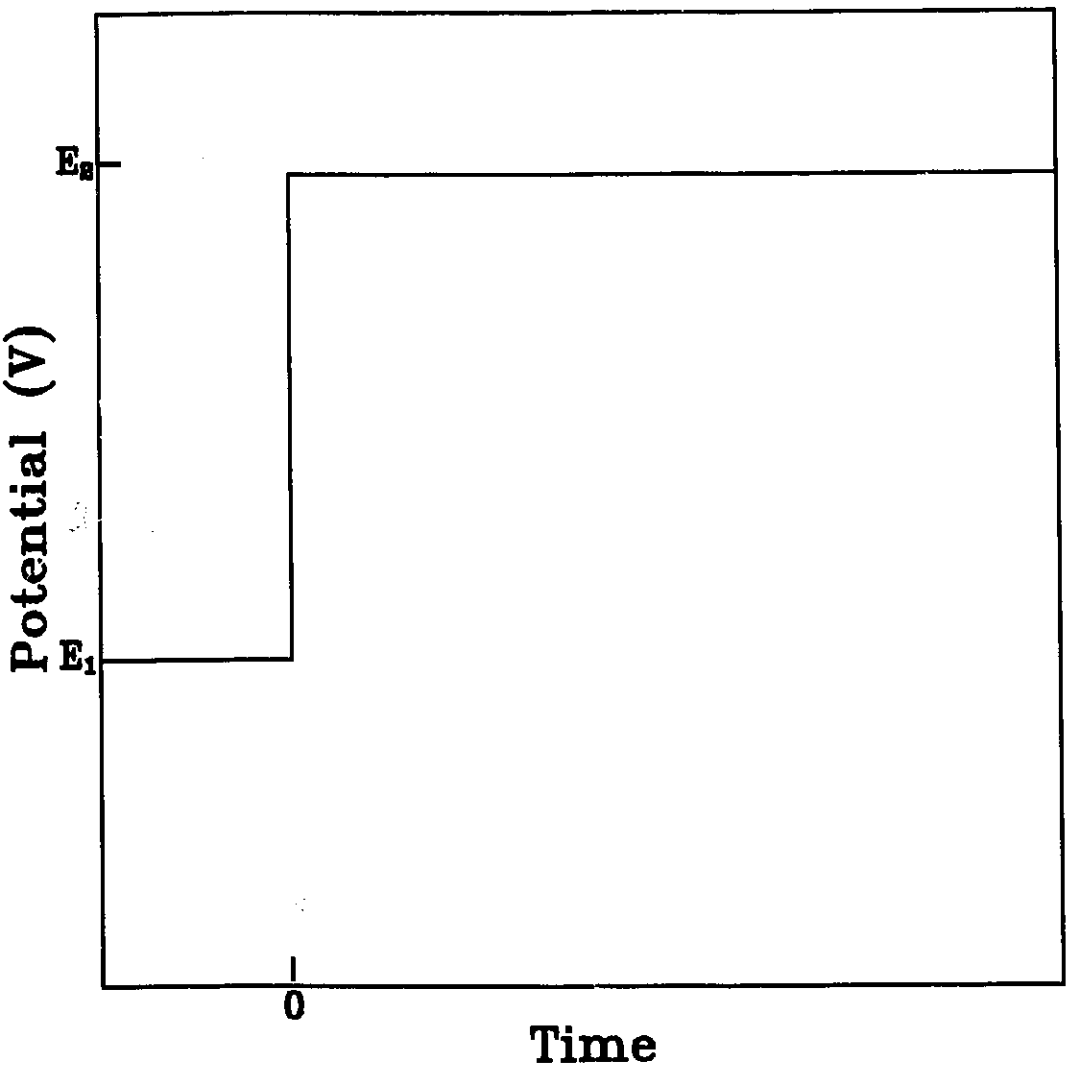

Figure 5.2: Form of the potential - time profile for a chronoamperometric experiment.

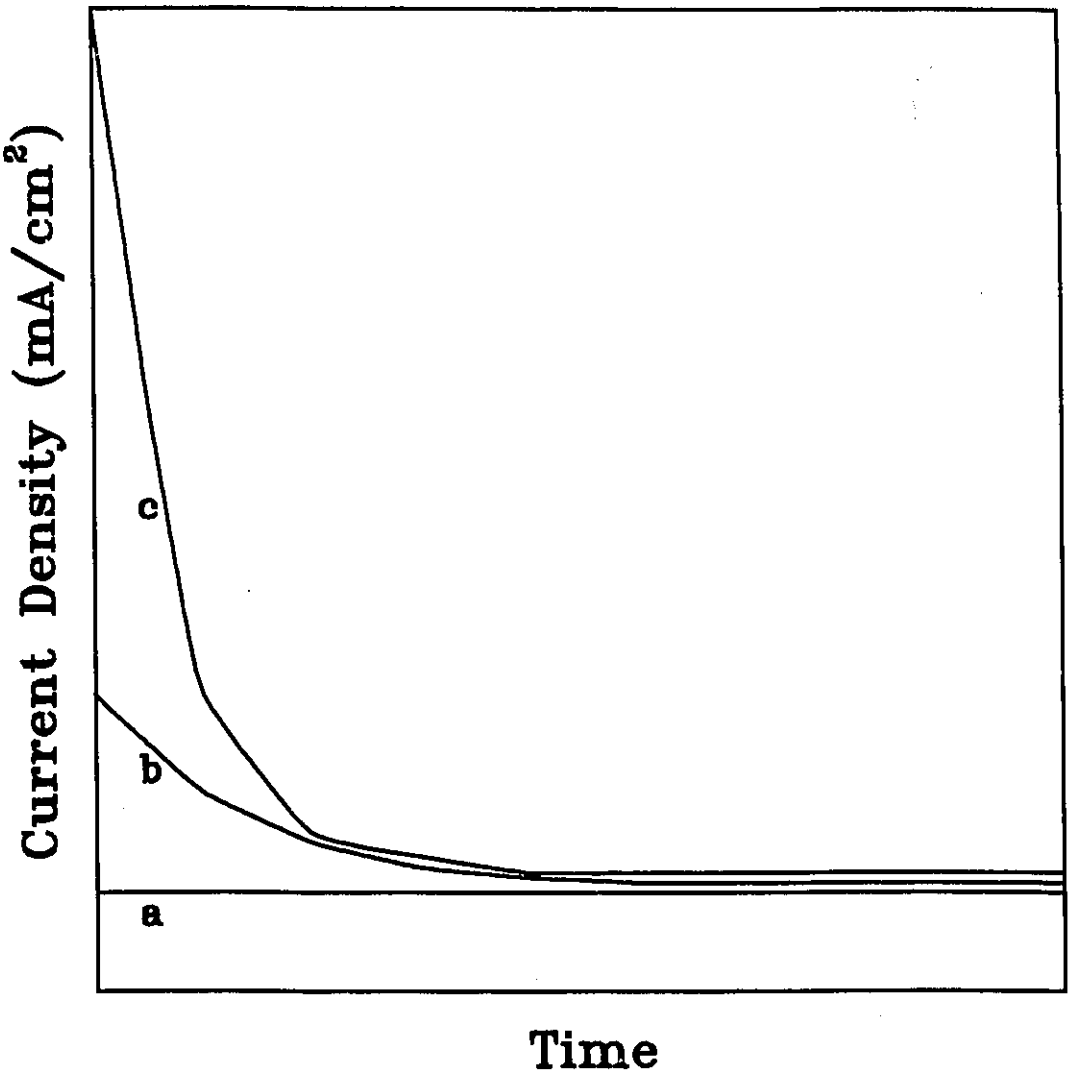

Figure 5.3: Form of chronoamperometric experiments: current density as a function of time. Curve a) describes a reaction under kinetic control, b) mixed control and c) diffusion control.

surface, through the deposit on the substrate electrode to the solution surface. This paper will generally discuss the mechanisms associated with the first of these applications, as they relate to zinc deposition on glassy carbon.

5.1.2.1 Rate Determining Step in Nucleation and Growth: Lattice Incorporation

The current response is observed from a potential where no reduction occurs to one where nucleation of the metal phase can occur. On the instant the potential is changed, there are no nuclei on the electrode surface and the deposition current is zero. The current will initially increase because the number of nuclei increases (progressive nucleation), the surface area of each nucleus increases with time (instantaneous nucleation) or a combination of the above. When overlap of the centres begins, the slope of the transient will decrease, and when a complete layer is formed, the current will plateau (if thickening is electron transfer controlled), or pass through a peak and decrease (if thickening is diffusion controlled). The shape of the transient can assume many forms. Analysis of current - time transients for deposition of metals have been considered by numerous authors(Bosco and Rangarajan, 1982; Sun *et al.*, 1991; Uceda *et al.*, 1991; Hills *et al.*, 1974; Gunawardena, *et al.*, 1982a; Gunawardena, *et al.*, 1982b). A detailed description of this theory is beyond the scope of this thesis but can be found in the literature (Fleishmann and Thirsk, 1963). Several important results are, however, presented below.

In electrocrystallization processes, discrete nuclei have been found to form at preferred sites. The value of the energy barrier depends on the nature of the substrate, and on the electrode potential. If the number of active sites under particular experimental conditions is N_0, then the rate of appearance of stable growth centres should follow first order kinetics, with the number density of centres, N, given by:

$$N(t) = N_o\,[1 - \exp(-At)] \qquad (5.4)$$

where N_o is the total number of sites available, and A is the nucleation rate constant.

Two limiting case of Equation 5.4 are of interest. If the nucleation of growth centres is essentially instantaneous, i.e., the nucleation rate constant A is very large, then

$$N(t) = N_o \tag{5.5}$$

If A is small, then the nucleation rate is linear with time, and

$$N(t) = AN_o t \tag{5.6}$$

If one assumes that each nuclei grows independent of the others and the rate determining step in electrocrystallization is the incorporation of atoms or molecules at the expanding periphery of the centres, the current flowing into the centres is shown below for several growth and nucleation mechanisms (Fleishmann and Thirsk, 1963).

One dimensional growth, instantaneous nucleation

$$I = nFN_o kS \tag{5.7}$$

One dimensional growth, progressive nucleation

$$I = nFAN_o Skt \tag{5.8}$$

Two dimensional growth, instantaneous nucleation

$$I = \frac{2nF\pi MhN_o k^2 t}{\rho} \tag{5.9}$$

Two dimensional growth, progressive nucleation

$$I = \frac{nF\pi MhAN_o k^2 t^2}{\rho} \tag{5.10}$$

Three dimensional growth, instantaneous nucleation

$$I = \frac{2nF\pi M^2 N_o k^3 t^2}{\rho^2} \tag{5.11}$$

Three dimensional growth, progressive nucleation

$$I = \frac{2nF\pi M^2 A N_o k^3 t^3}{3\rho^2} \qquad (5.12)$$

Equations 5.7 to 5.12 show that the time dependence of the growth current is a function of the nucleation and growth mechanisms. Further, the current density time dependence does not uniquely determine the law, Equations 5.8 and 5.9, and Equations 5.10 and 5.11 exhibit dependence on t and t^2 respectively.

The above equations assume that each nuclei grows independent of the others. This is generally true for the first stages of nucleation, after which adjacent centres will come into contact with one another, reducing the edge area available for the incorporation of materials into the lattice. The limitation on the size of the centres is confined to the axes parallel to the plane of the substrate, and the current density must eventually approach steady state, at a value corresponding to the outward growth perpendicular to the surface. In order to properly calculate the current density - time transient it is necessary to estimate the extent of the overlap for the model chosen. Assuming that the probability of finding a centre growing in two dimensions is uniform over the surface, and assuming that the growth of any centre is not limited by overlap with bounding surfaces of the parent phase, or of the substrate, expressions for the current density associated with two dimensional growth have been developed and are presented below (Fleishmann and Thirsk, 1963).

$$I(\textit{instantaneous}) = \frac{2\pi nFMhN_o k^2 t}{\rho} \exp\left(-\frac{\pi N_o M^2 k^2 t^2}{\rho^2}\right) \qquad (5.13)$$

and

$$I(\textit{progressive}) = \frac{\pi nFMhAN_o k^2 t^2}{\rho} \exp\left(-\frac{\pi M^2 A N_o k^2 t^3}{3\rho^2}\right) \qquad (5.14)$$

In these equations (5.13 and 5.14), the exponential curve gives the leading correction term which is due to the overlap and causes the deviation from the current

density associated with freely growing centres. Approximations, based on the evaluation of the first overlap integral are shown below. The approximations yield the same solution as Equations 5.13 and 5.14 above at short times. They give a maximum which is at different time and of different height, and at long time the approximations yield negative current, while Equations 5.13 and 5.14 approach zero asymptotically. These results indicate that approximations based on first order overlap only are valid at short times.

$$I(\textit{instantaneous}) = \frac{2\pi nFMhN_o k^2 t}{\rho}\left(1-\frac{\pi M^2 N_o k^2 t^2}{\rho^2}\right) \qquad (5.15)$$

$$I(\textit{progressive}) = \frac{\pi nFMhAN_o k^2 t^2}{\rho}\left(1-\frac{\pi M^2 A N_o k^2 t^3}{3\rho^2}\right) \qquad (5.16)$$

Electrocrystallization of a new phase on a foreign substrate may involve the formation of three dimensional growth centres. These centres eventually overlap to give a continuous deposit. It is possible to consider simple growth geometries, such as right circular cones and hemispheres, to develop analytical expressions for the current transient under potentiostatic conditions. Hemispherical models assume a single radial growth-rate, and the right circular conical growth assumes one vertical and one horizontal growth-rate. Consider a right circular conical model, in which growth parallel to the surface takes place with rate constant k, and growth perpendicular to the surface takes place with rate constant k'. The total current associated with the growing cone can be obtained by integration of the contributions of a stack of discs. For the problem involving growth of a number of discrete centres, accounting for the overlap problem as discussed above, the expressions for instantaneous and progressive nucleation have the following form (Southampton Electrochemical Group, 1990b).

$$I\ (\textit{instantaneous}) = nFk'\left(1-\exp\left(-\frac{\pi M^2 k^2 N_o t^2}{\rho^2}\right)\right) \qquad (5.17)$$

and

$$I\ (progressive) = nFk' \left(1 - \exp\left(-\frac{\pi M^2 k^2 N_o A t^3}{3\rho^2}\right)\right) \qquad (5.18)$$

The general behaviour of these expressions can be seen by considering the limiting forms of the equations. At short time, the arguments of the exponential terms are sufficiently small that the expansion reduces to a function of t^2, and t^3 for instantaneous and progressive nucleation respectively. At long times, for both instantaneous and progressive nucleation, the current approaches nFk', as the growth is restricted to the perpendicular direction.

5.1.2.2 Rate Determining Step in Nucleation and Growth: Diffusion of the Electroactive Species

If the rate determining step is not the electron transfer reaction as assumed above, but the slowest step in the growth of the three-dimensional deposit is diffusion of the electroactive species to the surface, the analysis above is no longer valid. A typical transient under mass transfer (diffusion) control includes an initial rising portion, corresponding to the growth of the electroactive area as established nuclei grow and as new nuclei form; a plateau region and a final decay portion. For the case of instantaneous nucleation, under conditions of overlap of the diffusion zones:

$$I = \left(\frac{nFD^{1/2}c}{\pi^{1/2}t^{1/2}}\right)[1-\exp(-N\pi kDt)] \qquad (5.19)$$

k is a numerical constant determined by the conditions of the experiment.

It is clear from the quantity of charge that has passed up to the observed current maximum, that before the overlap of the growing centres occurs, overlap of the diffusion zones develops. For short time scales, the above equation can be simplified by substituting 1-x for exp(-x), and Equation 5.19 becomes:

$$I = \left(\frac{nF(Dc)^{3/2}\pi 8^{1/2}M^{1/2}N}{\rho^{1/2}}\right)t^{1/2} \qquad (5.20)$$

For progressive nucleation, under conditions of overlap of the diffusion zones:

$$I = \left(\frac{nFD^{1/2}c}{\pi^{1/2}t^{1/2}}\right)[1-\exp(-AN\pi k'Dt^2/2)] \qquad (5.21)$$

k' is also a numerical constant.

At short times Equation 5.21 can be reduced to:

$$I = \left(\frac{nF(Dc)^{1/2}AN\pi 2(8M)^{1/2}}{\rho^{3/2}}\right)t^{3/2} \qquad (5.22)$$

In each case (equations 5.19 and 5.21), the current passes through a maximum and then approaches the limiting current for diffusion to a planar electrode. At long times the behaviour of systems undergoing progressive nucleation approaches that of those undergoing instantaneous nucleation. As the diffusion zones grow, the fractional area left uncovered is continuously decreasing and, under the assumptions prevailing here, a nucleus born at a site already crossed by the perimeter of a diffusion zone will not contribute to the observed current. The transient, therefore, invariably approaches that of instantaneous nucleation. It has been observed that an exclusion zone for further nucleation always develops around an already nucleated centre. Thus, what was regarded as a transition from progressive to instantaneous nucleation, is really the interruption of the nucleation process.

5.2 Experimental

Electrochemical electrolyte studies were performed in a constant temperature bath between -25 and 25 °C (±1 °C). The bath included an insulated chamber containing ethylene glycol, and an insulated Neslab circulating bath containing a heating knife(110 V, 250 W) and two immersion coolers (Neslab PBC-4 Bath Cooler, Cryocool Immersion Cooler, CC-65A). Temperature was controlled using an OMEGA CN9000A

thermocouple sensor temperature controller. Cyclic voltammetry and chronoamperometric studies were performed using a Hokuto Denko potentiostat/galvanostat HAB-151. The data were recorded digitally on an IBM-compatible computer using a DAS 16 A/D board, and UnkelScope Software, (Copyright 1984, M.I.T. 1985, 1987, Unkel Software).

5.2.1 Electrochemical Cell Design

The electrochemical cell used in the voltammetry and amperometry experiments included a glassy carbon working electrode(3 mm diameter), a zinc metal counter electrode and a Ag/AgBr reference electrode. The working and counter electrodes were contained in a single compartment cell, and a Luggin capillary connected the reference electrode to the rest of the cell. The counter electrode was formed from 1 mm diameter zinc rod (Johnson Mathey, 99.9999 %) sealed in a glass tube holder with Araldite epoxy. The exposed end of the zinc rod was shaped into small coils having about three turns and an apparent geometric area in the range of 2 cm^2. The working electrode (3 mm diameter glassy carbon) was secured to a silver wire with E-SOLDER Conductive Adhesive (Insulating Materials Incorporated) and sealed in a glass tube holder with Araldite epoxy.

The Ag/AgBr electrode was prepared in-house (Donepudi and Conway, 1984). A silver electrode was lightly polished with emery cloth, then rinsed in distilled water. It was then refluxed in acetone for 1 to 3 hours. The electrode was removed from the acetone bath and rinsed in distilled water in an ultrasonic cleaner. The electrode was next placed in 50 ml of 1 M spectroscopic grade KBr solution. Platinum mesh was used as the counter and reference electrodes. A current of 0.075 mA was applied and the Ag/AgBr electrode was left for 16 hours. At the conclusion of the plating, the Ag/AgBr electrode was pale yellow coloured, and the potential was measured against a standard calomel electrode. A schematic diagram of the electrochemical cell used in these studies is shown in Figure 5.4.

Between electrochemical zinc deposition experiments, the carbon working electrode was held at anodic potential, -0.800 V with respect to the Ag/AgBr reference electrode, until the positive anodic current fell to 0 mA. The working electrode was then

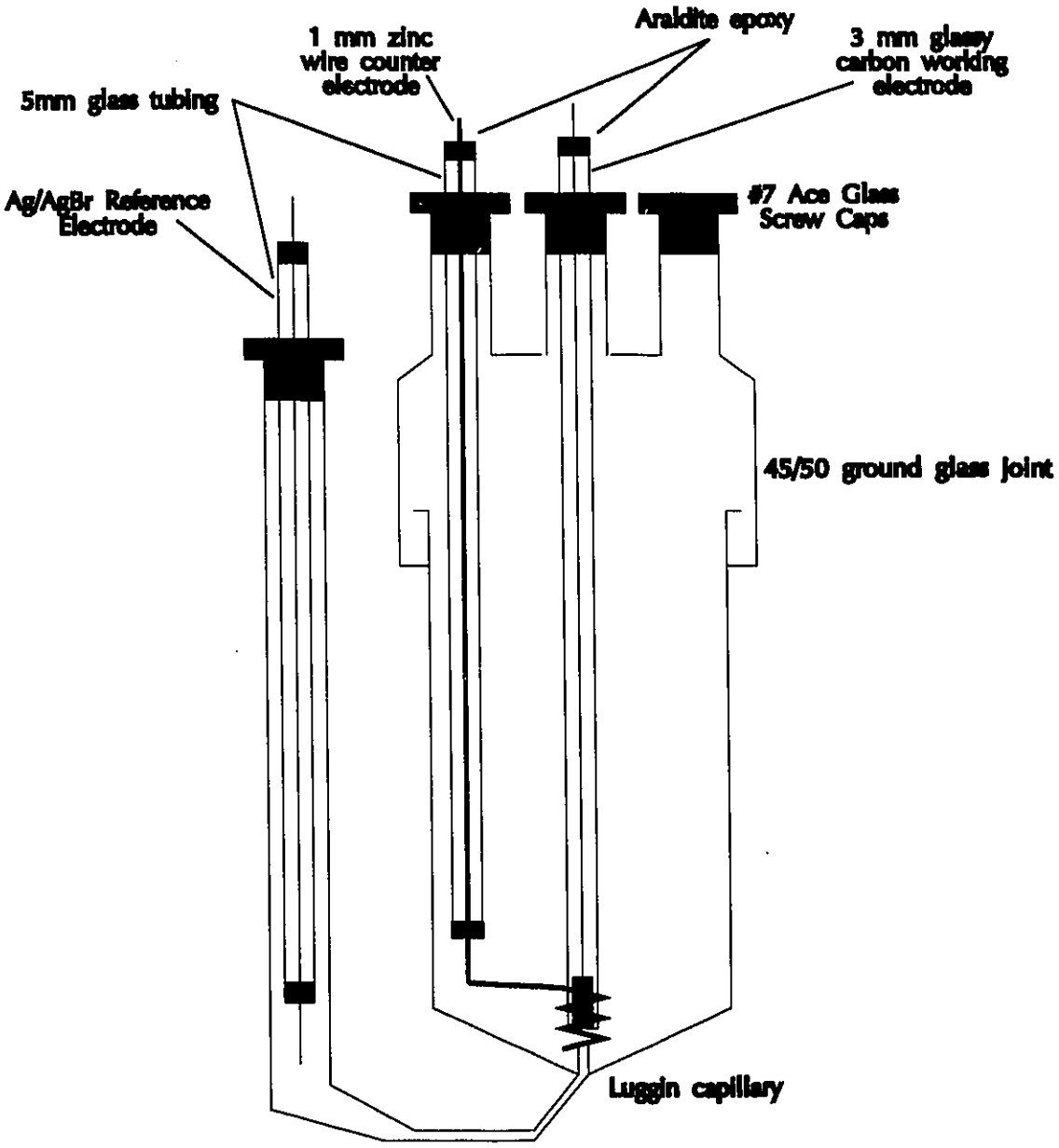

Figure 5.4: Schematic diagram of the electrochemical cell used in cyclic voltammetric and chronoamperometric studies.

removed from the cell, and polished with 1 μm alumina. The electrode was rinsed with distilled water, then cleaned in distilled water in an ultrasonic bath. Finally the electrode was rinsed, dried, and returned to the cell. Each electrochemical experiment was conducted three or more times to ensure reproducibility. Between electrochemical bromide/bromine experiments the carbon working electrode was held at 0.400 V with respect to the Ag/AgBr reference electrode until the cathodic current fell to 0 mA. The glassy carbon working electrode was then polished as described above. The rest potential prior to each experiment was noted, and the experiment was repeated twice.

5.2.2 Solution Preparation

All solutions were prepared volumetrically from standard $ZnBr_2$ solution (7.64 M purchased from Johnson Controls, Inc.), N-ethyl-N-methylpyrrolidinium bromide (2.94 M from Johnson Controls, Inc.), liquid bromine (99.5 %, laboratory reagent grade, BDH Chemical, Inc), BDH AnalR grade $ZnCl_2$(98.0 %), BDH AnalR propan-2-ol (99.7 %), and BDH Assured ethylene glycol (99 %).

5.3 Discussion of Electrode Selection for Electrochemical Experiments

The electrochemical cell used in this work included a Ag/AgBr reference electrode, a high purity metallic zinc wire counter electrode, and a polished glassy carbon working electrode. The Ag/AgBr electrode has been found to be stable in zinc/bromide electrolytes (Donepudi and Conway, 1984). Although near commercial zinc/bromine batteries use carbon plastic composite electrodes, glassy carbon was chosen as the working electrode in the electrochemical cell. As it is important to ensure a stable electrode resistance over a series of tests, Cathro *et al.* (1986) chose to study bromide oxidation on platinum. Most metals, including platinum and titanium, are subject to corrosion in zinc bromide solutions. The presence of metal impurities in the electrolyte can significantly alter the zinc plating morphology. Glassy carbon also provides a stable

resistance, which is of the order of (10 to 50)x10^{-4} $\Omega \cdot cm^{-1}$. Carbon plastic composite electrodes can have as much as 50 % by weight non-conductive material, and have resistance as low as 0.1 $\Omega \cdot cm^{-1}$ (Zagrodnik *et al.*, 1989). Graphite electrodes are subject to bromine intercalation. At ambient temperatures bromine intercalation results in the saturated graphite compound C_8Br. Extended exposure results in flaking of graphite particles and electrode failure (Kinoshita, 1988). Glassy carbon is a good alternative as it is impermeable to gases, resistant to chemical attack, electrically conductive and available in relatively high purity. Polishing of the electrode with a sequence of smaller particle sized abrasive powders ensures a uniform surface for experimentation. The polished surface has a mirror like finish and is covered by a thin layer of finely divided carbon microparticles. This surface provided reproducible experimental results (Kinoshita, 1988). Furthermore, porous glassy carbon, bonded to a graphite substrate has provided a bromine active electrode, but is brittle, difficult to bond to plastic cell frames, and is expensive (Cathro *et al.*, 1987). Finally, several other electrochemical studies on zinc/bromine battery components have been performed at glassy carbon working electrodes (McBreen and Gannon, 1983; Vogel and Mobius, 1991; Mastragostino and Gramellini, 1985).

McBreen and Gannon (1983) have studied the kinetics of zinc deposition in aqueous zinc/bromide solutions in the absence of quaternary ammonium salts. The Br_2/Br^{-1} reactions have been previously studied at glassy carbon in pure polybromide and 0.25 M $ZnBr_2$, NaBr and NH_4Br aqueous solutions (Vogel and Mobius, 1991). Glassy carbon was also selected as the working electrode by Mastragostino and Gramellini (1985) in their study of bromide oxidation in 0.5 M $NaClO_4$. The results of this study can be compared, where possible, to these earlier works.

5.4 Cyclic Voltammetry Study of Bromide Oxidation/Bromine Reduction at Glassy Carbon in Aqueous Zinc Bromide Electrolytes

5.4.1 Results of Bromide Oxidation Study in Aqueous $ZnBr_2$ Electrolytes

The bromide/bromine oxidation/reduction reaction:

$$2Br^- \rightleftharpoons Br_2 + 2e^- \tag{5.23}$$

was studied at a polished glassy carbon electrode in three different aqueous electrolytes. The first electrolyte, SOLA (electrolyte low concentration, A) consisted 0.051 M $ZnBr_2$, the second, SOLB (electrolyte low concentration, B) of 0.046 M $ZnBr_2$ and 0.018 M MEPBr, and the third electrolyte, SOLC, (electrolyte standard battery) of 2.25 M $ZnBr_2$, 0.5 M $ZnCl_2$, and 0.80 M MEPBr. Electrolytes SOLA and SOLB contained 1.0 and 0.51 M $AlCl_3$, respectively. Cyclic voltammetry was used to determine the effects of active species and complexing agent concentration on mechanism and rate of the bromide/bromine redox reaction. The initial voltage for the low concentration studies was 0.900 V versus the Ag/AgBr reference potential, and the system was scanned anodically, at rates ranging from 10 to 500 mV/s, to 1.700 and 1.400 V versus a Ag/AgBr reference electrode potential 0.073 V for SOLA and SOLB respectively. The scan was then continued in the cathodic direction to 0.400 V versus the Ag/AgBr reference electrode, and returned to rest at 0.900 V. The studies in standard battery electrolyte were conducted between the limits of 0.800 V, 1.200 V and 0.400 V versus a Ag/AgBr reference electrode. Experiments were conducted in a constant temperature bath at 0 and 20 °C for SOLA, 20 °C for SOLB.

Cyclic voltammograms (CV) for bromide oxidation/bromine reduction in SOLA, 0 °C, 500 mV/sec are presented in Figure 5.5. These CVs are representative of the experimental results obtained in both SOLA and SOLB at 20 °C and 0 °C, and illustrate the reproducibility of experimental results in these solutions. Results were tabulated and

are presented in Table 5.1. Cyclic voltammetry parameters E_{PA}, E_{PC}, ΔE_P, I_{PA} and I_{PC} are defined in Figure 5.5.

Table 5.1: Cyclic voltammetry results of Br^-/Br_2 oxidation/reduction at a glassy carbon working electrode. Results presented here are the average of three experiments.

Potential Scan Rate (mV/sec)	SOLA, 20 °C				SOLB, 20 °C			
	E_{PA} (V) (±0.02)	E_{PC} (V) (±0.02)	ΔE_P (V) (±0.04)	I_{PA} (mA/cm²) (±1)	E_{PA} (V) (±0.02)	E_{PC} (V) (±0.02)	ΔE_P (V) (±0.04)	I_{PA} (mA/cm²) (±1)
500	1.53	0.52	1.02	59	1.33	0.71	0.62	54
200	1.47	0.56	0.90	41	1.31	0.75	0.56	37
50	1.39	0.65	0.75	23	1.26	0.74	0.52	20
10	1.35	0.64	0.71	12	1.22	0.85	0.36	10
	SOLA, 0 °C							
500	1.52	0.60	0.93	46				
200	1.47	0.63	0.84	32				
50	1.40	0.69	0.71	18				
10	1.35	0.74	0.65	9				

Maximum anodic and cathodic current densities were larger at 20 °C than at 0 °C. As well, anodic current density increased as the potential scan rate increased. The anodic peak maxima shifted to higher potentials, and the cathodic peak to more negative potentials as the potential scan rate increased. This trend was evident at both 0 and 20 °C, and in both electrolytes. Furthermore, the peak separation was sufficiently large to indicate the reaction was irreversible or quasi-reversible. Interestingly, the peak separation decreased in the presence of the polybromide complexing agent.

The standard zinc/bromine battery electrolyte, SOLC, was studied between -15 and 25 °C. Cyclic voltammograms for SOLC at -15 °C, 500 mV/s shown in Figure 5.6, illustrate the reproducibility of the experiments in the concentrated electrolyte. The results of the cyclic voltammetry experiments are presented below in Table 5.2. Both

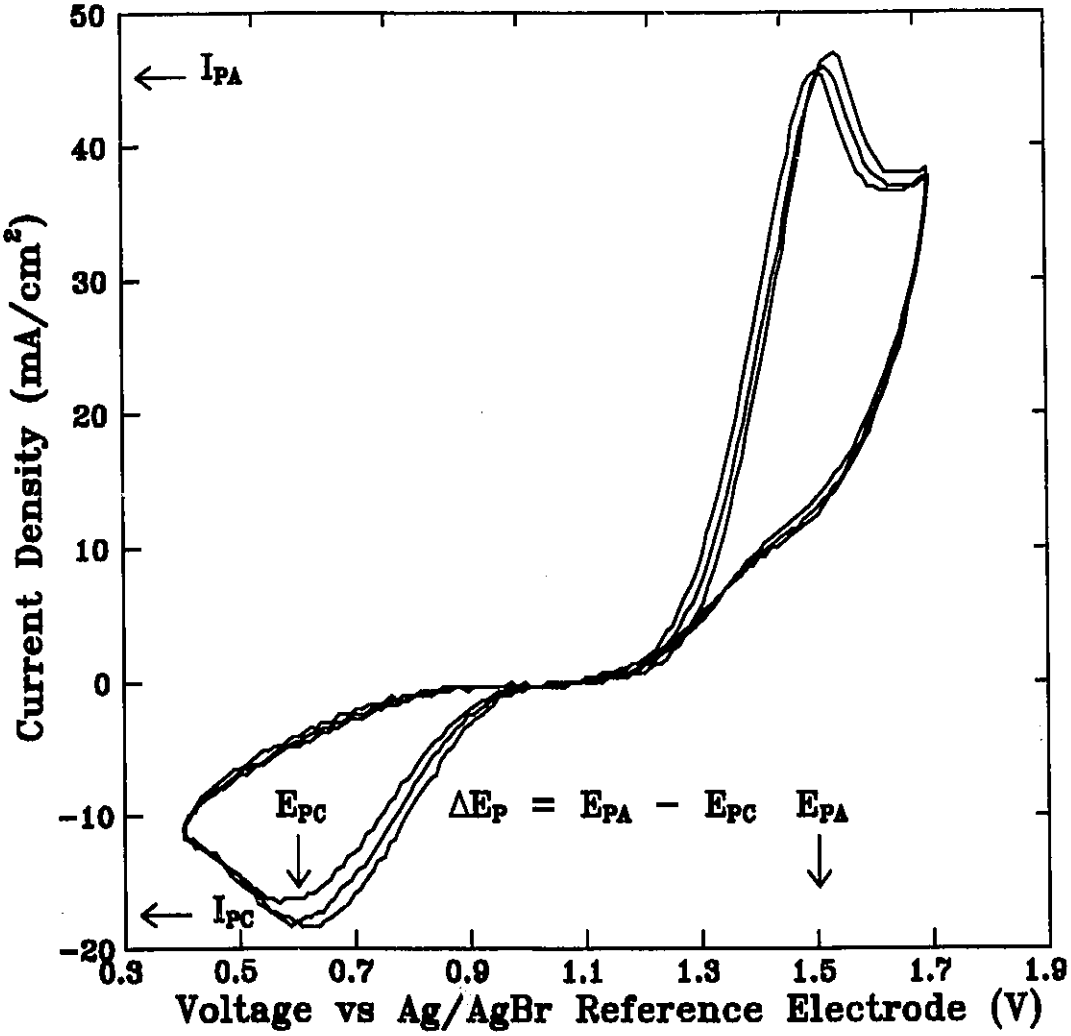

Figure 5.5: Cyclic voltammograms for three experiments showing bromide oxidation/bromine reduction in SOLA (0.05 M $ZnBr_2$), at 0 °C, 500 mV/s.

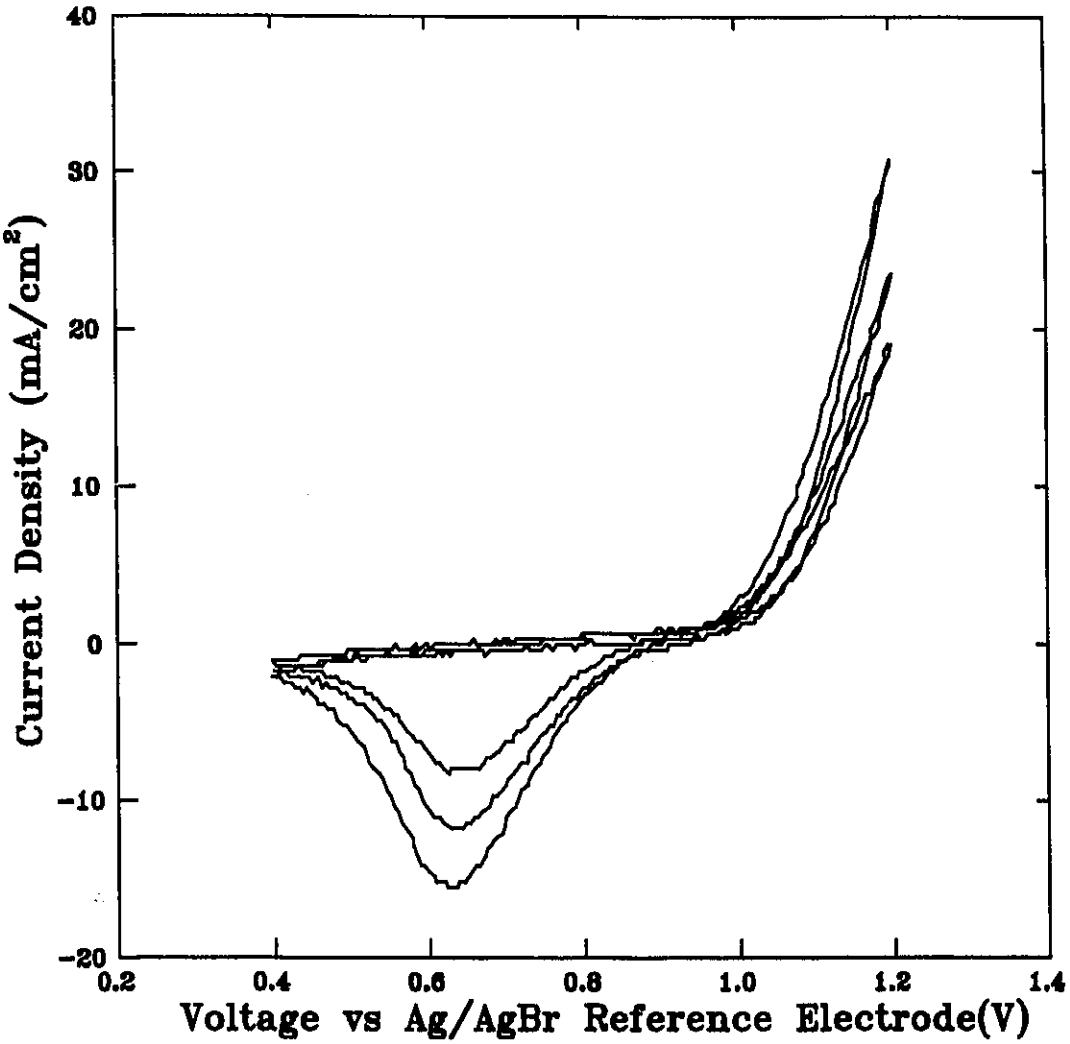

Figure 5.6: Cyclic voltammograms for three experiments showing bromide oxidation/bromine reduction in SOLC (aqueous 2.25 M $ZnBr_2$), -15 °C, 500 mV/s.

anodic and cathodic current density increased with increasing potential scan rate, and with temperature. The position of the cathodic peak maxima, and the peak separation showed no trends with either temperature or potential scan rate.

Table 5.2: Cyclic voltammetry results for standard battery electrolyte (SOLC). Results presented in this table were calculated as the average of three separate experiments.

Scan Rate (mV/s)	I_{PC} (mA/cm^2) (±3)	I_{PA} (mA/cm^2) (±4)	E_{PC} (V) (±0.003)	E_{PA} (V) (±0.003)	ΔE_P (V) (±0.006)
	Temperature -15 °C				
500	12	24	0.629	1.200	0.571
10	10	17	0.610	1.200	0.590
	Temperature 0 °C				
500	22	57	0.609	1.200	0.591
10	13	33	0.634	1.200	0.566
	Temperature 20 °C				
500	41	84	0.650	1.200	0.550
10	17	71	0.657	1.200	0.543

5.4.2 Discussion of Bromide Oxidation Cyclic Voltammetry in Aqueous $ZnBr_2$ Electrolytes

The maximum anodic current densities for SOLA and SOLB were plotted as a function of the square root of the potential scan rate in Figure 5.7, in order to determine if the reaction was reversible, irreversible or quasi-reversible.

The experimental data shown in Figure 5.7 were fitted by an equation of the form (Southampton, 1990a):

$$I_{PA} = c_1 * \sqrt{v} + c_2 \qquad (5.24)$$

The coefficients and fitting parameters for each set of experimental data are presented in

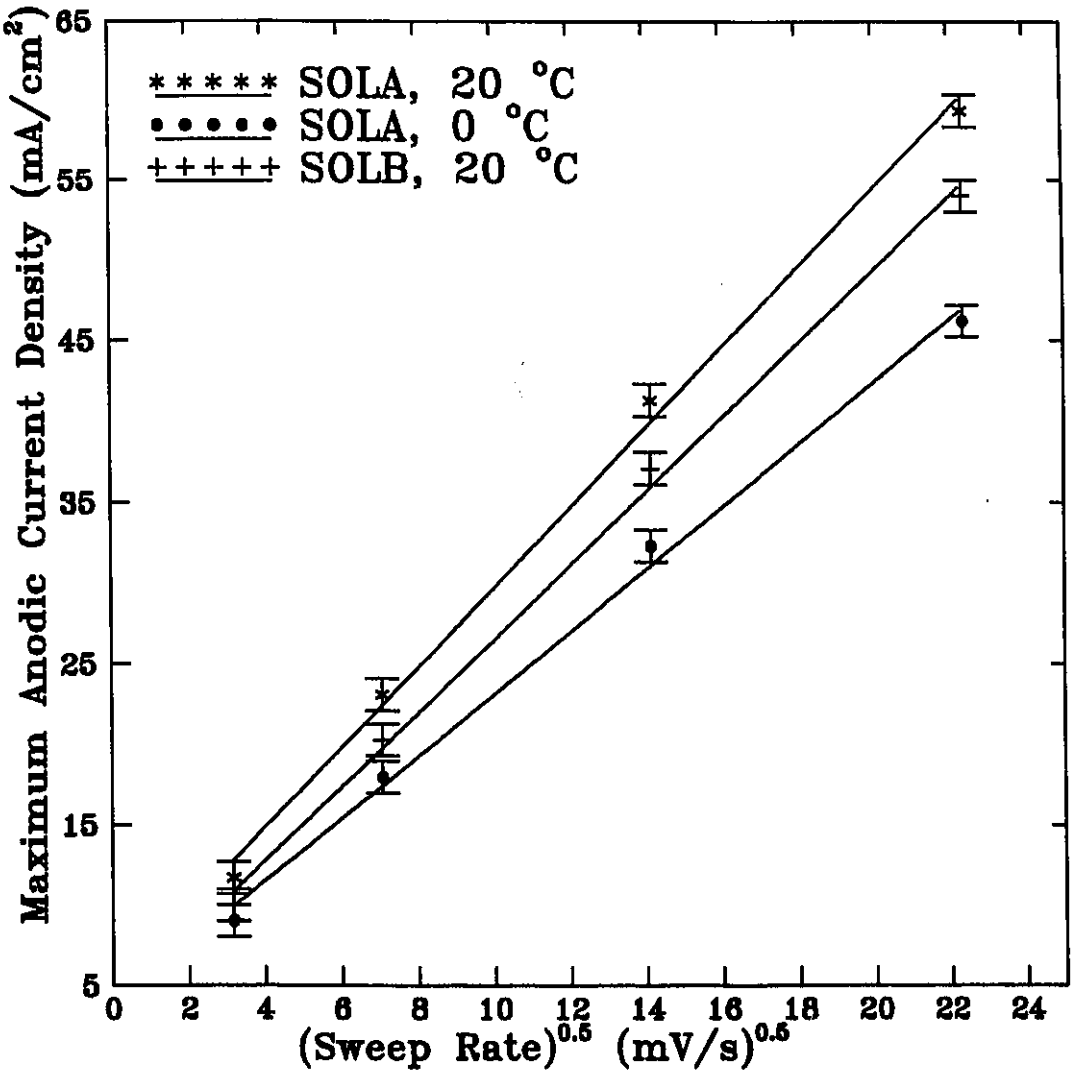

Figure 5.7: Maximum anodic current density for bromide oxidation plotted as a function of the square root of sweep rate for solutions SOLA and SOLB. Each point represents an average of three experiments.

Table 5.3 below.

Table 5.3: Coefficients and fitting parameters for maximum anodic current density as a function of the square root of the potential scan rate (see equation 5.24 for definition of parameters).

	SOLA, 20 °C	SOLA, 0 °C	SOLB, 20 °C
c_1	2.48	1.94	2.29
Standard error of c_1	0.10	0.08	0.08
c_2	4.96	3.76	3.65
Standard error of y estimate	1.45	1.19	1.19
R^2	0.9968	0.9965	0.9975

Examination of the residuals as a function of the potential scan rate indicated, however, that while current density increased with the square root of the potential scan rate, it was not proportional to it (i.e., the residuals were not randomly distributed as shown in Table 5.4).

Table 5.4: Residuals of the equation for maximum anodic current density as a function of the square root of the potential scan rate as shown in Figure 5.7 and Table 5.3.

Potential Scan Rate (mV/s)	√(Scan Rate) $(mV/s)^{1/2}$	Residual (I_{calc} - I_{expt}) (mA/cm^2)		
		SOLA, 20°C	SOLA, 0°C	SOLB, 20°C
500	22.3607	0.8979	0.7394	0.7479
200	14.1421	-1.3416	-1.1059	-1.1328
50	7.0711	-0.6413	-0.5249	-0.4914
10	3.1623	1.0851	0.8914	0.8763

Application of standard diagnostic tests, as described by the Southampton Electrochemistry Group (1990), to the cyclic voltammograms for SOLA identified the bromide oxidation reaction at glassy carbon to be quasi-reversible. The diagnostic tests and results are shown in Table 5.5. It was concluded that the oxidation of bromide at a

glassy carbon electrode, in 0.05 M $ZnBr_2$ electrolyte, was a quasi-reversible reaction.

Table 5.5: Diagnostic tests applied to cyclic voltammograms recorded for 0.05 M $ZnBr_2$ electrolyte. Similar results were realized in electrolytes containing 0.018 M MEPBr.

Observed Behaviour	Reaction Mechanism
Reverse peak obtained	quasi-reversible or reversible
$\lvert I_{PA}/I_{PC} \rvert > 1$	quasi-reversible
E_{PA} is dependent on ν, and shifts positively with increasing potential scan rate	quasi-reversible
ΔE_P is greater than 59/2 = 29.5 mV, and increases with increasing potential scan rate	quasi-reversible
I_{PA} increases with $\nu^{0.5}$ but is not proportional to it	quasi-reversible

Once a potential has been reached at which the oxidation of bromide can occur, the concentration of bromide, Br^-, at the electrode will decrease as predicted by the Nernst equation, and a concentration gradient is established. A current proportional to the concentration gradient flows through the external circuit. The gradient once established begins to relax as Br^- ions diffuse from the bulk to the surface. At the same time, the potential continues to increase, the surface concentration continues to decrease, and the concentration gradient increases. Once the surface concentration effectively reaches zero, the concentration gradient begins to decrease due to relaxation effects. At this time the current also begins to decrease. For an irreversible reaction, however, the rate of mass transfer is similar to the rate of electron transfer, and the surface concentration of Br^- will not be at equilibrium, and the Nernst Equation will not be satisfied. As a result, the surface concentration takes longer to reach zero, the concentration gradient is smaller than for the reversible case, and the peak separation will be larger than for the reversible case, and will increase with increasing potential scan rate as was observed in these experiments.

Peak separation is a measure of the heterogeneous reaction rate. A large separation indicates that the reverse reaction is significantly slower than the forward

reaction. These experimental results indicated that bromide oxidation was significantly faster than bromine reduction at a glassy carbon working electrode.

At low potential scan rates, and 20°C, the reverse peak (cathodic) was non-existent in the SOLA, indicating that the reaction was irreversible under these conditions, and that bromine was weakly adsorbed to the surface of the working electrode (Wopschall and Shain, 1967).

On addition of the quaternary ammonium complexing agent (MEPBr) to the electrolyte, several interesting features were noted in the cyclic voltammograms. In the complex-free electrolyte, the potential of the anodic peak maximum shifted to higher values, and the potential of the cathodic peak maximum shifted to lower potentials with increasing potential scan rate. Thus, peak separation increased with increasing potential scan rate in both solutions. The anodic current density in electrolyte containing MEPBr, corresponding to the oxidation of bromide ions to bromine was roughly the same as in the complex free electrolyte, whereas the cathodic current density, corresponding to the reduction of bromine to bromide was significantly higher at high potential scan rates in electrolytes containing MEPBr. Further, the potential of the anodic maximum current was lower, and the potential for the cathodic maximum current was higher, in electrolytes containing MEPBr than in electrolytes free from MEPBr. As a result, the peak separation was considerably reduced in the presence of the quaternary ammonium salt.

Several mechanistic conclusions can be based on the above information. It is proposed that adsorption processes occur at the surface of the glassy carbon electrode. Strongly adsorbed species can result in multiple peaks, one corresponding to the adsorbed species, and another to the solution species. A strongly adsorbed reactant is stabilized at the surface with respect to the electrode reaction, and results in oxidation at higher potential. A strongly adsorbed product favours the reaction, and results in a peak at potential lower than the solution peak. For weak adsorption, two distinct peaks will not be realized, rather a single distorted peak will result. Thus it is proposed that bromine is more readily adsorbed at the surface of the glassy carbon electrode, in the presence of MEPBr, thus reducing the potential corresponding to the maximum anodic current and increasing the maximum anodic current.

In electrolyte not containing MEPBr, the rate of transport of bromine away from the glassy carbon electrode was similar to the rate of electron transfer for the reduction of bromine. In the presence of MEPBr, bromine formed during oxidation of bromide was more readily adsorbed to the surface of the glassy carbon electrode. As a result, the rate of mass transport of bromine away from the electrode was reduced and the cathodic maximum current increased.

Thus the polybromide complexing agent facilitates bromine adsorption on glassy carbon in $ZnBr_2$ solutions. This hypothesis is in agreement with the earlier work of Mastragostino and Gramellini (1991) and Vogel and Mobius (1991). Mastragostino and Gramellini (1991) identified bromine adsorption on glassy carbon as the rate determining step in bromine reduction in $NaClO_4$ solutions, and Vogel and Mobius (1991) found that, in pure polybromide solutions, the carbon electrodes became coated in polybromide during prolonged exposure.

The bromide/bromine oxidation/reduction reaction was quasi-reversible in the presence of polybromide complexing agent. The addition of the complexing agent did, however, improve the reversibility of the reaction.

The cyclic voltammograms associated with the high concentration electrolyte are much more complex than the low concentration curves. In all high concentration cases, the anodic current density maximum occurred at the maximum anodic potential, 1200 mV. A peak in the cyclic voltammogram results when the concentration of the active species at the electrode surface reaches zero. At this time the concentration gradient associated with the active species begins to decrease, as does the current density. In the concentrated battery electrolyte, solution concentration was sufficiently high that the surface concentration did not reach zero. A maximum was reached for the cathodic portion of the scan (bromine reduction). The cathodic peak tended to be relatively broad, without a well defined E_{PC}. The cathodic current was associated with the reduction of the adsorbed bromine and was limited by the extent bromine had been adsorbed to the surface. During much of the experiment, concentration gradients continued to drive the newly formed bromine away from the electrode, and toward the bulk of the solution. As a result, the value of the cathodic current density maximum was much less than that of

the anodic current density. Bromide oxidation was quasi-reversible in 2.25 M $ZnBr_2$ solutions, at a glassy carbon working electrode, as well as in low concentration electrolytes.

If the current response to the cyclic voltammetric changing potential is plotted as a function of time, the charge for the anodic and cathodic processes can be calculated as the area of the function. The charge, Q, associated with bromide oxidation and bromine reduction was calculated for each electrolyte at several temperatures and potential scan rates, and is presented in Table 5.6. The ratio of the charge associated with the cathodic process (Br_2 reduction) to the charge associated with the anodic process (Br^- oxidation) can be used as a measure of reversibility.

For an irreversible reaction in the absence of adsorption, the rate of mass transfer approached the rate of electron transfer as the potential scan rate increased, and the anodic peak maximum shifted to more positive potentials. This can generally be interpreted as the degree of reversibility decreasing as the potential scan rate increased. In SOLA and SOLB the anodic peak shifted to more positive potential as the potential scan rate increased, indicating that reversibility decreased with increasing potential scan rate. The ratio of the charge associated with the reduction reaction to that of the oxidation reaction in low concentration $ZnBr_2$ solution (SOLA, SOLB), indicated that the degree of reversibility increased with increasing potential scan rate. This result showed that the Br^-/Br_2 is not a simple electron transfer reaction, thus supporting the hypothesis that bromine reduction occurs in the presence of adsorbed bromine. Removal of bromine from the electrode surface via diffusion will reduce the charge associated with the reduction peak, and therefore reduce the degree of reversibility determined from the ratio of redox charges.

The voltage of the maximum anodic current exhibited no dependence on temperature, indicating the reversibility is not affected by temperature. The ratio of redox charges, however, show an increase in the degree of reversibility as temperature is decreased. As temperature is reduced, the mobility of the bromine molecules is reduced and the rate of diffusion of bromine away from the electrode is reduced. Further, the current density decreased with decreasing scan rate, indicating that the concentration

Table 5.6: Charge associated with bromide oxidation and bromine reduction for several electrolytes.

Electrolyte	Temperature (°C)	Scan Rate (mV/s)	Charge (mA·s)		Degree of Reversibility (%)
			Bromide Oxidation	Bromine Reduction	
SOLC	25	500	2.5±0.1	-1.7±0.1	66±1
SOLC	25	10	91±10	-50±3	55±5
SOLC	0	500	1.3±0.1	-0.9±0.1	64±2
SOLC	0	10	34±4	-24±3	72±2
SOLC	-15	500	0.7±0.1	-0.4±0.1	65±8
SOLC	-15	10	23±2	-17±2	79±10
SOLA	25	500	3.94±0.01	-1.37±0.01	35±1
SOLA	25	200	6.3±0.6	-2.0±0.5	32±5
SOLA	25	50	16.5±.1	-3.81±0.05	23±1
SOLA	25	10	56±1	-3±1	5±2
SOLA	0	500	2.78±0.01	-1.14±0.04	41±2
SOLA	0	10	31±1	-5.8±0.1	18±1
SOLB	25	500	2.5±0.1	-1.6±0.1	65±1
SOLB	25	200	4.26±0.09	-2.7±0.1	63±1
SOLB	25	50	9.2±0.2	-4.8±0.1	52±1
SOLB	25	10	25.7±0.5	-5.6±0.6	22±2

gradient decreased with temperature, and therefore the driving force for the diffusion of bromine from the electrode was lower at low temperatures.

On addition of MEPBr to 0.05 M $ZnBr_2$, the degree of reversibility increased, from 35 to 64 % for electrolyte at 25 °C, and 500 mV/s potential scan rate, and from 5 to 22 % at 25 °C, and 10 mV/s. The cathodic charge is directly related to the quantity of bromine available for reduction, thus indicating that in the presence of quaternary ammonium complexing agent, there was more bromine available at the electrode surface. This fact

supports the theory that bromine was preferentially adsorbed to the surface of the glassy carbon electrode in the presence of MEPBr.

In concentrated electrolyte (SOLC), the charge efficiency was independent of temperature between -15 and 25 °C, at fast potential scan rates, (65 % for 500 mV/s), and increased with temperature at low potential scan rates. Further, the charge efficiency at low potential scan rates was much higher than for the low concentration electrolytes (compare results at 25 °C, 10 mV/s, SOLC 55 %, SOLA 5 %, SOLB 22 %). In high concentration battery electrolytes mass transfer of bromide ions, the active species, did not limit the maximum oxidation current achieved. The reduction current was dependent on the quantity of bromine adsorbed at the electrode surface, and the higher degree of reversibility, determined from anodic and cathodic charges, indicated that increasing the quaternary ammonium salt concentration, facilitated bromine adsorption on glassy carbon.

5.4.3 Conclusions of the Cyclic Voltammetry Study of Bromide Oxidation

Bromide oxidation/bromine reduction was a quasi reversible reaction at glassy carbon in aqueous zinc bromide electrolytes. The CVs obtained were characteristic of a weak product adsorption mechanism (Wopschall and Shain, 1967). Addition of MEPBr facilitated bromine adsorption on glassy carbon. This conclusion is supported by earlier work of Mastragostino and Gramellini (1991) and Vogel and Mobius(1991). Finally, the ratio of redox charge associated with the anodic to cathodic processes was found to be independent of temperature.

5.5 Cyclic Voltammetric Study of Zinc Deposition on Glassy Carbon in Aqueous Zinc Bromide Electrolytes

5.5.1 Results of Zinc Deposition in Aqueous Zinc Bromide Electrolytes

The zinc deposition reaction was studied at a glassy carbon electrode in aqueous solutions SOLA, SOLB, and SOLC described previously. The overall deposition reaction is given in the equation:

$$Zn^{2+}(aq) + 2e^- \rightleftharpoons Zn(s) \qquad (5.25)$$

Cyclic voltammetry experiments were conducted in SOLA and SOLB over the voltage range -0.475 to -1.300 V versus the Ag/AgBr reference electrode potential of 0.073 V. The system was scanned cathodically (decreasing voltage), (-0.970 to -1.300 V versus Ag/AgBr), then anodically (-1.300 to -0.475 V versus Ag/AgBr). Scan speed ranged from 10 to 200 mV/s, corresponding to experiments of 200 seconds at the slow rate, and 8 seconds at the fast rate. Each experiment was repeated three times. The cathodic peak corresponds to zinc deposition on carbon, and the anodic peak to zinc dissolution.

Typical cyclic voltammograms recorded for SOLA and SOLB electrolytes at a glassy carbon electrode are shown in Figures 5.8, 5.9, and 5.10.

A typical Zn^{2+}/Zn cyclic voltammogram for electrolyte containing 2.25 M $ZnBr_2$, 0.5 M $ZnCl_2$, 0.8 M MEPBr (SOLC) is presented in Figure 5.11. It is important to note the potential limits for the voltammetry experiments shown in Figure 5.11. The glassy carbon electrode was cycled between -1.0 V and -0.5 V versus the Ag/AgBr reference electrode at -15 °C, and between -0.940 V and -0.565 V versus the Ag/AgBr reference electrode at 0 °C and 20 °C. As a result the maximum cathodic and anodic currents densities recorded at -15 °C were greater than those at 0 °C.

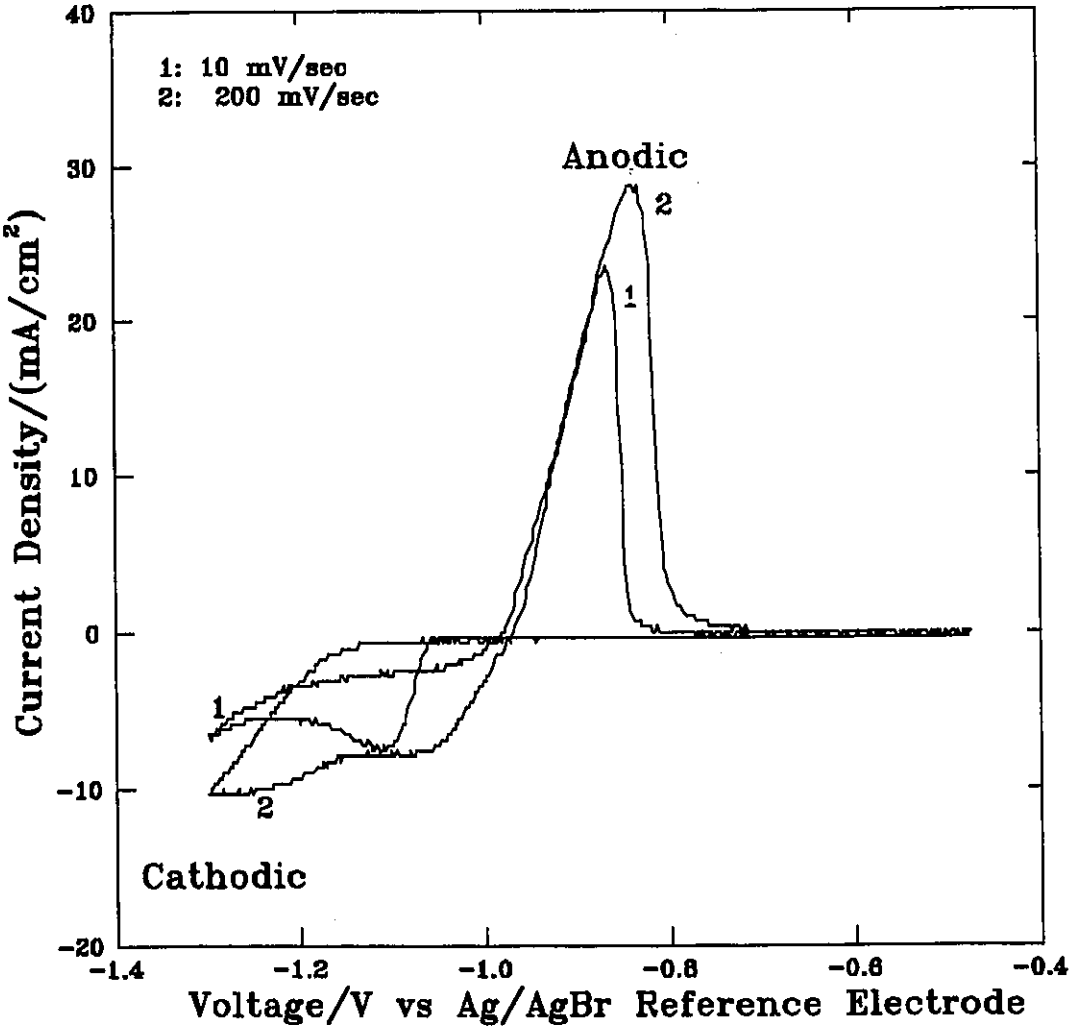

Figure 5.8: Cyclic voltammograms of zinc deposition on glassy carbon in 0.05 M $ZnBr_2$ solutions as a function of scan rate, no added polybromide complexing agent, 25 °C, (SOLA).

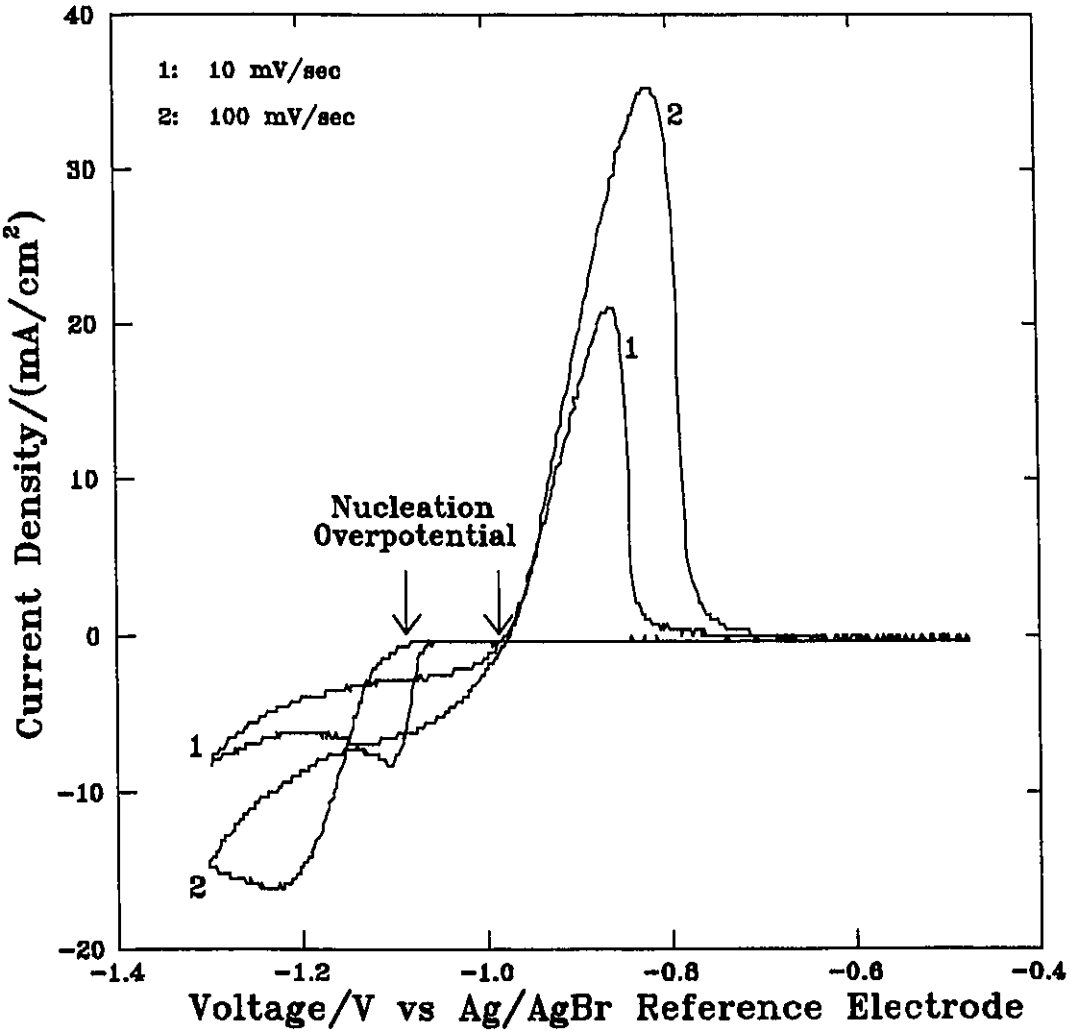

Figure 5.9: Cyclic voltammograms of zinc deposition on glassy carbon in 0.05 M $ZnBr_2$ solutions as a function of scan rate, 0.018 M N-ethyl-N-methylpyrrolidinium bromide added, 25 °C, (SOLB).

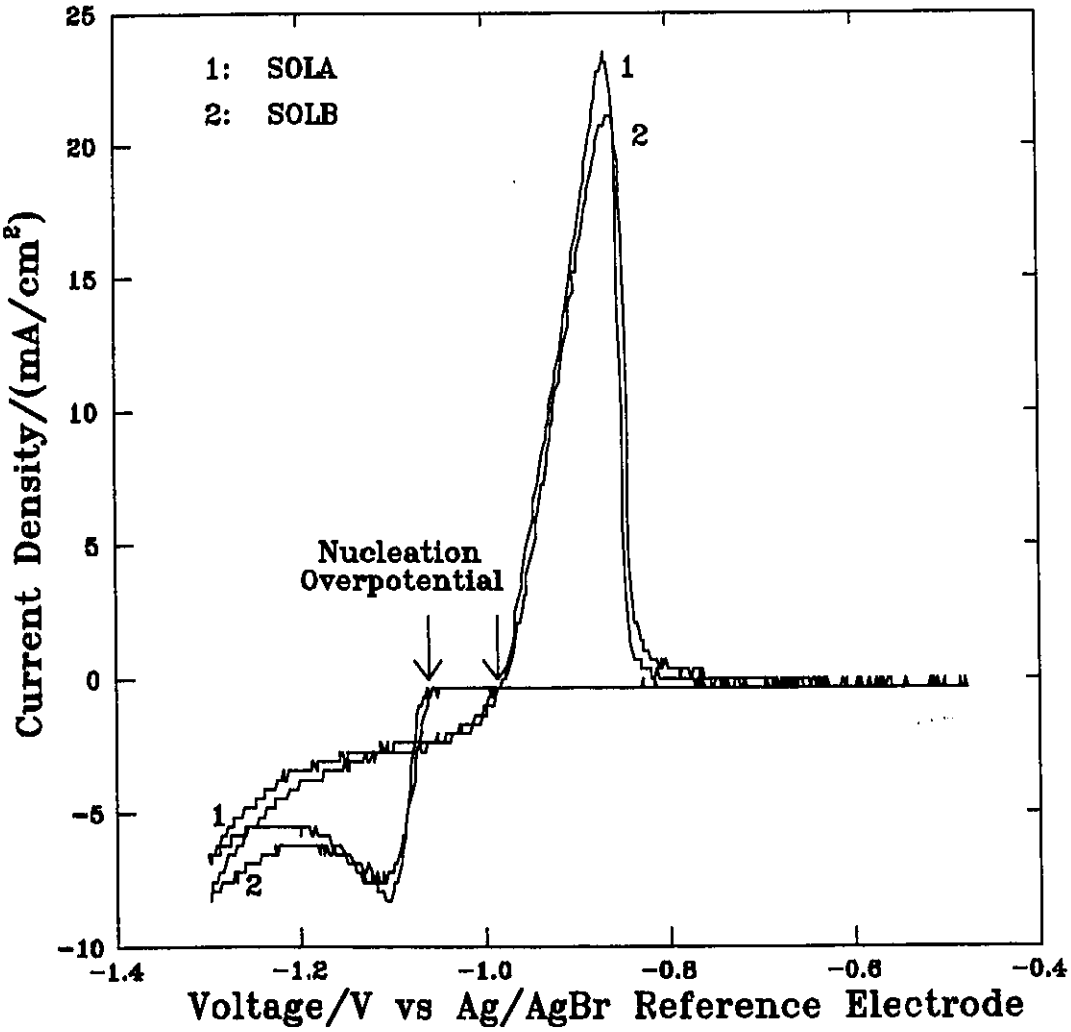

Figure 5.10: Cyclic voltammograms of zinc deposition on glassy carbon in 0.05 M $ZnBr_2$ solutions illustrating the effects of MEPBr addition, 10 mV/s, 25 °C.

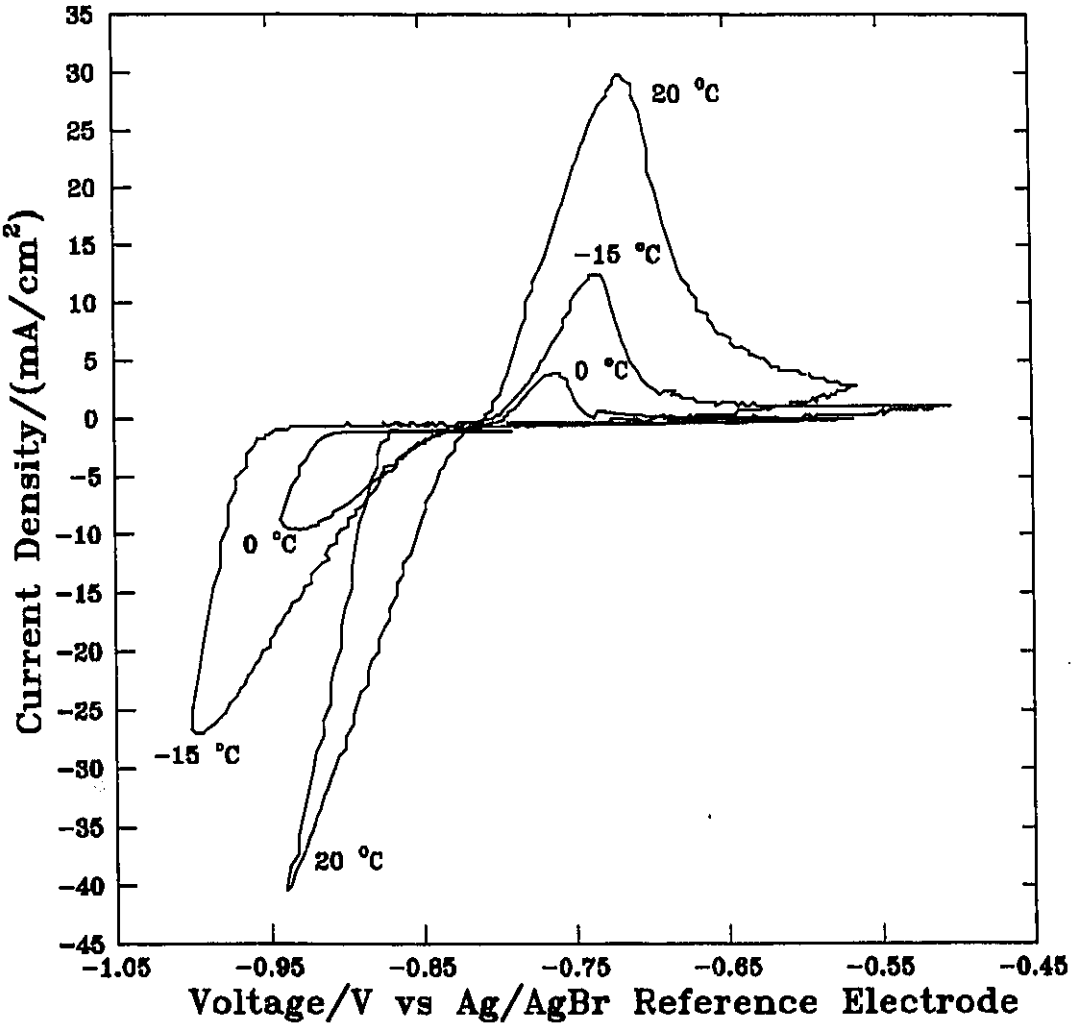

Figure 5.11: Cyclic voltammograms for zinc deposition on glassy carbon in 2.25 M $ZnBr_2$, 0.5 M $ZnCl_2$, and 0.8 M MEPBr at various temperatures (SOLC).

5.5.2 Discussion of Zinc Deposition in Aqueous Zinc Bromide Electrolytes

The cyclic voltammograms obtained for solutions SOLA and SOLB were characteristic of metal deposition onto a foreign substrate. The forward peak of the first cathodic scan of an experiment was identifiable by a very steep leading edge, and on reverse the cathodic current density was higher than on the forward scan over the potential range -1.1 to -0.9 V versus Ag/AgBr. On the forward scan, a potential significantly more negative than the equilibrium potential for the Zn/Zn^{2+} couple was required before deposition began. On the reverse scan, zinc deposition occurred at a zinc surface and continued until the equilibrium potential was reached. This gave rise to the high cathodic current density on the reverse scan. The second cross-over observed in the cyclic voltammograms corresponded to the equilibrium potential for fast M/M^{n+} couples, and under these conditions the difference between this and the potential at which deposition began on the forward scan, was the nucleation overpotential. The anodic peak was sharp and relatively symmetrical, as the reacting material was deposited on the electrode and, therefore, did not need to diffuse there in order to react. The peak current density for the anodic portion of the scan was very high as the zinc was already present at the electrode surface, and diffusion did not limit the supply of reactants.

The cathodic peak current density, I_c, (mA/cm^2), (zinc deposition) is plotted as a function of the square root of potential scan rate at -10, 0 and 20 °C for Quat free solutions, (SOLA), and 20 °C for solutions containing MEPBr, (SOLB), in Figure 5.12. The maximum cathodic current for SOLA decreased with decreasing temperature. Nucleation overpotential was found to increase as temperature decreased for SOLA and to increase with increasing scan rate.

Over the potential scan rates 10 to 100 mV/sec, the peak cathodic current density for zinc deposition in the absence of polybromide complexing agent increased with the square root of potential scan rate. The cathodic current density was not, however, proportional to the square root of potential scan rate. Above 100 mV/sec, the cathodic peak current density decreased with increasing potential scan rate. Furthermore, the shape

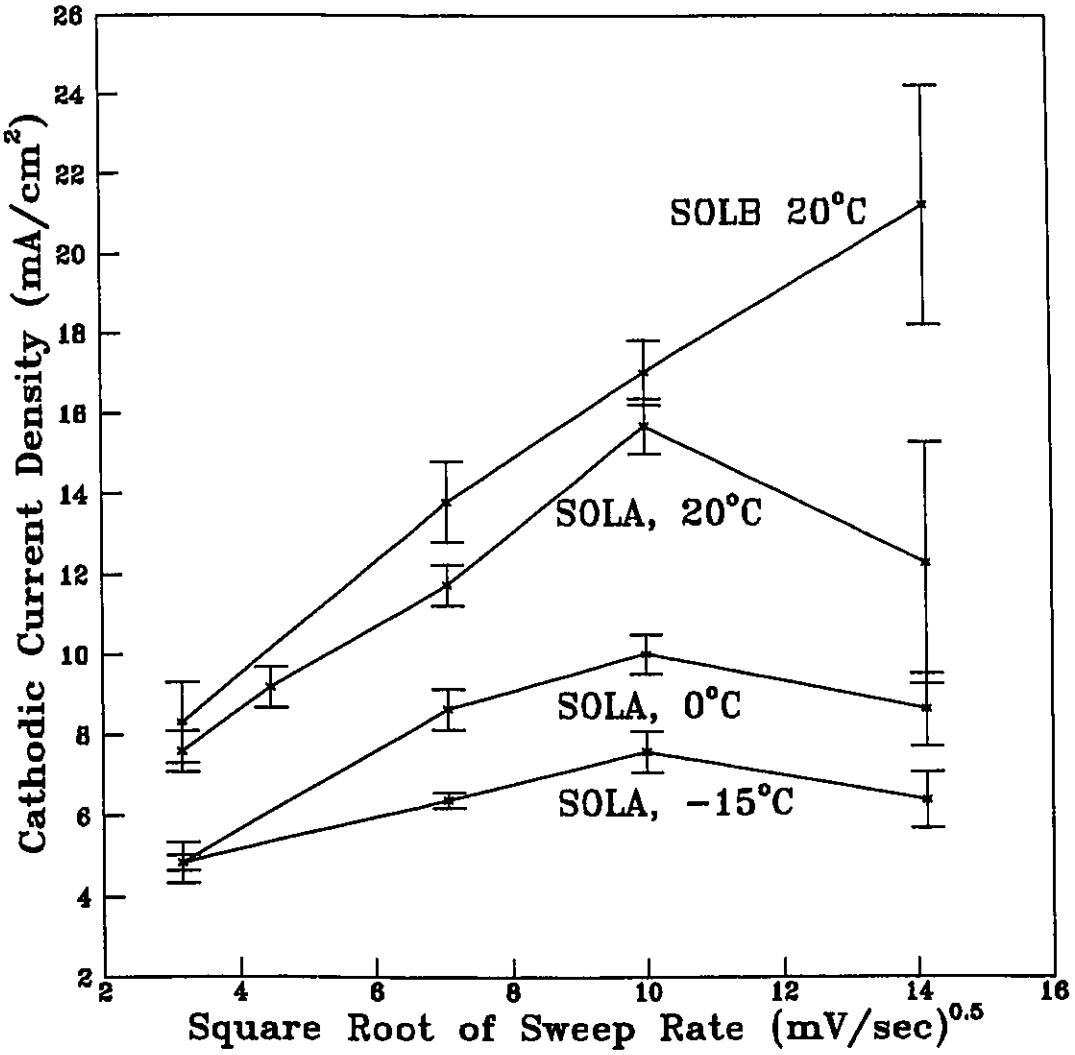

Figure 5.12: Maximum cathodic current density of zinc deposition as a function of temperature and sweep rate.

of the deposition (cathodic) response changed at high potential scan rate. In the presence of Quats, the cathodic peak current density increased with the square root of the potential scan rate over the range of potential scan rates 10 to 200 mV/s. The shape of the current density versus potential scan rate curve remained the same throughout the experiments. The overpotential, η, associated with zinc deposition and the anodic and cathodic peak separation, ΔE_P are shown in Table 5.7 for SOLA and SOLB.

Table 5.7: Cyclic voltammetry results for zinc deposition on glassy carbon from 0.05 M $ZnBr_2$ solutions (SOLA, SOLB). Each data point in this table was calculated as the average from three experiments.

Scan Rate (mV/sec)	I_{PC} (mA/cm^2)	E_{PC} (mV)	I_{PA} (mA/cm^2)	E_{PA} (mV)	η (mV)	ΔE_P (mV)
Polybromide free solution (SOLA), 20 °C						
10	7.6±0.5	-1115±7	24.0±0.7	-868±1	78±5	247±8
50	11.7±0.5	-1193±5	33.4±0.5	-848±6	91±6	350±10
100	15.4±0.7	-1223±3	39±2	-831±4	117±6	392±7
200	13±3	-1300±5	31±3	-831±2	170±10	469±7
Polybromide free solution (SOLA), 0°C						
10	4.8±0.5	-1140±1	17.6±0.5	-861±1	95±15	279±2
50	8.6±0.5	-1230±10	23±1	-836±2	128±2	395±10
100	10.0±0.5	-1295±7	23.8±0.5	-825±2	183±13	470±9
200	8.6±0.9	-1240±10	21±1	-830±3	232±5	410±20
Polybromide free solution (SOLA), -10°C						
10	4.5±0.2	-1130±10	14.3±0.2	-832±2	118±5	300±20
50	6.4±0.2	-1280±20	17±1	-809±1	160±6	470±20
100	7.6±0.5	-1300±10	18±1	-808±5	191±7	490±15
200	6.4±0.7	-1270±40	15±2	-813±5	189±3	450±40
Polybromide solution (SOLB), 20 °C						
10	8±1	-1120±20	21.6±0.7	-864±9	90±20	250±30
50	14±1	-1160±10	33±3	-839±3	74±6	320±10
100	17.0±0.8	-1220±10	37±3	-823±2	110±20	390±20
200	21±2	-1280±10	42±4	-806±6	110±20	470±20

In the quat containing solutions, overpotential was independent of the potential scan rate, and was generally lower than in the absence of the quats. Low overpotential is good, as it favours higher voltaic efficiency. The peak separation in both solutions was very large, greater than 200 mV, and increased as the potential scan rate increased, indicating zinc deposition was quasi-reversible on glassy carbon. For a reversible reaction the peak separation would be 59/2 = 29.5 mV. Peak separation, ΔE_p, exhibited no dependence on quat concentration indicating that quaternary complexing agents do not influence the homogeneous reaction rate of zinc deposition on glassy carbon from 0.05 M $ZnBr_2$ solutions.

Cyclic voltammograms obtained for SOLC also showed characteristic metal deposition behaviour. A comparison of cathodic current densities at -0.940 V versus the Ag/AgBr reference electrode (see Figure 5.11) indicated that current density decreases as temperature decreases. Ionic mobility decreases as the viscosity of the medium increases and increases as the size of the ion increases. As the temperature was decreased, the viscosity of the solution increased and the electrolyte began to freeze at 0 °C, thus resulting in a negative contribution to ionic mobility. Raman spectroscopic results obtained in battery electrolytes indicated a shift to higher order species ($ZnBr_4^{2-}$, $ZnBr_3^-$) from ($ZnBr_2$, $ZnBr^+$) as temperature was decreased. The higher order species contributed to negative migration effects (i.e., negative species will migrate away from the negative electrode). Activity measurements indicated that Zn^{2+} carries twelve more waters than $ZnCl_3^-$, which in turn has four more waters than $ZnCl_4^{2-}$ (Hsie and Selman, 1985). They predict that ionic diffusivity will increase as $Zn^{2+}<ZnCl_3^-<ZnCl_4^{2-}$. It has been suggested that zinc/bromine complexes follow a similar trend (Hsie and Selman, 1985). Ionic mobility will, therefore, be increased due to the increased number of smaller ions at low temperature, but will be decreased due to the increase in solution viscosity and the negative migration effects. As a result of these competing phenomena, the current density decreased as temperature decreased. Nucleation overpotential, characteristic of metal deposition on a foreign substrate, was readily visible in these voltammograms. A summary of these experiments is presented in Table 5.8.

Table 5.8: Results from cyclic voltammetry experiments on zinc deposition/dissolution in 2.25 M $ZnBr_2$, 0.5 M $ZnCl_2$, 0.8 M MEPBr (SOLC). Each data point in this table was calculated as the average from three experiments.

Temperature (° C)	Scan Rate (mV/s)	I_C (mA/cm^2) (±3)	E_C (V) (±0.002)	I_A (mA/cm^2) (±3)	E_A (V) (±0.005)	η (mV)
-15	50	-24	-0.998	13	-0.728	113±2
0	50	- 9	-0.932	4	-0.760	93±7
0	1	-35	-0.940	32	-0.700	42±2
25	50	-41	-0.940	29	-0.722	55±3
25	1	-56	-0.940	65	-0.658	31±1

Nucleation overpotential was observed to increase with decreasing temperature and increasing potential scan rate as was generally observed in SOLA and SOLB. A cathodic current density peak was not obtained in SOLC within the potential range considered in these experiments. A maximum in cathodic current will occur only when the surface concentration of active species is zero. Due to the high concentration of Zn^{2+}(aq) in solution, the timescale of the experiment, and the potential range over which current density was recorded, a maximum cathodic current was not recorded. On reverse of the potential scan, the cathodic current density was always higher than on the forward scan. Again, on the forward scan a potential significantly more negative than the equilibrium Zn/Zn^{2+} potential was required to deposit zinc on the glassy carbon electrode. On the reverse scan, the deposition was occurring at a zinc surface, and the minimum potential required was much lower. The cathodic current density was seen to increase with increasing temperature. Cathodic current density did not however increase with the potential scan rate or the square root of the potential scan rate as is typically found in cyclic voltammetry experiments. Current density generally increases with potential scan rate due to an increasing concentration gradient between active species in the bulk and at the electrode surface. In these experiments, the concentration of active species was very high, and significant changes in the concentration gradient did not occur.

The quantity of charge, Q, associated with zinc deposition and stripping was

calculated and is presented in Tables 5.9 and 5.10 below as a function of potential scan rate and temperature for SOLA and SOLB, and SOLC, respectively.

Table 5.9: Charge efficiency as a function of temperature and potential scan rate for SOLA and SOLB. Results in this table were calculated as the average from three experiments.

Temperature (°C)	Scan Rate (mV/s)	SOLA Q_A/Q_C (%)	SOLB Q_A/Q_C (%)
25	200	83 ± 3	84 ± 2
25	100	84 ± 3	83 ± 2
25	50	82 ± 3	68 ± 1
25	20	69 ± 1	
25	10	66 ± 1	61 ± 3
0	200	80 ± 2	
0	100	83 ± 1	
0	50	79 ± 1	
0	10	70 ± 4	
-10	200	75 ± 3	
-10	100	81 ± 1	
-10	50	79 ± 1	
-10	10	67 ± 1	

Charge efficiency relates the amp hours of charge used to deposit zinc, to the amp hours of charge recovered during the stripping cycle. If the only electrode processes occurring are $Zn^{2+} \rightleftharpoons Zn(s)$, the anodic charge and the total cathodic charge (area under both the forward and reverse scans at cathodic potential) must be equal, as all the metal deposited onto the electrode surface will be redissolved in the anodic process. In the case of zinc deposition/stripping at room temperature in SOLC the charge efficiency was essentially 100 % indicating that $Zn^{2+} \rightleftharpoons Zn(s)$ was the only reaction occurring. At low temperatures (0, -15 °C), the charge efficiency was reduced, indicating that the process was more

complicated. At these temperatures, the solution began to freeze. Visual inspection of the glassy carbon working electrode at the completion of the cyclic voltammetry experiment indicated that isolated zinc deposits remained on the electrode surface. As well, at low temperatures the rest potential at the completion of the experiment was between -0.75 and -0.80 V versus the Ag/AgBr reference electrode, indicating that metallic zinc remains deposited on the electrode at the completion of the cyclic voltammogram. Holding the working electrode at an anodic potential (sufficient to oxidize Zn(s) to Zn^{2+}) resulted in very low current density, and eventually to a falling rest potential. On inspection of the glassy carbon working electrode, after holding it at anodic potential, the electrode appeared free of zinc. Thus, the isolated zinc deposits were insolated from the glassy carbon working electrode possibly by a layer of non-conductive ice. The ice layer could have been trapped between the freshly depositing zinc, and the carbon surface. High cathodic current densities indicate that zinc deposition occurs quickly in SOLC once the potential surpasses the nucleation overpotential. During solid zinc oxidation to Zn^{2+}, metallic zinc deposited directly on the carbon surface was readily oxidized as indicated by the high initial anodic current. Zinc deposited on an ice surface would only be oxidized at high potential and low current density. As a result, the ratio of anodic charge to cathodic charge decreased with decreasing temperature as shown in Table 5.10.

Table 5.10: Charge efficiency as a function of temperature and potential scan rate for solutions of 2.25 M $ZnBr_2$, 0.5 M $ZnCl_2$, and 0.8 M MEPBr(SOLC). Results in this table were calculated as the average from three experiments.

Temperature (°C)	Scan Rate (mV/s)	Q_A/Q_C (%)
-15	50	38±2
0	50	65±10
0	1	84±5
25	50	72±5
25	1	94±1

The effect of added quaternary ammonium salt was also studied in high concentration $ZnBr_2$ electrolyte. This study was performed in electrolyte containing 2.25 M $ZnBr_2$ and varying concentrations of MEPBr. The concentration of $ZnCl_2$ throughout this study was 0 M. Results of this study are presented in Table 5.11.

Table 5.11: Cyclic voltammetry results as a function of MEPBr concentration and potential scan rate. Experiments conducted at 25 °C, in electrolyte containing 2.25 M $ZnBr_2$.

MEPBr Concentration	Scan Rate (mV/s)	I_C (mA/cm^2)	E_C (mV) (±0.002)	I_A (mA/cm^2)	E_A (V) (±5)	η (mV)
0	50	-49±8	-0.938	48±6	-0.671	56±2
0	10	-43±2	-0.937	47±1	-0.653	47±2
0	5	-62±5	-0.936	69±6	-0.651	40±1
0	1	-53±8	-0.937	58±10	-0.645	30±1
0.01	50	-69±7	-0.938	70±8	-0.669	57±2
0.01	10	-59±2	-0.938	60±2	-0.659	46±1
0.01	5	-63±10	-0.936	69±10	-0.651	44±1
0.01	1	-52±1	-0.936	56±1	-0.648	36±1
0.1	50	-50±1	-0.937	43±5	-0.699	59±10
0.1	5	-59±2	-0.937	53±3	-0.679	38±8
0.1	1	-70±10	-0.937	69±10	-0.659	19±1
0.5	50	-30±6	-0.936	22±2	-0.747	69±9
0.5	10	-52±6	-0.937	38±3	-0.729	51±6
0.5	5	-61±2	-0.937	52±7	-0.713	34±8
0.5	1	-60±5	-0.936	59±6	-0.698	22±2

In summary, the cathodic and anodic current densities were of the same order of magnitude in the presence of MEPBr. Further, the maximum cathodic current density occurred at the maximum cathodic potential, -0.94 V versus the Ag/AgBr reference

electrode, in all experiments. The nucleation overpotential also remained of the same order in the presence of MEPBr. These results indicated that the addition of MEPBr to the concentrated battery electrolyte does not effect the zinc deposition/dissolution reactions, and were in agreement with the experiments performed with low concentrations of $ZnBr_2$. Raman spectroscopic studies further indicated that zinc/bromine complex distribution was not affected by the addition of quaternary ammonium salts, thus supporting the above conclusion.

5.5.3 Conclusions of CV Study of Zinc Deposition on Glassy Carbon

The maximum cathodic current density obtained in electrochemical cells, at room temperature ranged from 40 to 70 mA/cm^2 for zinc deposition on glassy carbon from solutions of 2.25 M $ZnBr_2$ and additives. Interestingly, this current density is of the same order of magnitude as current densities used to test operating zinc/bromine batteries. Fujii *et al.* (1986) in a study of 80 kWh zinc/bromine batteries for electric power storage operated 1 to 10 kW batteries at current densities between 10 and 20 mA/cm^2. A 50 KWh battery was also operated in this same range of current densities (Fujii *et al.*, 1988). Technical feasibility of zinc/bromine batteries was demonstrated by Exxon, with a 30 kWh battery operating with current density in the 30 to 45 mA/cm^2 range. As zinc deposition has been found to be dependent on the cathodic current density it is important to conduct electrochemical studies at similar current densities (McBreen and Gannon, 1983; McBreen, 1993; Leo and Charkey, 1986).

Cyclic voltammograms characteristic of metal deposition on a foreign substrate were obtained. Addition of quaternary ammonium bromide complexing agent did not affect the zinc deposition cyclic voltammograms.

Overpotential was found to increase with decreasing temperature. Stripping of zinc from the electrode surface was incomplete at low temperatures and isolated zinc deposits were visible at the completion of the cyclic voltammetry experiment. This is a significant result, as it indicates that coulombic efficiency will be reduced at low temperature due to incomplete oxidation of metallic zinc.

5.6 Chronoamperometric Studies of Zinc Deposition on Glassy Carbon in Aqueous Zinc Bromide Electrolytes

5.6.1 Results of Chronoamperometric Study in Aqueous $ZnBr_2$ Electrolytes

Chronoamperometric experiments were performed at room temperature in both SOLA and SOLB. Experiments ranged from 1 to 20 seconds in length, the initial potential was -0.940 V (SOLA), or -0.950 V (SOLB), and E_2 ranged from -1.100 to -1.200 V. The sweep rate was 5 x 10^4 mV/sec. Between each experiment the carbon working electrode was held at anodic potential, -0.800 V, until the positive anodic current fell to 0 mA. It was then removed from the cell, and polished with 1 μm alumina. The electrode was rinsed in distilled water and cleaned in distilled water in an ultrasonic bath. The electrode was again rinsed, then was dried and returned to the electrochemical cell. The transient current density responses were plotted as a function of time, and a typical result is presented in Figure 5.13.

A series of chronoamperometry experiments were performed using SOLC (2.25 M $ZnBr_2$, 0.5 M $ZnCl_2$, 0.8 M MEPBr) at 25 °C, 0 °C, and -15 °C. The potential steps used in these experiments were -0.210 V and -0.310 V. In each of these cases, the current initially increased, the slope of the transient then decreased, and finally a current plateau was reached and maintained for the length of the experiment (10 to 25 seconds). Typical chronoamperometry experiments are presented in Figure 5.14.

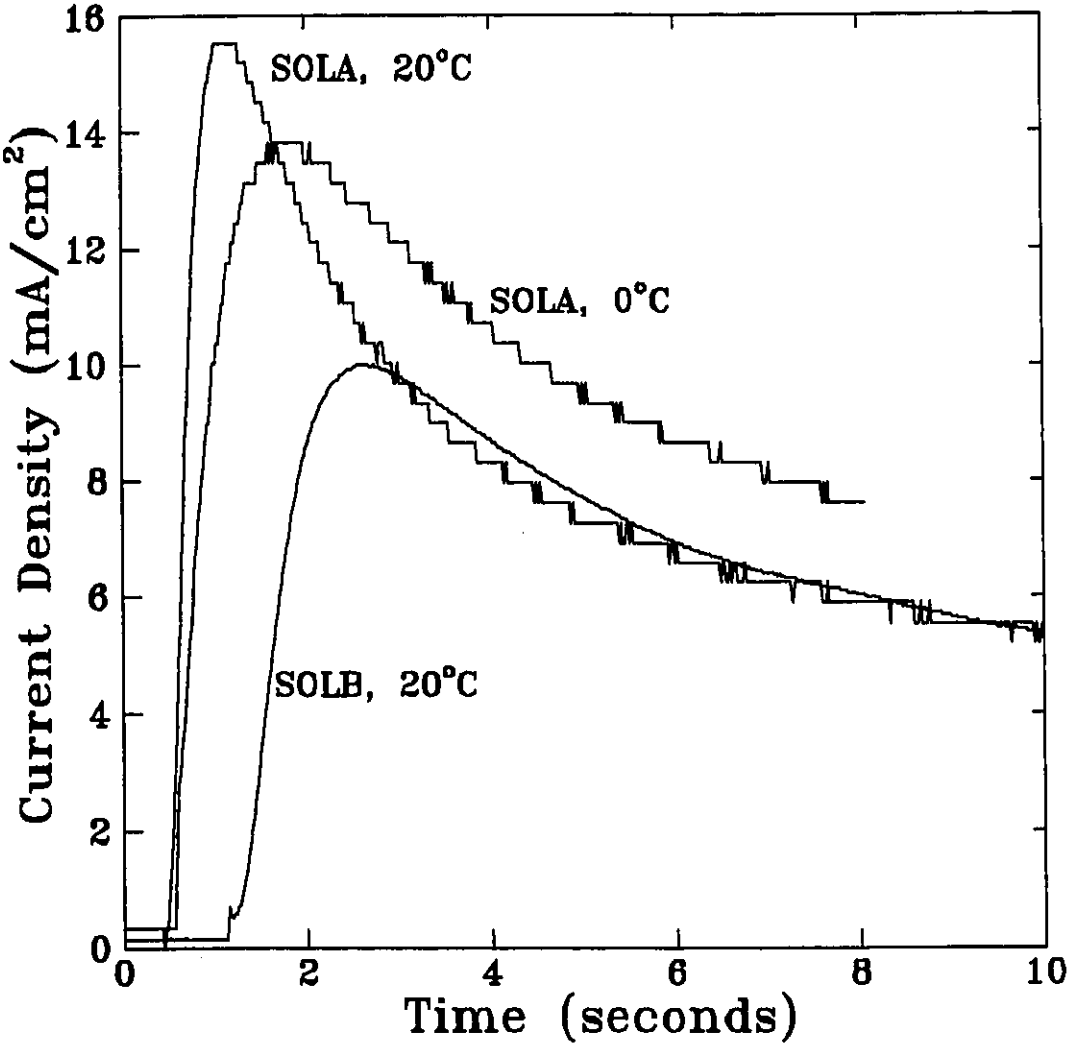

Figure 5.13: Chronoamperometric study of zinc deposition in solutions of 0.05M $ZnBr_2$ and 0.05M $ZnBr_2$ and 0.018M MEPBr, on glassy carbon, E_2 = -1.200 V vs Ag/AgBr reference electrode.

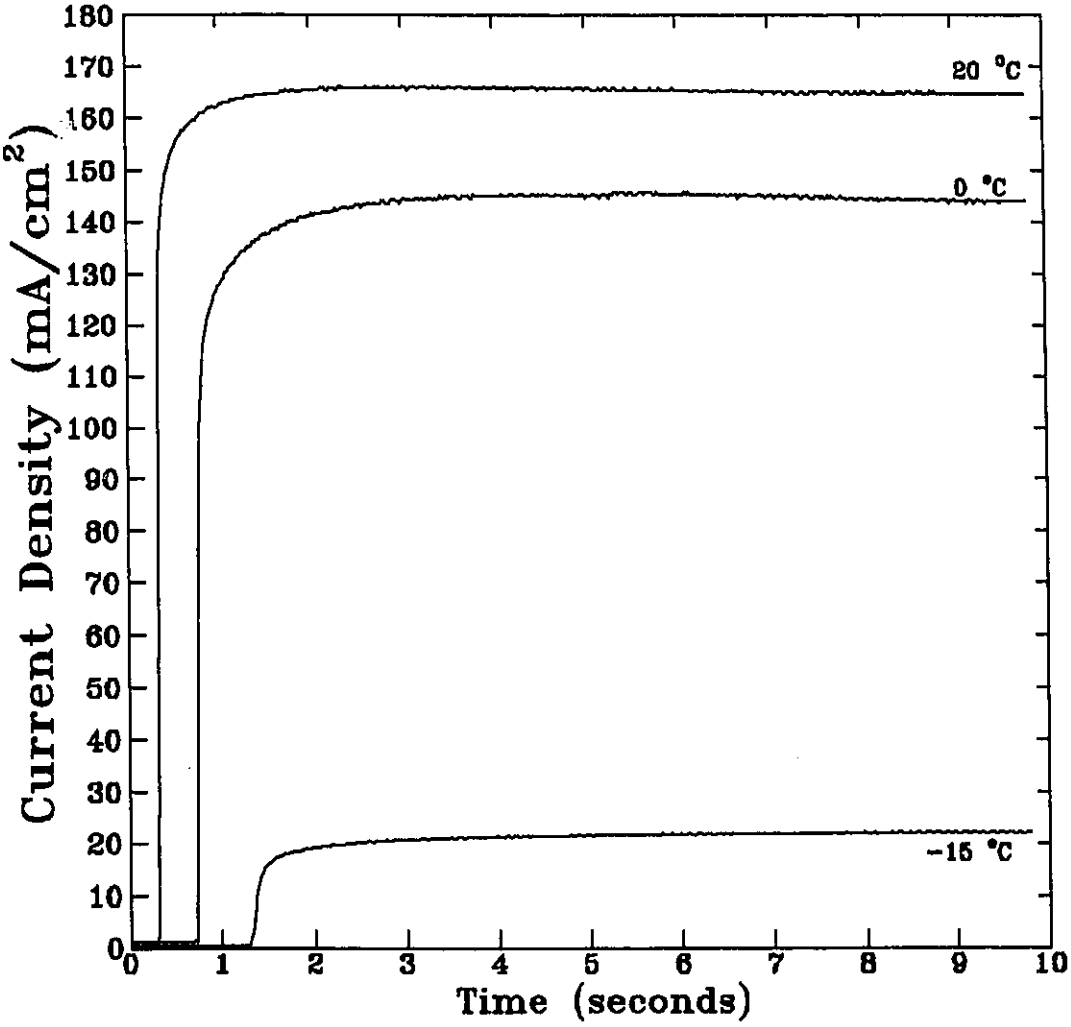

Figure 5.14: Result of chronoamperometric studies of zinc deposition on glassy carbon from SOLC(2.25M $ZnBr_2$, 0.5M $ZnCl_2$, 0.8M MEPBr) as a function of temperature. Potential step -0.310 V.

5.6.2 Discussion of the Chronoamperometric Study in Aqueous $ZnBr_2$ Electrolytes

Figure 5.13 illustrates that the current response to the step potential was similar for both solutions, SOLA and SOLB, indicating that the zinc deposition mechanism was independent of the presence of the quaternary ammonium salt (SOLA: 0 M MEPBr, SOLB: 0.018 M MEPBr). The rising portion of this current density transient (I) was plotted as a function of time (t), the square root of time ($t^{0.5}$), and time raised to the power 1.5 ($t^{1.5}$). Each of these plots was then fit to a linear equation using Asystant GPIB curve fitting software (Asyst, 1988). A linear dependence of I on $t^{0.5}$ is characteristic of instantaneous nucleation, diffusion control, and a linear dependence of j on $t^{1.5}$ is characteristic of progressive nucleation, diffusion control (Southampton, 1990b). Instantaneous nucleation occurs when the nuclear number density rapidly reaches a limiting constant value because the number of sites available at that overpotential has been exhausted or because the onset of depletion and concentration polarization attenuates the overvoltage at the equipotential surface of the substrate. Progressive nucleation occurs when fresh nuclei are formed continuously. The overlap of neighbouring depletion zones is responsible for the current maxima in the I versus t transient. As diffusion zones overlap, replacement of material in the planes close to the electrode surface becomes restricted and the only source of depositing species is that of diffusion down to the surface. The current then approaches a limiting value for diffusion to a planar electrode, and at long times the behaviour of systems undergoing progressive nucleation approaches that of those undergoing instantaneous nucleation. As the diffusion zones grow, the fractional area left uncovered is continuously decreasing and a nucleus born at a site of another diffusion zone will not contribute to the observed current.

Results of analysis of the rising portion of the chronoamperometric experiments are presented in Table 5.12 for the data shown in Figure 5.13 (SOLA at 20 and 0 °C, and SOLB at 20 °C). Similar results were obtained in replicate experiments.

The standard error of the y estimate for the expression $y = mx_i + b$, where x_i is t, $t^{1/2}$, or $t^{3/2}$, is given by:

$$s_y = \sqrt{\frac{\sum (mx_i + b - y_i)^2}{n - 2}} \qquad (5.26)$$

where $mx_i + b$ is the calculated value

y_i is the experimental value

and n is the total number of experimental data points.

The value of R^2, the square of the coefficient of correlation (or the coefficient of determination) is also calculated, and is defined below:

$$R^2 = \frac{\sum (mx_i + b - \bar{y})^2}{\sum (y_i - \bar{y})^2} \qquad (5.27)$$

where $\bar{y}$ is the average of the y_i observations.

Table 5.12: Results of the analysis of the rising portion of chronoamperometric experiments shown in Figure 5.13 for zinc deposition on glassy carbon in electrolytes of 0.05 M $ZnBr_2$ and 0.05 M $ZnBr_2$, 0.018 M MEPBr. s_y is the standard error of the y estimate, s_m is the standard error of the slope, R^2 is the coefficient of determination.

X	b	s_y	R^2	m	s_m
SOLA, 20 °C					
t	-20.8370	0.2943	0.9938	42.6991	0.9757
$t^{1/2}$	-49.2091	0.2234	0.9964	69.7401	1.2078
$t^{3/2}$	-11.3787	0.3794	0.9897	34.7299	1.0250
SOLA, 0 °C					
t	-8.9886	0.1782	0.9949	19.5577	0.3210
$t^{1/2}$	-23.9997	0.1312	0.9972	34.3745	0.4151
$t^{3/2}$	-3.9837	0.2479	0.9901	14.7456	0.3376
SOLB, 20 °C					
t	-14.2341	0.1667	0.9924	11.7798	0.2060
$t^{1/2}$	-33.7198	0.1281	0.9955	30.3345	0.4069
$t^{3/2}$	-7.7386	0.2059	0.9884	6.0857	0.1317

Figures 5.15, 5.16, and 5.17 are plots of the residuals as a function of time for each of the three experiments presented in Table 5.12 and Figure 5.13. These plots indicated that models based on I dependence on both $t^{0.5}$ and $t^{1.5}$ tended to underestimate current density at long times. This is to be expected as the linear dependence of j on $t^{0.5}$ and $t^{1.5}$ is characteristic of the nucleation phase only. At longer times, deposition was diffusion controlled. At short times, the model based on I dependence on $t^{1.5}$ underestimated the experimental value for several experiments (as shown in Figures 5.16, 5.17). Results presented in Figures 5.15 to 5.17 and Table 5.12 showed, for both Quat containing and Quat free solutions, that the rising transient was best plotted as a linear function of $t^{0.5}$, indicating instantaneous nucleation. Also, addition of the quaternary solution to the electrolyte did not influence the zinc deposition mechanism. Further, the fact that the current passes through a maximum and decreases indicated that the thickening of the zinc layer is diffusion controlled.

These results are in agreement with the work of McBreen *et al.* (1983) who found an instantaneous nucleation, kinetic growth control mechanism for zinc deposition on glassy carbon in 3 M zinc bromide electrolyte. Due to the high concentration of the electrolyte in the study of McBreen *et al.* (1983), no diffusion control stage was observed for the zinc deposition reaction.

A plateau in the current density response to a step in potential, as shown in Figure 5.14 (SOLC), is indicative of electron transfer or steady state control of the deposition mechanism. Models applied to current density response of electrolytes SOLA and SOLB are not applicable to the standard high concentration battery electrolytes as these models are based on diffusion control mechanisms. Models have been developed which assume the rate determining step in the electrocrystallization process is the incorporation of atoms or molecules at the expanding periphery of the growth centres. The model based on three dimensional growth, and instantaneous nucleation is (Southampton, 1990b):

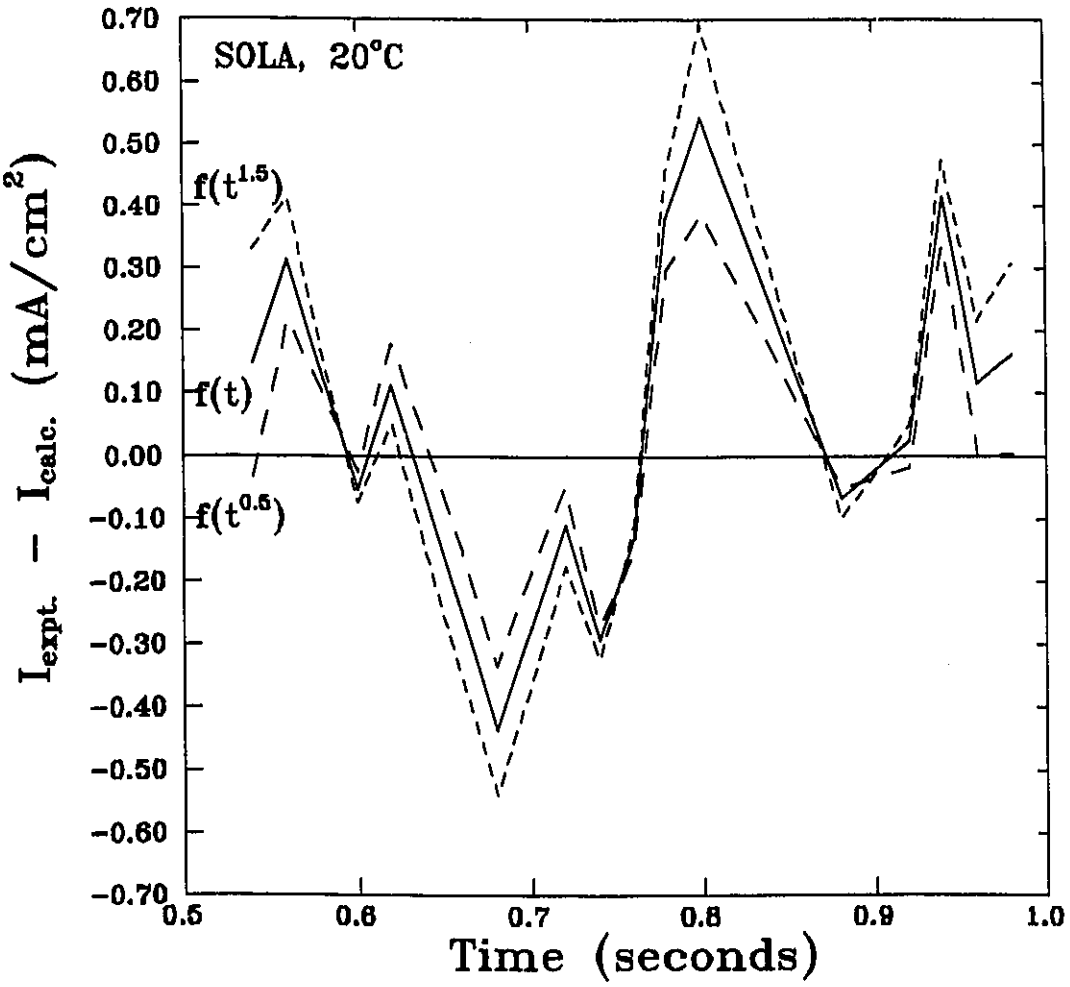

Figure 5.15: Residuals as a function of time for the rising portion of the chronoamperometric experiment shown in Figure 5.13 for SOLA, 20 °C, E_2=-1.2 V vs Ag/AgBr reference electrode.

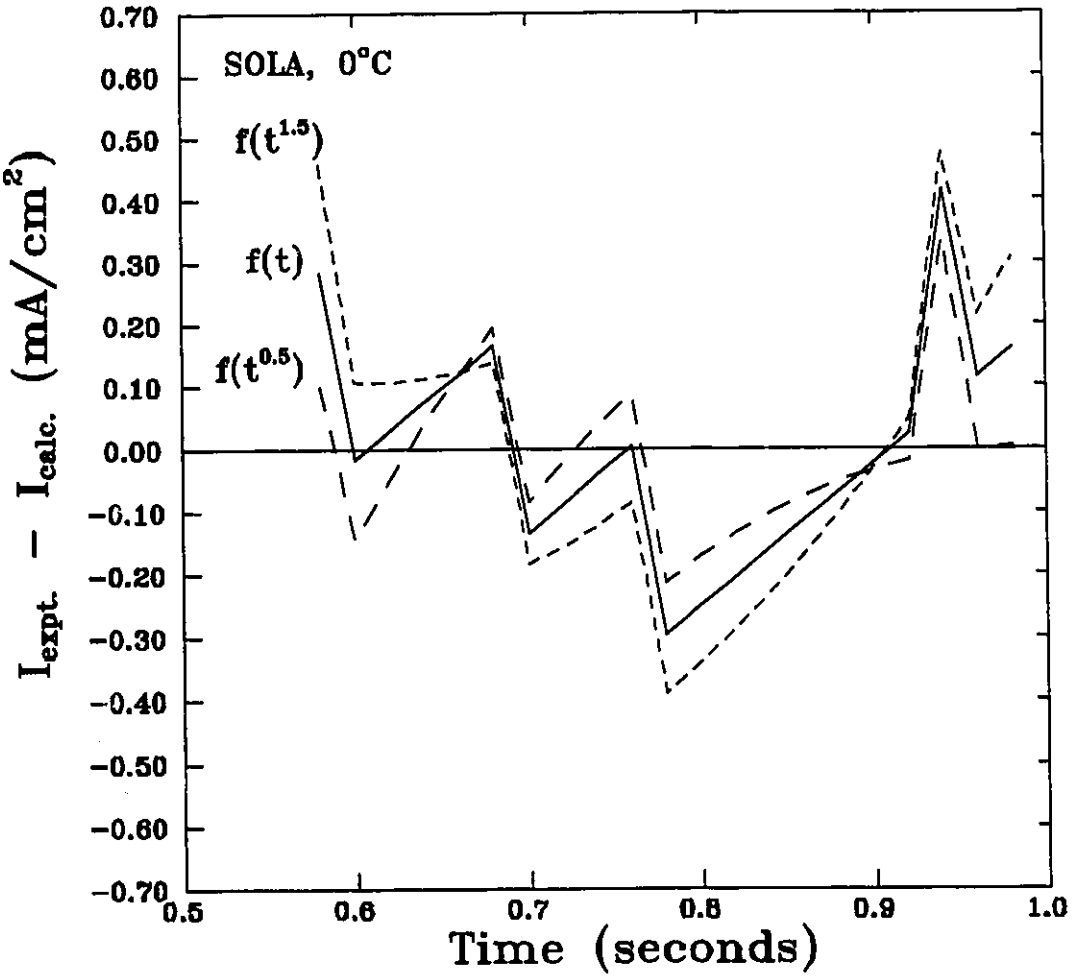

Figure 5.16: Residuals as a function of time for the rising portion of the chronoamperometric experiment shown in Figure 5.13, 0 °C, E_2=-1.2 V vs Ag/AgBr reference electrode.

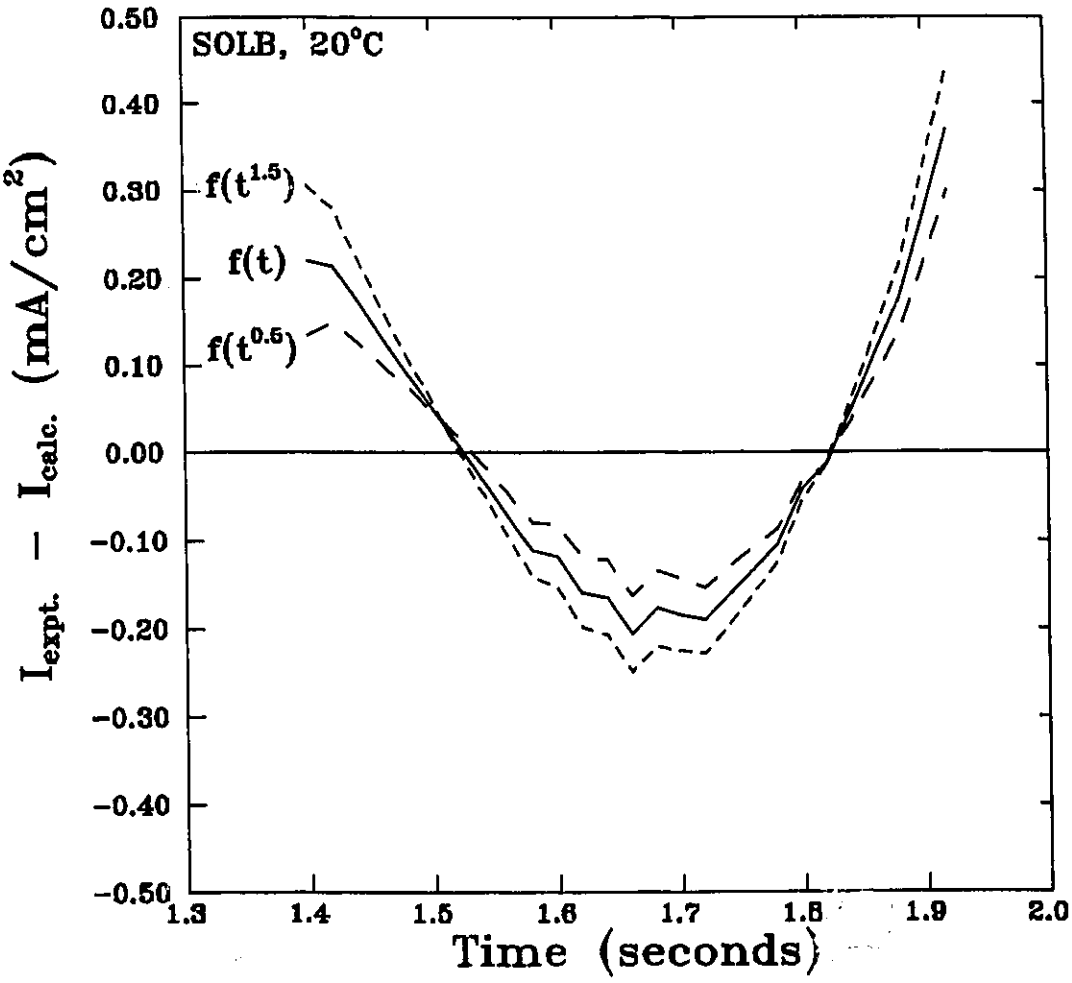

Figure 5.17: Residuals as a function of time for the rising portion of the chronoamperometric experiment shown in Figure 5.13 for SOLB, 20 °C, E_2=-1.20 V vs Ag/AgBr reference electrode.

$$I(instantaneous) = nFk' \left(1 - \exp\left(-\frac{\pi M^2 k^2 N_o t^2}{\rho^2}\right)\right) \qquad (5.17)$$

and that based on three dimensional growth, and progressive nucleation is:

$$I(progressive) = nFk' \left(1 - \exp\left(-\frac{\pi M^2 k^2 N_o A t^3}{3\rho^2}\right)\right) \qquad (5.18)$$

The general chronoamperometric behaviour predicted by these equations can be seen by examination of the limiting forms of the equations. At short times, the exponential terms in equations 5.17 and 5,18 are sufficiently small that the expressions reduce to functions of t^2, and t^3 for instantaneous and progressive nucleation, respectively. At long times, both expressions approach nFk', as growth is restricted to the perpendicular direction.

For models based on two distinct growth rates, one lateral and one vertical, several other equations have been developed by Bosco and Rangarajan (1982). For lateral growth rate proportional to $t^{-1/2}$, and vertical growth under electron transfer control (i.e., constant current), then the current law is:

$$\begin{aligned} I &= \frac{nF\rho v}{M}\left(1 - \exp\left(-4N_o\pi\mu^2 t\right)\right) \text{ for } t \to 0 \\ &= \frac{nF\rho v}{M}\left(1 - \frac{1}{4N_o^{1/2}\mu t^{1/2}} + \frac{\exp(-4N_o\pi\mu^2 t)}{8N_o\pi\mu^2 t}\right) = \frac{nF\rho v}{M} \text{ for } t \to \infty \\ &= A\left(1 - 0.88(Bt)^{-1/2} + \frac{\exp(-Bt)}{2Bt}\right) \end{aligned} \qquad (5.28)$$

Each of the equations 5.17 and 5.18 and 5.28, describe the basic shape of the transients obtained for chronoamperometry experiments for zinc deposition on glassy carbon from standard battery electrolytes. Figure 5.18 shows a typical experimental chronoamperometric response at 20 °C, potential step -0.210 V. Equations 5.17, 5.18

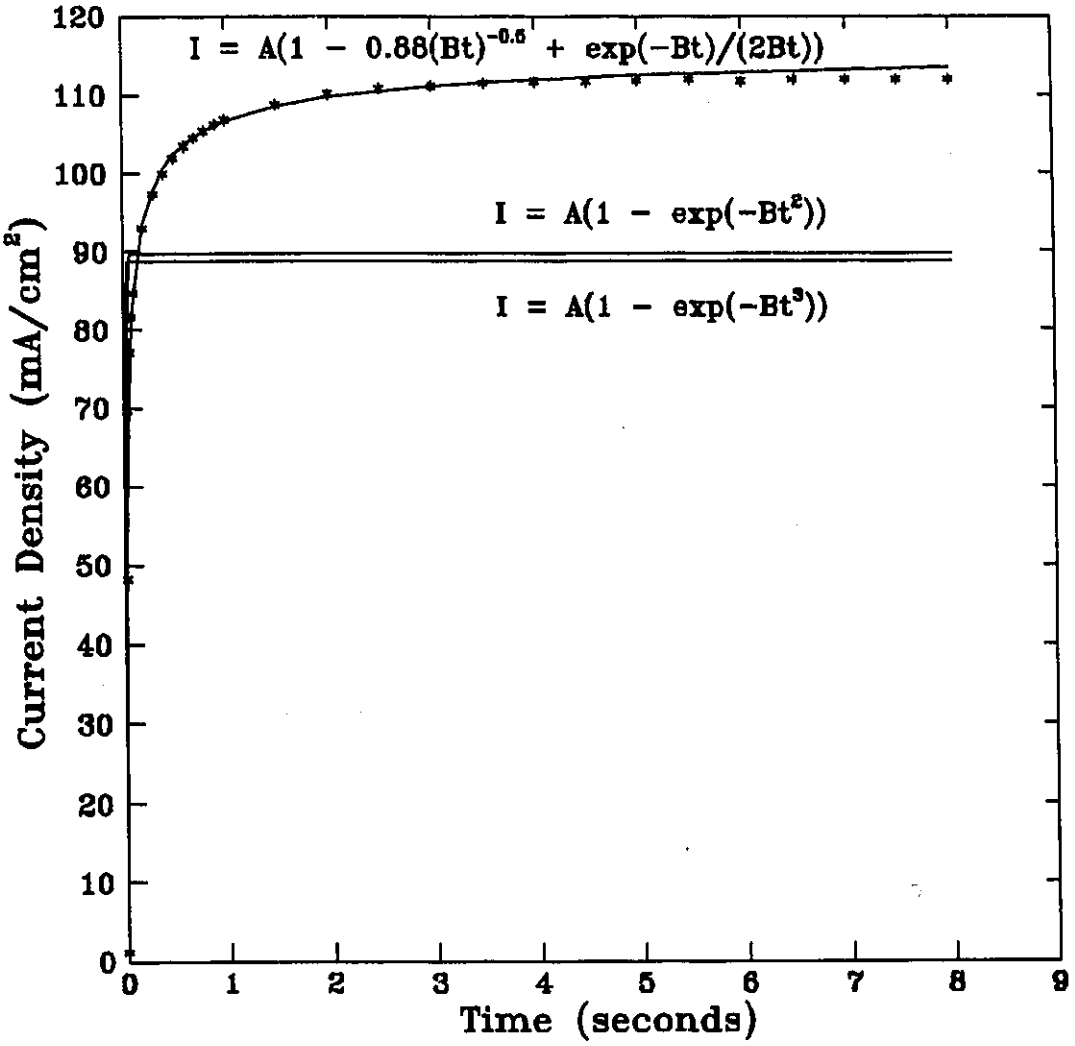

Figure 5.18: Potentiostatic transients for zinc deposition from aqueous solution SOLC (2.25M $ZnBr_2$, 0.5M $ZnCl_2$, 0.8M MEPBr) onto glassy carbon at 25 °C, E_2=-0.210.

were fit to the data with Asystant GPIB Curve Fitting Software using a Gauss-Newton curve fitting algorithm (Asyst, 1988), and are plotted in Figure 5.18. Equation 5.28, for time approaching infinity, was also fit to the data and is also shown in Figure 5.18.

Clearly models based on instantaneous and progressive nucleation (Equations 5.17 and 5.18) fail to describe the behaviour of the transient at times greater than 1 second. The two rate model of Equation 5.28, for large time, best described the behaviour of the transient. Results of individual experiments for each temperature (-15, 0, 25 °C) and overpotential (-0.210 V, -0.310 V) were fit by the two rate model of Equation 5.28. The average values for $nF\rho v/M$ and $4N_o\pi\mu^2$ are shown in Table 5.13.

Table 5.13: Average values obtained for $nF\rho v/M$ and $4N_o\pi\mu^2$ for potentiostatic transient for the deposition of zinc from an aqueous solution of 2.25 M $ZnBr_2$, 0.5 M $ZnCl_2$, 0.8 M MEPBr onto glassy carbon determined for the two rate model described in Equation 5.28

Temperature (°C)	Overpotential (mV)	$(nF\rho/M)v$ (mA/cm^2)	$(4N_o\pi)\mu^2$ (s)	$2\sqrt{N_o}\sqrt{\pi}\mu$ (s$^{0.5}$)
20	-210	117±15	95±2	9.7±0.2
20	-310	176±15	369±8	19.2±0.4
0	-210	99±15	10±4	3±1
0	-310	154±15	110±10	10±1
-15	-210	39±6	9±1	3.0±0.3
-15	-310	54±7	62±2	7.9±0.2

Parameter $(nF\rho/M)v$ is related to the vertical growth rate of the zinc deposit, and parameter $(4N_o\pi)\mu^2$ is related to the lateral growth rate of the zinc deposit. Increasing the overpotential increased both the vertical and lateral growth rates. Decreasing temperature decreased both the vertical and lateral growth rates, but appears to have a greater effect on the lateral growth rate. According to this model, lateral growth dominates initially, and at long times, vertical growth is the dominant mechanism. Thus, the lateral growth corresponds to zinc deposition on carbon, and the vertical growth is predominantly zinc depositing on zinc. These results indicate that deposition on carbon (lateral growth) is

more significantly affected by both temperature and overpotential than is the vertical growth rate (zinc deposition on zinc). As a result, both the maximum current density achieved and the rate at which the current density increases were reduced as temperature and overpotential were reduced. A kinetic growth control mechanism is suggested as the current density versus time transient reaches a maximum value and then remains constant.

McBreen and Gannon (1983) identified instantaneous nucleation and growth under kinetic control as the deposition mechanism for zinc on glassy carbon from 3 M $ZnCl_2$ aqueous solution. McBreen and Gannon (1983) were unable to fit data obtained for deposition from aqueous 3 M $ZnBr_2$ to the instantaneous nucleation, kinetic growth mechanism, but microscopic observations indicated that all zinc growths were identical in size, thus suggesting instantaneous nucleation.

5.6.3 Conclusions of The Chronoamperometric Study of Zinc Deposition

Chronoamperometric studies in solutions SOLA and SOLB were in agreement with the work of McBreen and Gannon (1983) that suggests zinc deposition on glassy carbon occurs via an instantaneous nucleation mechanism. Addition of quaternary ammonium complexing agent did not effect the shape of the current density transient.

An equation based on a two rate model (distinct growth rates in vertical and lateral directions) described the current density transient obtained in standard battery electrolytes (2.25 M $ZnBr_2$, 0.5 M $ZnCl_2$, 0.8 M MEPBr) (Bosco and Rangarajan, 1982). Our work suggests a kinetic control mechanism at long times (i.e., when vertical growth dominates). It was not possible to fit the current density transients obtained in SOLC (2.25 M $ZnBr_2$, 0.5 M $ZnCl_2$, 0.8 M MEPBr) by an expression describing an instantaneous nucleation three dimensional growth mechanism as suggested by McBreen and Gannon (1983). However, both our study and the earlier work of McBreen and Gannon (1983) suggest that zinc deposition is under kinetic control after initial nucleation occurs.

5.7 Electrochemistry of Alternate Electrolytes

5.7.1 Zinc Electrochemistry

The zinc deposition reaction was studied at a glassy carbon electrode in alternate electrolyte solutions, SOLD, SOLE, and SOLF. The composition of these electrolytes is shown below in Table 5.14.

Table 5.14: Composition of solutions used in electrochemistry experiments

Electrolyte	Composition
SOLC	2.25 M $ZnBr_2$, 0.5 M $ZnCl_2$, 0.8 M MEPBr
SOLD	2.25 M $ZnBr_2$, 0.5 M $ZnCl_2$, 0.8 M MEPBr, 3.1 M ethylene dichloride (25 volume %)
SOLE	2.25 M $ZnBr_2$, 0.5 M $ZnCl_2$, 0.8 M MEPBr, 3.3 M propan-2-ol (25 volume %)
SOLF	2.25 M $ZnBr_2$, 0.5 M $ZnCl_2$, 0.8 M MEPBr, 4.5 M ethylene glycol (25 volume %)

Cyclic voltammetry experiments were conducted between -20 and 25 °C over the voltage range -0.500 to -1.0 V versus a Ag/AgBr reference electrode. Cyclic voltammograms collected in these solutions were similar to those in SOLC (standard battery electrolyte) and are shown in Figures 5.19 to 5.21. In each case, zinc deposition on glassy carbon required a considerable overpotential. The nucleation overpotential increased with both potential scan rate and decreasing temperature in all solutions. Generally, the cyclic voltammograms recorded in alternate electrolytes were characterized by lower current density and higher overpotential at ambient temperatures. Table 5.15 shows the overpotential as a function of temperature for each of the alternate electrolytes. The results presented in Table 5.15 were calculated as the average of three separate experiments. A comparison of the maximum current densities achieved indicated that the mixed aqueous/organic electrolytes have higher solution resistance, and therefore, batteries incorporating these electrolytes will require higher overvoltage to charge. Further, they will also discharge at lower rates.

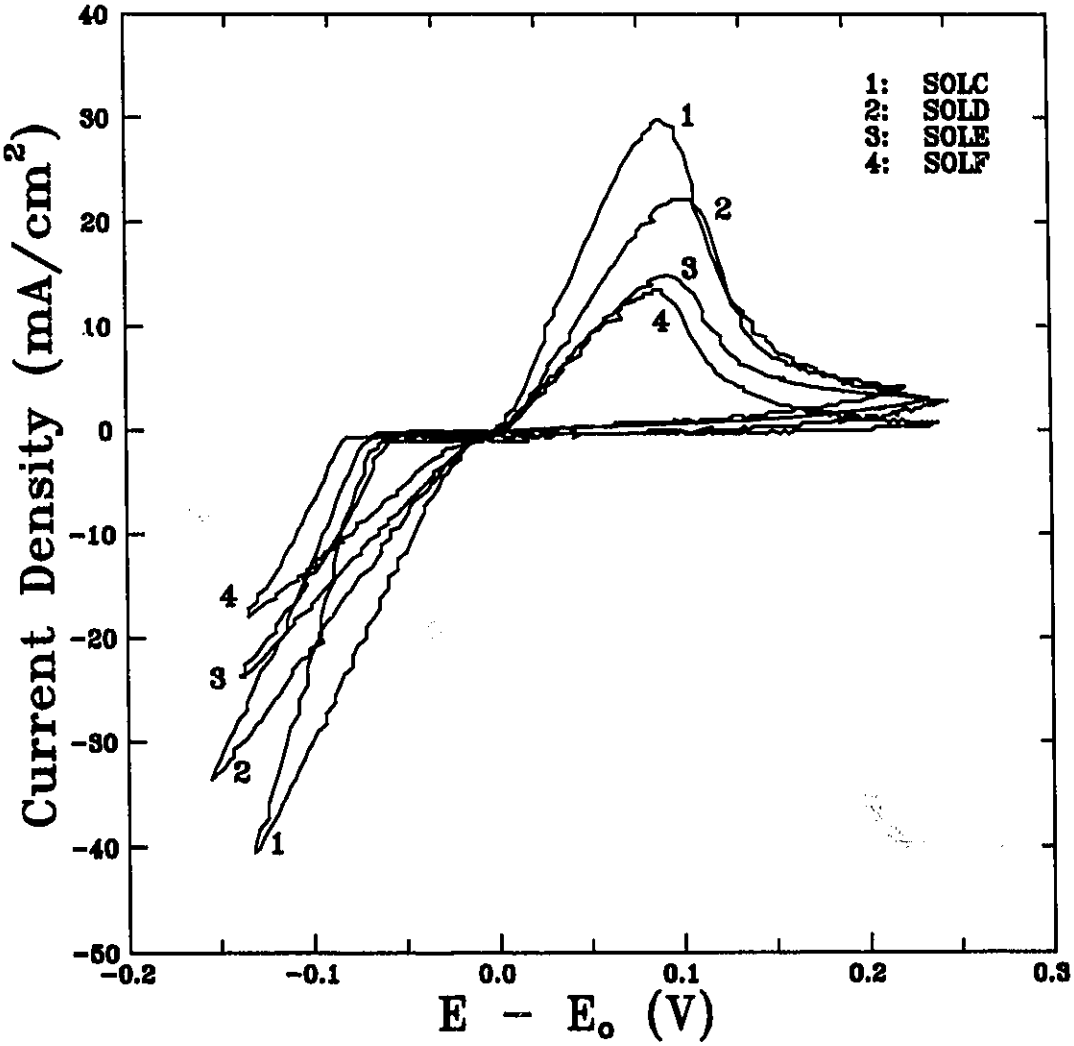

Figure 5.19: Cyclic voltammograms for zinc deposition/stripping on glassy carbon at 25 °C, and sweep rate 50 mV/s, for SOLC, SOLD, SOLE, and SOLF.

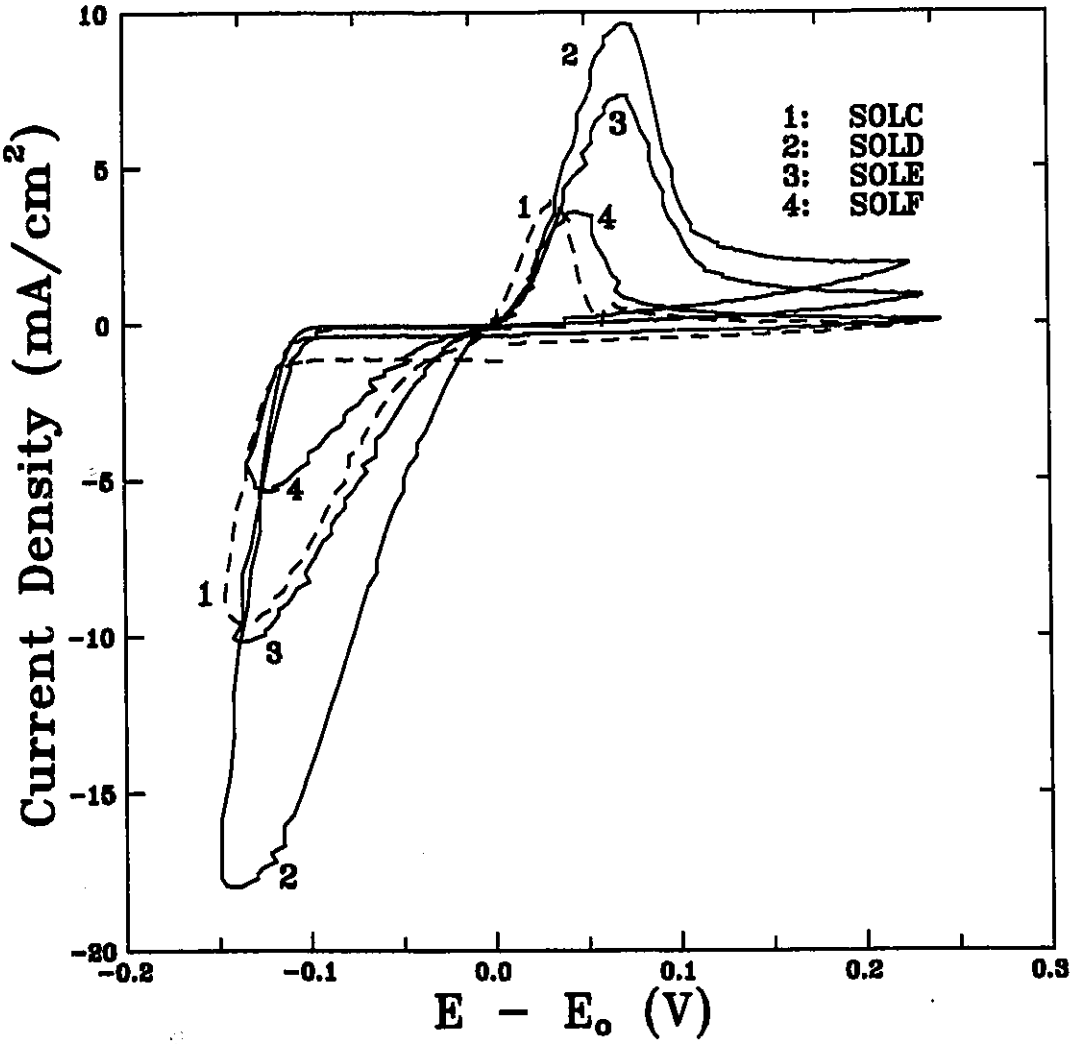

Figure 5.20: Cyclic voltammograms for zinc deposition/stripping on glassy carbon at 0 °C, and sweep rate 50 mV/s, for SOLC, SOLD, SOLE, and SOLF.

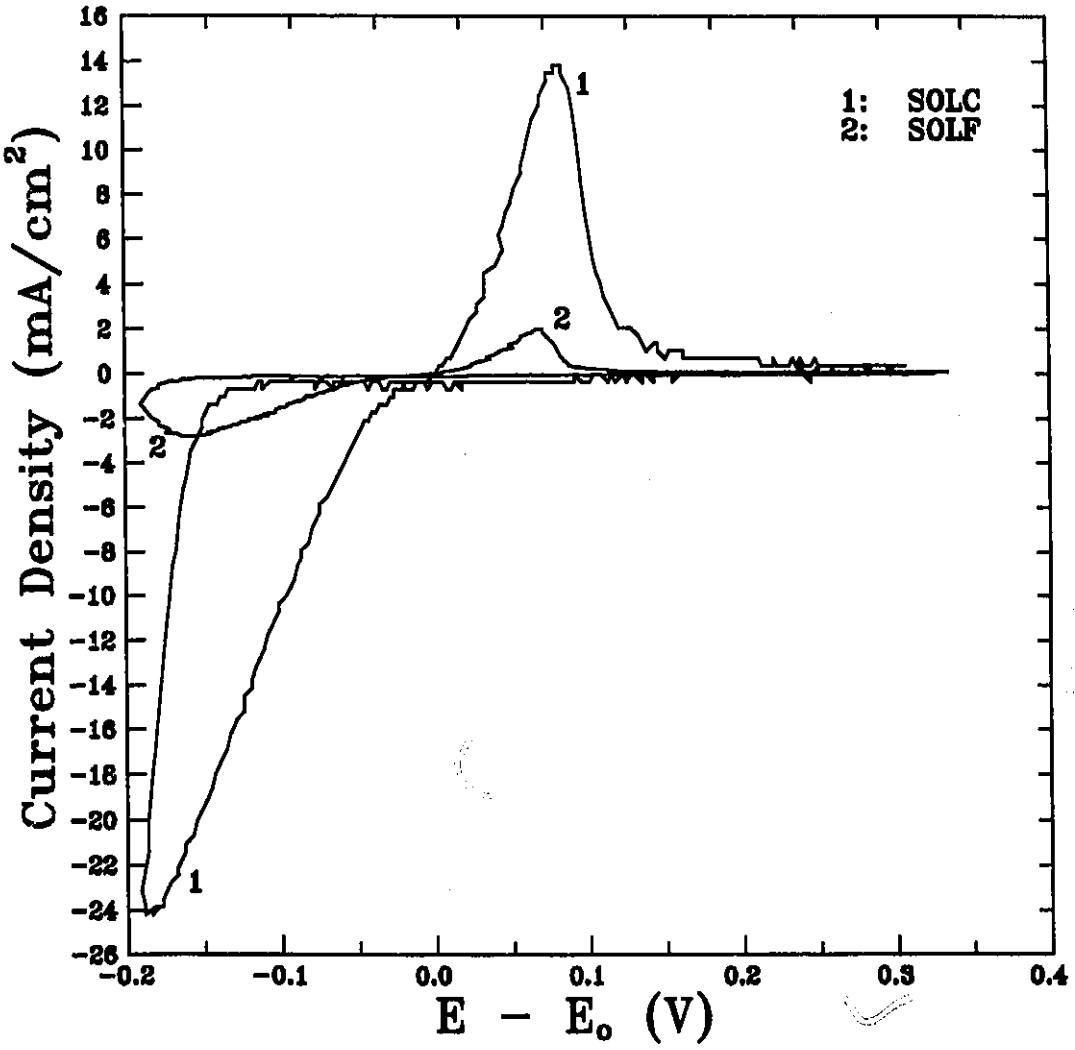

Figure 5.21: Cyclic voltammograms for zinc deposition/stripping on glassy carbon at -15 °C, and sweep rate 50 mV/s, for SOLC and SOLF.

Table 5.15: Zinc deposition overpotential and redox charge ratios as a function of scan rate and temperature.

Solution	Temperature (° C)	Scan Rate (mV/s)	Overpotential (mV)	Q_A/Q_C(%)
SOLC: 2.25 M $ZnBr_2$, 0.5 M $ZnCl_2$, 0.8 M MEPBr	25	50	55±3	72±5
	25	1	31±1	94±1
	0	50	93±7	65±10
	0	1	42±2	84±5
	-15	50	113±2	38±2
SOLD: 2.25 M $ZnBr_2$, 0.5 M $ZnCl_2$, 0.8 M MEPBr, 3.1 M ethylene dichloride	25	50	64±3	80±10
	25	5	47±2	85±5
	0	50	92±7	76±10
	0	5	61±9	88±9
	-20	10	96±7	73±10
	-20	5	85±5	85±3
SOLE: 2.25 M $ZnBr_2$, 0.5 M $ZnCl_2$, 0.8 M MEPBr, 3.3 M propan-2-ol	25	50	76±4	66±4
	25	10	60±7	70±2
	25	5	44±1	69±9
	25	1	33±2	74±7
	0	50	78±3	69±10
	0	10	62±1	80±2
	0	5	57±1	78±4
	0	1	42±1	79±8
	-10	50	97±8	45±7
	-10	5	55±1	76±6
SOLF: 2.25 M $ZnBr_2$, 0.5 M $ZnCl_2$, 0.8 M MEPBr, 4.5 M ethylene glycol	25	50	73±3	66±6
	25	10	59±7	38±10
	25	5	43±2	53±2
	25	1	35±3	69±5
	0	50	79±4	52±9
	0	1	43±2	78±6
	-15	50	123±15	66±10
	-15	1	58±4	81±4

As temperature was decreased, however, the overpotential associated with the alternate electrolytes decreased with respect to that of standard battery electrolyte. Batteries incorporating these alternate electrolytes will show relatively better performance than standard electrolyte batteries, as temperature is decreased.

Chronoamperometric studies of zinc deposition were conducted in alternate (SOLE, SOLF) electrolytes as well as the standard battery electrolyte (SOLC). The experimental results achieved in SOLE and SOLF were similar in form to those in standard Zn/Br_2 battery electrolyte and results of the curve fitting analysis are summarized in Table 5.16. For all electrolytes, the two rate model of Bosco and Rangarajan (1982) best fit the data.

Table 5.16: Calculated values of lateral and vertical growth rate constants for standard battery electrolyte and alternate electrolytes as a function of potential step and temperature. Each table entry represents an average of three experiments, parameter A is related to the vertical growth rate, and B is related to the lateral growth rate (see Equation 5.28 and Table 5.13 for definition of parameters A and B).

Over - potential (V)	Temperature 20 °C		Temperature 0 °C		Temperature -15 °C	
	A	B	A	B	A	B
STANDARD BATTERY ELECTROLYTE: SOLC						
0.200	117 ± 15	95 ± 2	99 ± 15	10 ± 4	39 ± 6	9 ± 1
0.300	176 ± 15	369 ± 8	154 ± 15	110 ± 10	54 ± 7	62 ± 2
2.25 M $ZnBr_2$, 0.5 M $ZnCl_2$, 0.8 M MEPBr, 3.3 M PROPAN-2-OL: SOLE						
0.100	23.1 ± 0.8	27.6 ± 4				
0.150	38.1 ± 0.5	67 ± 4				
0.200	55.9 ± 0.8	106 ± 14	23.8 ± 0.6	40 ± 5	8.8 ± 0.1	6.3 ± 0.3
0.300	96 ± 1	611 ± 50	60 ± 1	157 ± 10	20.1 ± 0.4	38 ± 4
2.25 M $ZnBr_2$, 0.5 M $ZnCl_2$, 0.8 M MEPBr, 4.5 M ETHYLENE GLYCOL: SOLF						
0.140	26.8 ± 0.2	5.1 ± 0.2				
0.200	46 ± 1	34 ± 4	26.5 ± 0.9	26 ± 4	17 ± 1	4.6 ± 0.8
0.300	80 ± 1	137 ± 8	52 ± 1	55 ± 8		

On increasing the potential from rest to a cathodic potential sufficient to deposit zinc, the current transient rose sharply. After the sharp rise, a current plateau was reached and maintained throughout the experiment. As the step potential increased both the lateral and vertical deposition rates increased (i.e., A and B from Equation 5.28 increased). As temperature decreased, in all electrolytes, the maximum current density of the plateau decreased. As well, the current transient increased at a slower rate as indicated by the decreasing value of B with decreasing temperature. In both mixed aqueous/organic and standard electrolytes, the lateral growth rate (parameter B) was more affected by both temperature and overpotential than was the vertical growth rate.

It was found that the addition of the organics reduced the maximum current density and electrolyte conductivity achieved, but the electrochemistry results indicated that it did not alter the deposition mechanism. Reduction in current density and reversibility must be balanced against the reduction in the freezing point when designing a low temperature electrolyte.

5.7.2 Bromine Electrochemistry

An electrochemical study of bromide oxidation/bromine reduction at a glassy carbon electrode was conducted in solutions SOLC, SOLD, SOLE, and SOLF. Cyclic voltammograms at 500 and 10 mV/s and 25 and 0 °C are shown in Figures 5.22 to 5.25.

The glassy carbon working electrode was initially scanned toward more positive potentials; at 1.200 V versus the Ag/AgBr reference electrode the scan direction was reversed. The anodic peak (between 0.9 to 1.2 V vs Ag/AgBr reference) corresponded to bromide oxidation to bromine, and the reverse peak (potential < 0.9 V vs Ag/AgBr reference) corresponded to bromine reduction to bromide. These voltammograms indicated that the bromide oxidation/bromine reduction reaction was quasi-reversible in all electrolytes. Results for cyclic voltammetry experiments on bromide oxidation/bromine reduction are shown in Tables 5.17 to 5.20.

The ratio of the charge associated with bromine reduction to that of bromide oxidation was generally lower than that for the zinc reactions discussed previously. If this

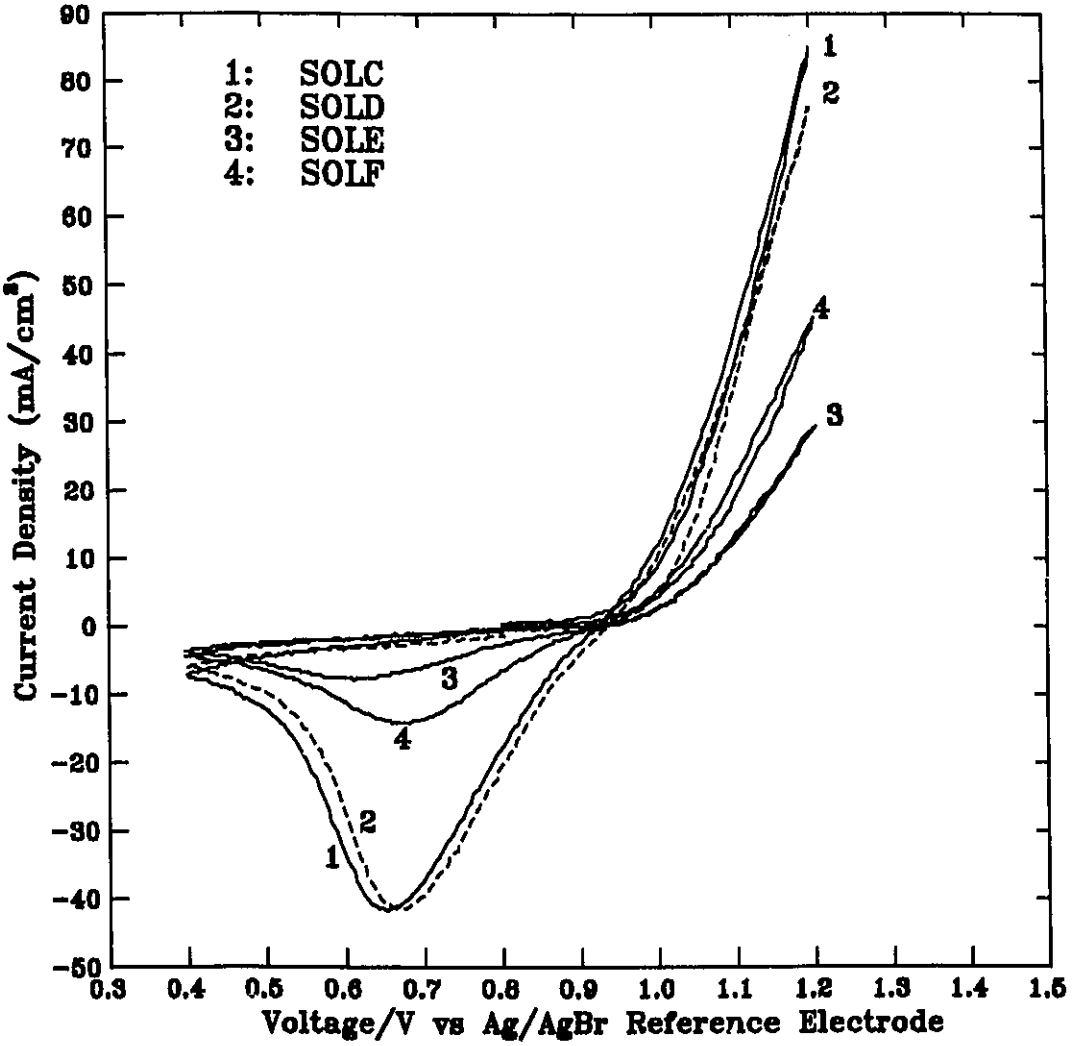

Figure 5.22: Cyclic voltammograms of bromide oxidation/bromine reduction on glassy carbon, 25 °C, 500 mV/s.

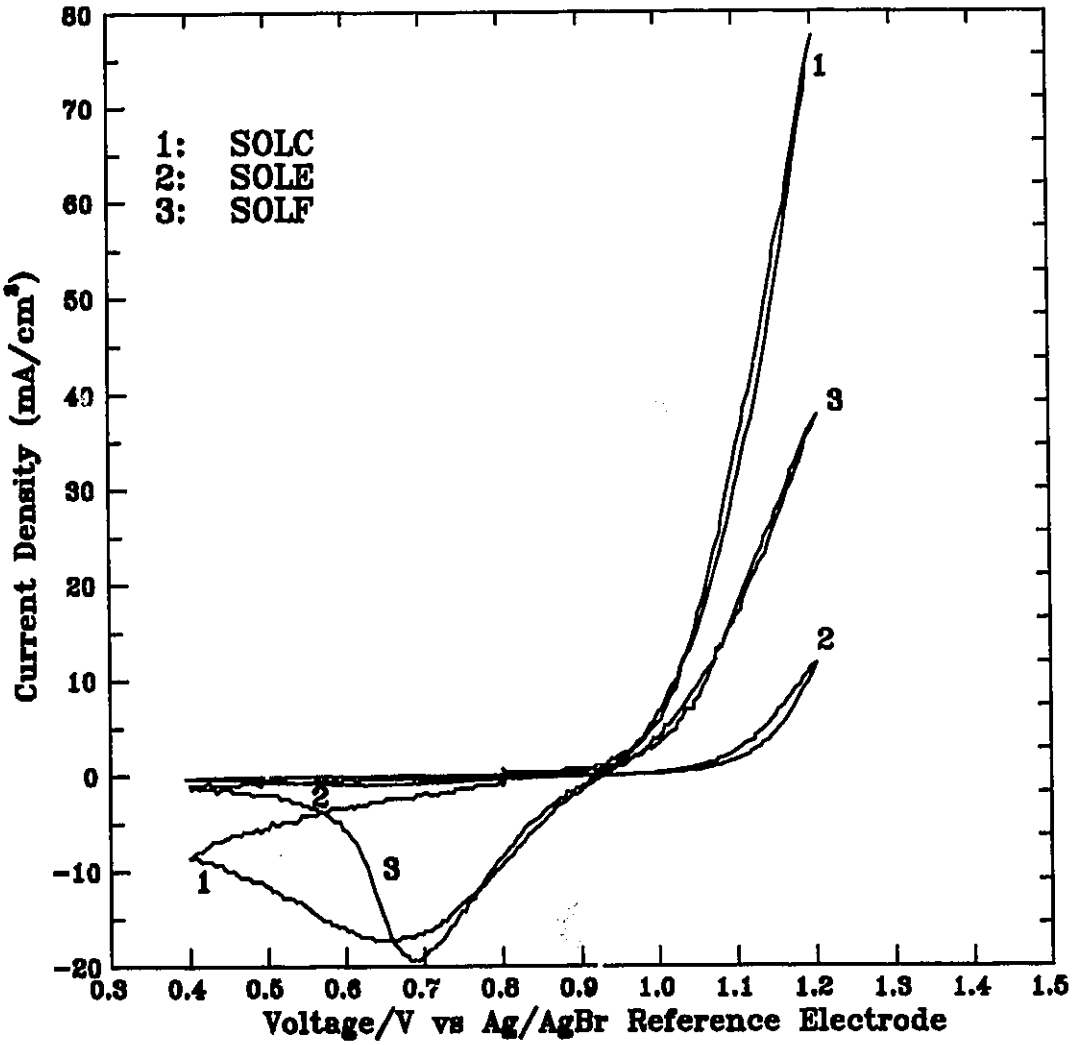

Figure 5.23: Cyclic voltammograms of bromide oxidation/bromine reduction on glassy carbon, 10 mV/s, 25 °C.

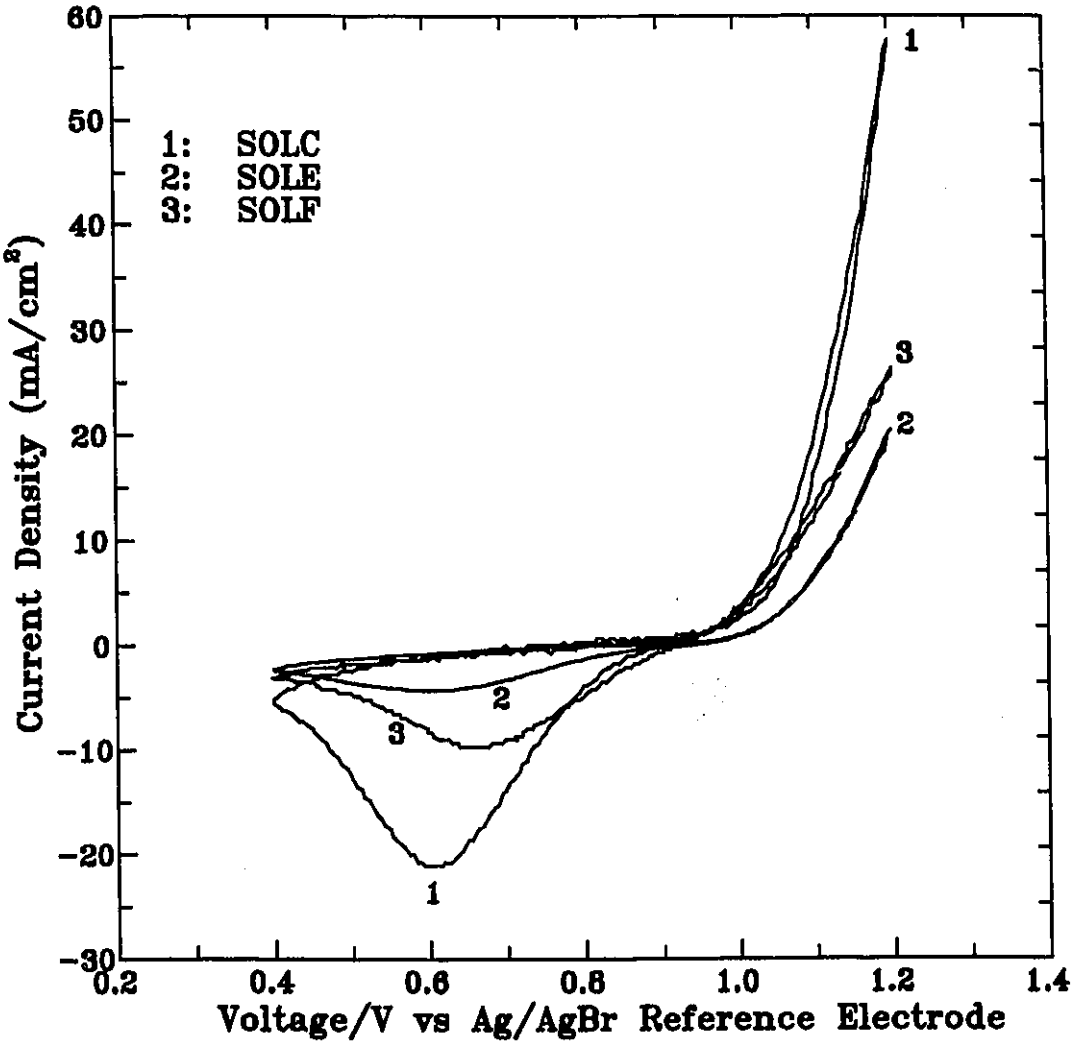

Figure 5.24: Cyclic voltammograms of bromide oxidation/bromine reduction on glassy carbon, 500 mV/s, 0 °C.

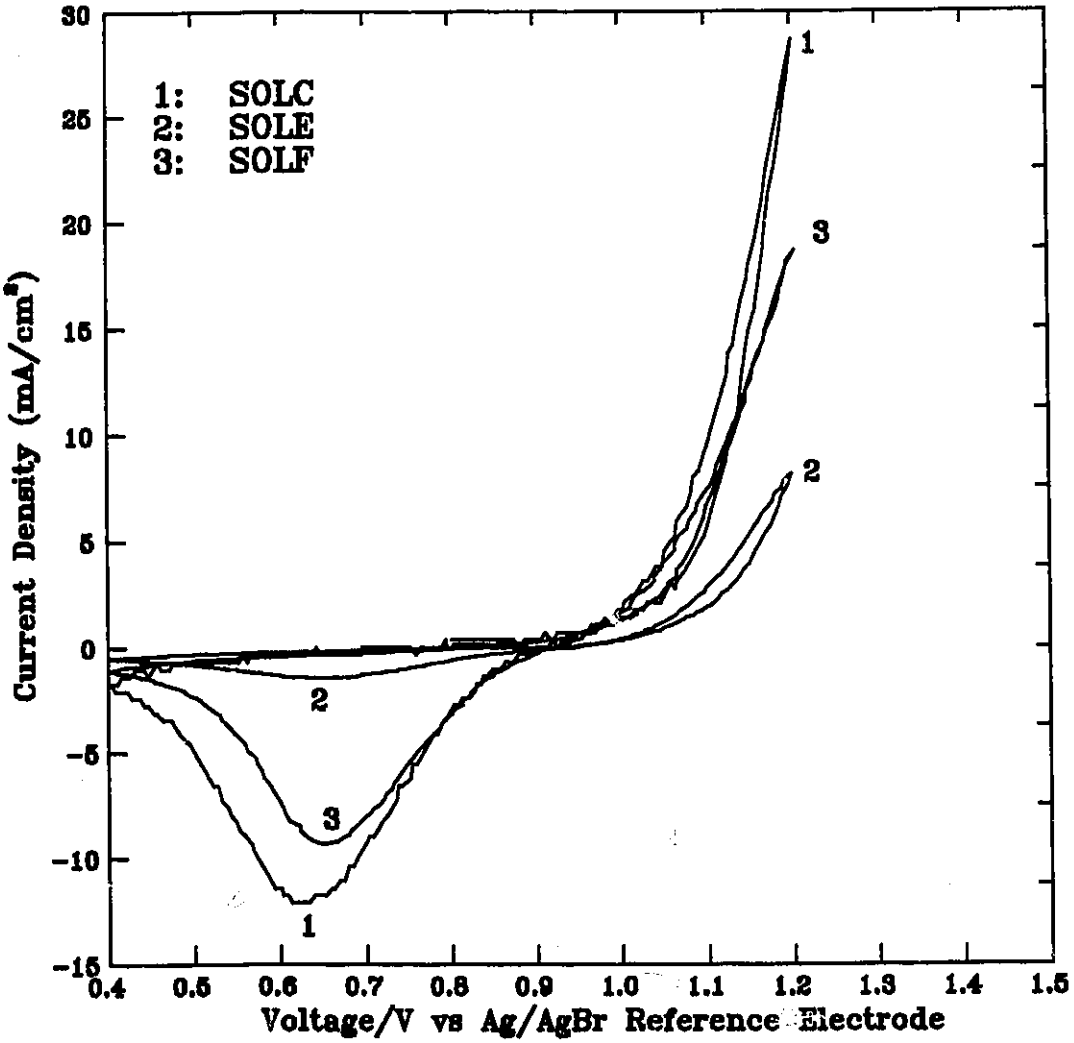

Figure 5.25: Cyclic voltammograms of bromide oxidation/bromine reduction on glassy carbon, 10 mV/s, 0 °C.

Table 5.17: Cyclic voltammetry results for bromide oxidation/bromine reduction on glassy carbon as a function of scan rate and temperature for standard battery electrolyte: SOLC.

Temperature (°C)	Scan Rate (mV/s)	Q_C/Q_A (%)	I_A (mA/cm^2)	I_C (mA/cm^2)	$E_O - E_C$ (mV)
STANDARD BATTERY ELECTROLYTE: SOLC					
25	500	66 ± 1	84 ± 4	41 ± 5	271 ± 4
25	10	55 ± 5	71 ± 5	17 ± 1	270 ± 9
0	500	64 ± 2	57 ± 5	22 ± 3	292 ± 12
0	10	72 ± 2	33 ± 5	13 ± 1	280 ± 21
-15	500	76 ± 7	24 ± 6	12 ± 4	295 ± 12
-15	10	83 ± 4	17 ± 1	10 ± 1	305 ± 14

Table 5.18: Cyclic voltammetry results for bromide oxidation/bromine reduction on glassy carbon as a function of scan rate and temperature for alternate battery electrolyte: SOLE.

Temperature (°C)	Scan Rate (mV/s)	Q_C/Q_A (%)	I_A (mA/cm^2)	I_C (mA/cm^2)	$E_O - E_C$ (mV)
2.25 M $ZnBr_2$, 0.5 M $ZnCl_2$, 0.8 M MEPBr, 3.3 M PROPAN-2-OL: SOLE					
25	500	54 ± 2	29 ± 2	8 ± 1	314 ± 17
25	100	57 ± 1	24 ± 1	6 ± 1	306 ± 11
25	50	53 ± 5	26 ± 10	7 ± 3	314 ± 80
25	10	28 ± 8	11 ± 2	1.0 ± 0.5	323 ± 28
0	500	57 ± 6	17 ± 4	4.0 ± 0.5	356 ± 45
0	200	56 ± 12	10 ± 1	2.1 ± 0.5	375 ± 40
0	100	51 ± 1	11 ± 1	2.4 ± 0.5	333 ± 12
0	50	51 ± 1	9 ± 1	2.0 ± 0.2	326 ± 15
0	10	44 ± 1	8 ± 1	1.4 ± 0.1	295 ± 2
-15	500	56 ± 1	7 ± 1	1.2 ± 0.2	271 ± 15
-15	10	60 ± 1	9 ± 4	2 ± 1	284 ± 33

Table 5.19: Cyclic voltammetry results for bromide oxidation/bromine reduction on glassy carbon as a function of scan rate and temperature for alternate battery electrolyte: SOLD.

Temperature (°C)	Scan Rate (mV/s)	Q_C/Q_A (%)	I_A (mA/cm^2)	I_C (mA/cm^2)	$E_O - E_C$ (mV)
2.25 M $ZnBr_2$, 0.5 M $ZnCl_2$, 0.8 M MEPBr, 3.1 M ETHYLENE DICHLORIDE: SOLD					
25	500	73 ± 1	73 ± 4	39 ± 3	262 ± 6
25	50	74 ± 4	49 ± 4	26 ± 1	281 ± 3
0	500	77 ± 1	40 ± 1	19 ± 1	280 ± 2
0	50	80 ± 1	30 ± 2	12 ± 1	308 ± 6
-20	500	88 ± 1	22 ± 1	13 ± 4	323 ± 4
-20	50	93 ± 1	23 ± 1	17 ± 1	336 ± 3

Table 5.20: Cyclic voltammetry results for bromide oxidation/bromine reduction on glassy carbon as a function of scan rate and temperature for alternate battery electrolyte: SOLF.

Temperature (°C)	Scan Rate (mV/s)	Q_C/Q_A (%)	I_A (mA/cm^2)	I_C (mA/cm^2)	$E_O - E_C$ (mV)
2.25 M $ZnBr_2$, 0.5 M $ZnCl_2$, 0.8 M MEPBr, 4.5 M ETHYLENE GLYCOL: SOLF					
25	500	55 ± 3	43 ± 4	14 ± 2	249 ± 12
25	200	62 ± 1	45 ± 3	19 ± 2	237 ± 5
25	50	68 ± 1	44 ± 3	25 ± 3	247 ± 7
25	10	48 ± 3	41 ± 3	19 ± 2	233 ± 13
0	500	60 ± 1	27 ± 2	10 ± 1	266 ± 7
0	10	70 ± 5	18 ± 1	9 ± 1	273 ± 18
-15	500		13 ± 3	4 ± 1	290 ± 17
-15	10		12 ± 1	7 ± 1	292 ± 9

redox ratio was one, then the reaction could be described as reversible; in this case, however, Q_C/Q_A ranged between 30 and 90 %. The ratio of anodic peak current to cathodic peak current is another way to view the behaviour of the bromine electrode as a function of electrolyte composition and temperature. The ratio of I_C/I_A for solutions SOLC, SOLD, and SOLF ranged from 0.3 to 0.6, and in solution SOLE this ratio was approximately 0.2 for all temperatures and potential scan rates considered. This is an indication that bromine did not stay as readily adsorbed to the surface of the electrode in the presence of propan-2-ol. The low cathodic current and Q_C/Q_A ratio indicated that either bromine reduction was irreversible or an irreversible chemical reaction was occurring after the bromine formed and before the bromine complexed reversibly with MEPBr. Furthermore, as the potential scan rate of the experiment decreased from 500 to 10 mV/s, the ratio of Q_C/Q_A in SOLE (propan-2-ol) decreased from 55 to 25 % at 25 °C, and 55 to 45 % at 0 °C. At the slow scan rate, the experiment takes considerably longer: compare 3.2 s at 500 mV/s, and 160 s at 10 mV/s. Thus at the slow rate, there was more time for an irreversible chemical reaction to consume bromine, and therefore, it can be expected that the ratio of cathodic to anodic charge would be lower at low potential scan rates. Alcohols can react with bromide ions in solution in an acid media. Reactivity of the halogen decreases according to the following trend: HI > HBr < HCl, and alcohol reactivity decreases according to the following trend: benzylic and allylic > 3° > 2° > 1° (Solomons, 1980). The following reaction mechanism was proposed (Solomons, 1980):

$$X:^- + R - \overset{\overset{+}{|}}{\underset{|}{O}}H \rightarrow R - X + H_2O \qquad (5.29)$$

The secondary alcohol, propan-2-ol can react with bromide anions in solution under acid catalized conditions to produce C_3H_7Br and water.

Secondary alcohols can also be oxidized to ketones at room temperature or slightly above, using strong oxidizing agents. Typically acid dichromate is used, but other strong

oxidizing agents such as potassium permanganate and bromine have also been employed. Bromine does not, however, oxidize primary alcohols. The following reaction of oxidation of secondary alcohols has been proposed (March, 1977):

$$RCHOHR' \xrightarrow[Br_2]{light,\ heat} RCOR' \qquad (5.30)$$

In oxidizing the secondary alcohol the bromine is itself reduced to bromide. Under operating battery conditions, bromine consumed in irreversibly oxidizing propan-2-ol will contribute to low coulombic, and energy efficiency. The extent of this reaction will determine the practicality of an electrolyte incorporating propan-2-ol.

For electrolytes SOLC, SOLD, and SOLF, decreasing the temperature increased (E_C - E_o). For SOLE (propan-2-ol), decreasing the temperature decreased the peak separation. It is proposed that decreasing the temperature in propan-2-ol solutions slowed the kinetics of the chemical reaction between bromine and propan-2-ol. In decreasing the rate of the chemical reaction, the reversibility of the bromine couple should be increased at low temperature.

5.7.3 Conclusions of the Alternate Electrolyte Study

In conclusion, it was found that the presence of propan-2-ol, ethylene glycol and ethylene dichloride in concentrations of 25 % by volume did not appear to effect the mechanism of zinc deposition on glassy carbon. Bromide oxidation/bromine reduction was found to be quasi-reversible in electrolytes containing 2.25 M $ZnBr_2$, 0.5 M $ZnCl_2$, and 0.8 M MEPBr. In electrolytes containing 25 % volume ethylene dichloride, propan-2-ol and ethylene glycol, bromide oxidation was also found to be quasi-reversible. As the potential scan rate was decreased, however, the reverse peak in the propan-2-ol electrolyte disappeared. This is an indication that an irreversible chemical reaction (oxidation of propan-2-ol) was occurring after the bromide ions were oxidized to bromine. A following chemical reaction could significantly reduce the efficiency of a battery incorporating this electrolyte.

5.8 Selection of Electrolytes for Pilot Scale Testing

5.8.1 Ethylene dichloride

Ethylene chloride is a colourless oily liquid, freezing point -35.3 °C, density 1.2351 kg/l. It is insoluble in water (CRC, 1984a). Electrochemical studies in 2.25 M $ZnBr_2$, 0.5 M $ZnCl_2$, 0,8 M MEPBr, 3.1 M ethylene dichloride indicated that neither zinc deposition, nor bromide oxidation was effected by the presence of ethylene chloride. Thus, ethylene dichloride would be a good additive for modification of battery electrolytes. However, as ethylene dichloride was insoluble in water and soluble only in the organic phase, the freezing point of the aqueous phase was not lowered by the addition of ethylene dichloride. Further, ethylene dichloride is a possible carcinogen, and if the battery is to be "environmentally friendly", then ethylene dichloride is not an ideal additive. As a result, ethylene dichloride was not tested in the single cell stack.

5.8.2 Propan-2-ol

Propan-2-ol is a clear colourless liquid, freezing point -89 °C, density 0.7855 kg/l (CRC, 1985b). Electrochemical studies of zinc deposition indicated that nucleation overpotential increased as propan-2-ol was added. The ratio of redox charge associated with anodic zinc oxidation to cathodic zinc cation reduction was, however, unaffected by the addition of propan-2-ol. Electrochemical investigation of bromide reduction/bromine oxidation indicated that an irreversible chemical reaction occurred in solutions containing propan-2-ol after bromine had formed. This will likely result in reduced coulombic efficiency in the pilot scale tests.

Propan-2-ol (25 % by volume) electrolytes were found to have approximately one third the conductivity of standard battery electrolytes. Thus solution resistance in a battery using this electrolyte will be higher and voltaic efficiency lower than in a standard electrolyte battery.

Propan-2-ol was selected to be tested in the single cell battery. It was expected that performance (efficiency and capacity) would not be as good as in standard battery

electrolyte.

5.8.3 Ethylene Glycol

Ethylene glycol is a clear, colourless, viscous liquid, freezing point -11.5 °C, density 1.1088 kg/l (CRC, 1985c). Electrochemical studies of zinc deposition indicated that nucleation overpotential increased as ethylene glycol was added. The ratio of charge associated with anodic zinc oxidation to cathodic zinc cation reduction was, however, unaffected by the addition of ethylene glycol.

Electrochemical investigation of bromide reduction/bromine oxidation indicated that the addition of ethylene glycol did not influence the efficiency of this reaction. It is expected that the coulombic efficiency of a battery incorporating ethylene glycol will be comparable to that of a standard electrolyte battery. The maximum current density for both zinc and bromine reactions was lower in ethylene glycol than in standard battery electrolyte. The solution resistance in a battery using this electrolyte will also be higher than in a standard electrolyte battery, and voltaic and energy efficiencies lower.

Ethylene glycol was selected to be tested in the single cell battery. It was expected that coulombic efficiency would be comparable to that of a standard electrolyte battery, and that voltaic and energy efficiency would be lower due to the increased solution resistance.

Chapter 6

Pilot Scale Testing of Aqueous and Mixed Aqueous/Organic Zinc/Bromine Single Cell Batteries

6.1 Experimental

6.1.1 The Single Cell Test Station

A single cell 52.5 Ah zinc bromine battery stack and station was acquired from Johnson Controls Inc.. This battery consisted of one anode, one cathode, a separator, approximately 700 ml of electrolyte and an electrolyte circulation system. The battery was constructed of high density polyethylene, polyvinyl chloride (PVC) and teflon. The high density polyethylene stack was bolted together and could be dismantled and the electrodes examined after cycling and replaced if required. Flow was maintained and controlled through March Mfg. Inc. Model 6C-2Cb-MD AC centrifugal pumps and PVC throttle valves. The stack was secured in the vertical position, with anolyte entering the bottom of the stack and exiting the top, and catholyte entering the top and exiting the bottom (see Figure 2.2). Flow rate and stack pressures were maintained within proprietary specifications provided by the manufacturer, Johnson Controls, Inc. A photograph of the operating single cell is shown in Figure 6.1.

Electrolytes were prepared volumetrically from 7.64 M stock $ZnBr_2$ solution (Johnson Controls, Inc.), 2.94 M stock MEPBr solution (Johnson Controls, Inc.), BDH AnalR grade $ZnCl_2$ (98.0 %), BDH AnalR propan-2-ol (99.7 %), BDH Assured ethylene glycol (99 %), and BDH Laboratory Reagent liquid bromine.

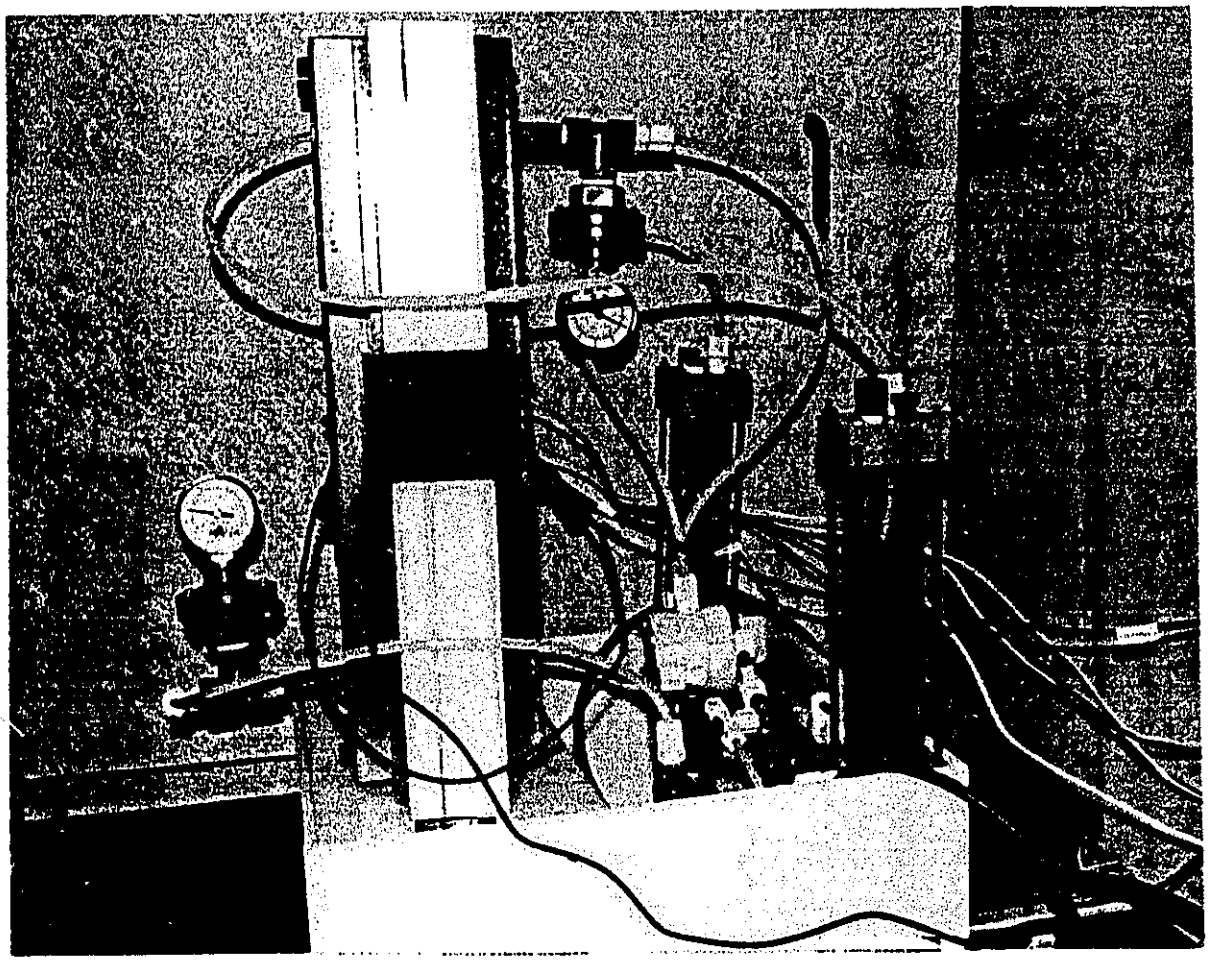

Figure 6.1: Zinc/bromine single cell battery under operation

6.1.2 Charge/Discharge Specifications

The standard test cycle included a five hour charge at 10 A (approximately 50 Ah), followed by a ten minute rest period, and a 10 A discharge to 0.7 V/cell. The charge cycle was voltage limited to 2.1 V. The discharge routine was followed by a strip cycle, discharge at progressively lower current until the battery voltage reached 20 mV. The stripping cycle was performed to maintain an initial state of 0 % charged for each experiment and to maximize the life of the battery. Manual flow reversal of the catholyte was executed for one minute of every hour of battery operation, excluding the stripping cycle. During charging, the second phase valve shown in Figure 2.2, was operated in the closed position. During discharge, the second phase valve was manually opened to allow heavy second phase to circulate throughout the battery.

Two charging systems were used to cycle the battery. A manual system was designed and built including a Hewlett-Packard 6260B DC power supply (0 - 10 V, 0 - 100 A) and is shown in Figure 6.2. The discharge circuit included two 1 ohm 175 watt Ohmite resistors connected in parallel (0.5 ohms). Battery current and voltage were monitored using a Fluke Hydra Data Logger, Model 2625A, Hydra Starter software and an IBM compatible computer. Data were recorded at 25 second intervals. A second automated charger, the Arbin Battery Testing System, Arbin Co., College Station, Texas, was also used for cycling. This system was capable of delivering ±10 A (±0.5 %), between -2 and 10 V (±0.5%). This charger was controlled and data collected using a PC computer.

Initially standard battery electrolyte (SOLC) was introduced, and the system efficiency and losses characterized. The system was drained of electrolyte, rinsed with two 500 ml aliquots of distilled water, and then filled with an alternate electrolyte. After a minimum of three charge/discharge cycles had been performed, the battery was again drained, and rinsed. It was then filled with standard battery electrolyte. In this way it was determined if performance degradation was caused by the introduction of modified electrolytes. Data were transferred to Borland Software QPRO for analysis where battery capacity, efficiency and losses (Equations 2.1 - 2.3, 2.5, and 2.6) were calculated.

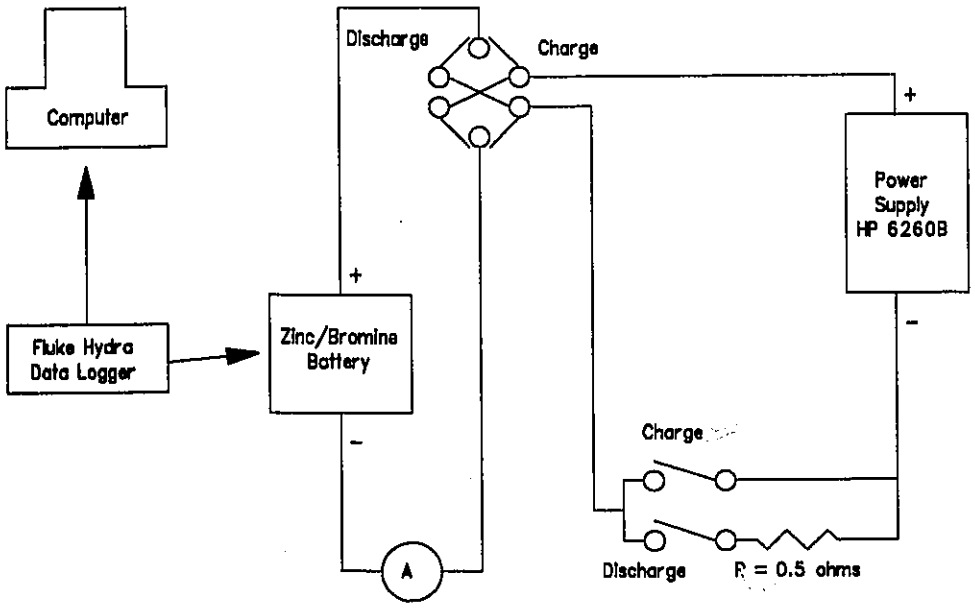

Figure 6.2: Schematic diagram of charge/discharge circuit for cycling 50 Ah zinc/bromine single cell battery.

6.2 Results and Discussion of Pilot Battery Testing

Based on the physical chemical and electrochemical experimental data, electrolytes containing ethylene glycol and propan-2-ol were selected for pilot scale testing. Electrolyte containing 2.25 M $ZnBr_2$, 0.5 M $ZnCl_2$, and 0.8 M MEPBr (SOLC) was used as the control battery electrolyte. The compositions of alternate electrolytes selected for testing in the single cell are shown in Table 6.1 below.

Table 6.1: Composition of electrolytes selected for testing in the single cell zinc/bromine battery.

Electrolyte	Composition
SOLC	2.25 M $ZnBr_2$, 0.5 M $ZnCl_2$, 0.8 M MEPBr
SOLE	2.25 M $ZnBr_2$, 0.5 M $ZnCl_2$, 0.8 M MEPBr, 3.3 M propan-2-ol (25 % by volume)
SOLF	2.25 M $ZnBr_2$, 0.5 M $ZnCl_2$, 0.8 M MEPBr, 4.5 M ethylene glycol (25 % by volume)
SOLG	2.25 M $ZnBr_2$, 0.5 M $ZnCl_2$, 0.8 M MEPBr, 2 % by volume propan-2-ol
SOLH	2.25 M $ZnBr_2$, 0.5 M $ZnCl_2$, 0.8 M MEPBr, 2 % by volume ethylene glycol

Typical discharge voltage profiles for SOLC, SOLG, and SOLH are shown in Figure 6.3. Each of the profiles shown in Figure 6.3 is characterized by a relatively flat charging voltage, and a moderately sloping discharge voltage. Generally the discharge voltage was lower in the electrolytes containing the mixed aqueous/organic electrolytes, than in SOLC. This was an indication that the voltaic and energy efficiencies will be lower in the alternate electrolytes. The single cell efficiencies and losses for each of these electrolytes are shown in Table 6.2. These results show that the overall efficiencies of the single cell battery were not significantly affected by the addition of propan-2-ol or ethylene glycol at low concentrations (2 % by volume). The results also show that while the efficiencies remain relatively constant, the distribution of losses was affected. For

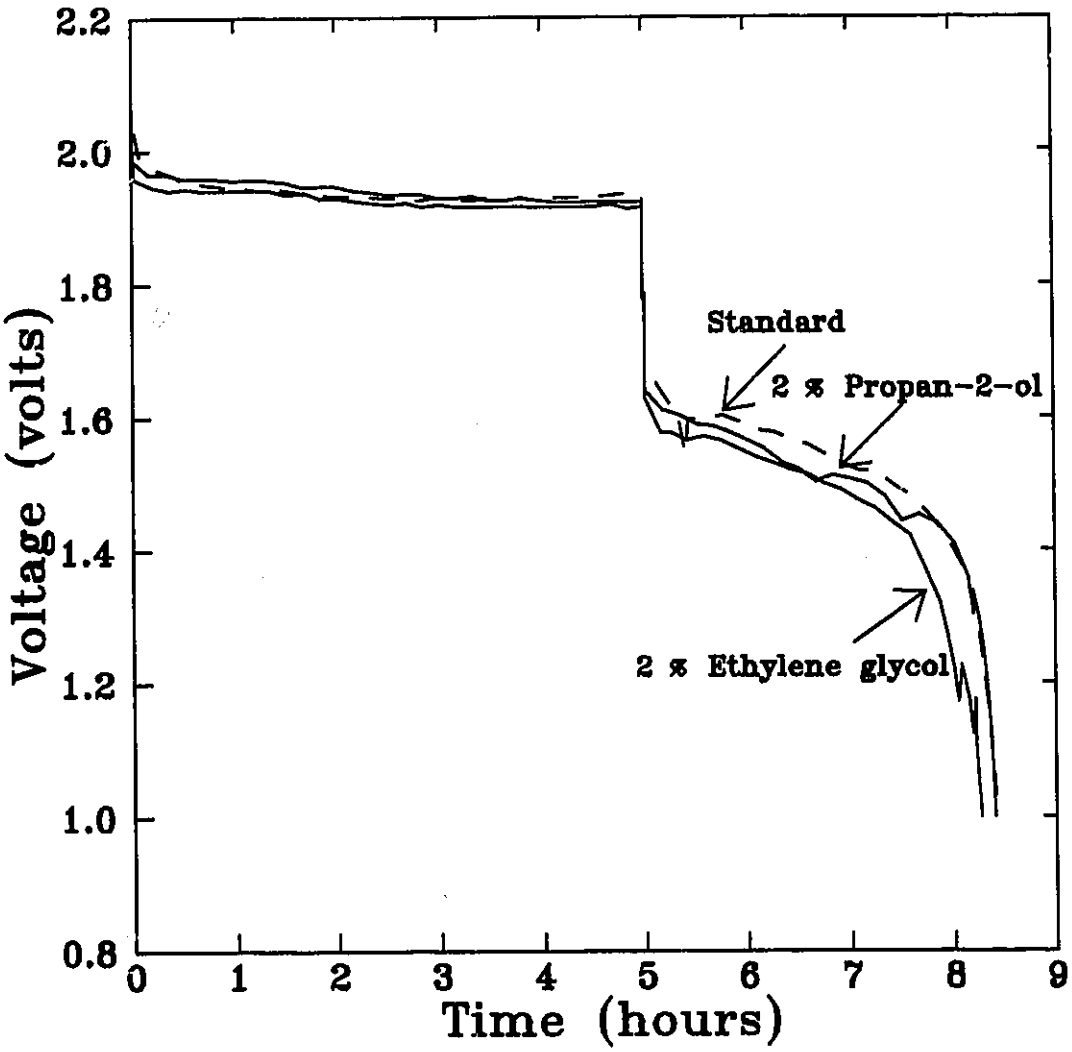

Figure 6.3: 10 A charge/10 A discharge voltage profiles for the zinc/bromine single cell battery shown in Figure 6.1, using electrolyte SOLC, SOLG, and SOLH.

both propan-2-ol and ethylene glycol, the transport losses increased from 20 % in standard electrolyte, to 25 %. The increase in transport losses was accompanied by a decrease in the residual capacity of the battery, thus the net losses remained relatively constant. This is an indication, however, that increasing the concentration of the organic alcohol or diol, will significantly affect the distribution of losses, and could potentially decrease the coulombic efficiency.

Table 6.2: Single cell stack efficiencies and losses at room temperature for electrolytes containing low concentrations of organic modifiers.

Solution	Efficiency (%)			Losses (%)	
	Coulombic	Voltaic	Energy	Residual Capacity	Transport Losses
SOLC	68 ± 2	77 ± 1	52 ± 1	12 ± 1	20 ± 2
SOLG	67 ± 1	78 ± 1	53 ± 1	8 ± 1	25 ± 1
SOLC	67 ± 1	77 ± 1	52 ± 1	12 ± 1	20 ± 1
SOLH	63 ± 2	75 ± 1	48 ± 2	11 ± 1	25 ± 2
SOLC	66 ± 1	75 ± 1	49 ± 1	13 ± 1	22 ± 1

The effect of higher concentrations of ethylene glycol and propan-2-ol was also investigated using the single cell zinc/bromine battery. Typical voltage profiles for SOLF (including 25 volume % ethylene glycol) and SOLC (control battery electrolyte) are shown in Figure 6.4. Results of cycling experiments for electrolytes containing high concentrations of ethylene glycol and propan-2-ol are presented in Table 6.3. The capacity of the battery employing SOLE (25 volume % propan-2-ol) was essentially zero as indicated by the coulombic efficiency of 1 ± 1 %. Losses were primarily due to transport phenomena, i.e., diffusion of bromine across the separator to the zinc electrode, or through subsequent chemical reaction with propan-2-ol. During charging, the bromine did not form a second phase with the MEPBr in solution. Rather a single phase, clear dark orange solution resulted. It is, therefore, not unexpected that the transport losses were found to be very high. The formation of the viscous second phase which settles in

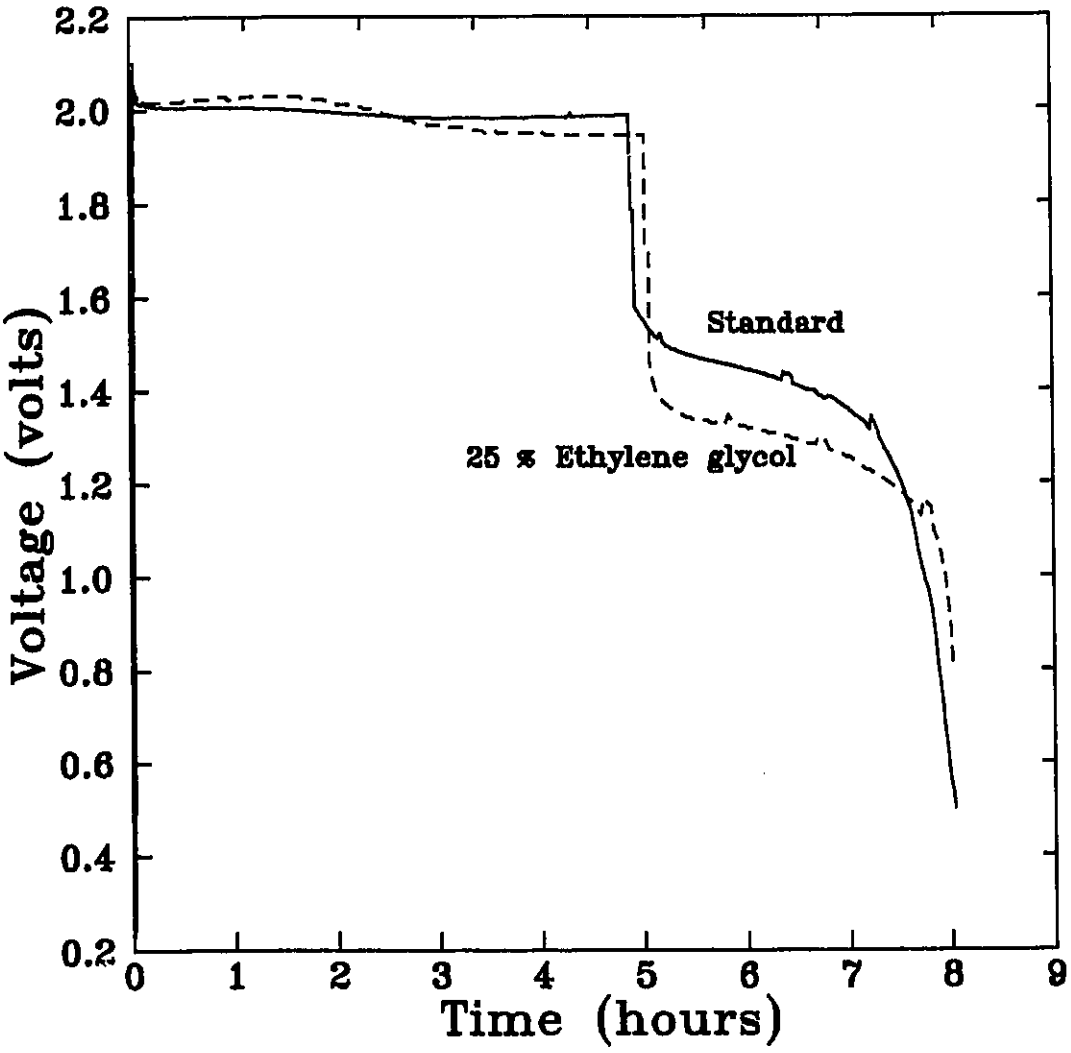

Figure 6.4: 10 A charge/10 A discharge voltage profiles for the zinc/bromine single cell battery shown in Figure 6.1 using electrolytes SOLC and SOLF.

Table 6.3: Single cell stack efficiencies and losses at room temperature for electrolytes containing high concentrations (25 % by volume) of organic modifiers.

Solution	Efficiency (%)			Losses (%)	
	Coulombic	Voltaic	Energy	Residual Capacity	Transport Losses
SOLC	68 ± 2	77 ± 1	52 ± 1	12 ± 1	20 ± 2
SOLE	1 ± 1	-	-	12 ± 4	87 ± 3
SOLC	68 ± 2	77 ± 1	52 ± 1	12 ± 1	20 ± 1
SOLC	58 ± 1	71 ± 2	41 ± 1	14 ± 3	28 ± 3
SOLF	60 ± 1	64 ± 1	38 ± 1	8 ± 1	32 ± 1

the bottom of the catholyte reservoir, is the prime method of self-discharge control in this design of the zinc bromine battery. Therefore, if the second phase does not form, then "charged" bromine is not confined to the catholyte reservoir when the battery is charging, and diffusion of bromine to the zinc electrode will be higher. The electrochemical studies at glassy carbon working electrodes predicted the rechargeability of the bromine electrode to be lower in solutions containing a high concentration of propan-2-ol, and suggested that after bromide oxidation to bromine, the bromine reacts chemically. The lack of second phase was also an indication that a chemical reaction between bromine formed by oxidation of bromide anions, and propan-2-ol was occurring, and that bromine was being consumed. In this case, bromine formed during charging (oxidation of bromide) reacted chemically before the discharge reaction occurred. This has the effect of increasing transport losses and decreasing the capacity of the battery.

Coulombic efficiency was the same in 25 % ethylene glycol (SOLF) as in standard control electrolyte (SOLC). Voltaic and energy efficiencies were lower in the alternate electrolyte. This can be predicted by examination of Figure 6.4. The discharge voltage was approximately 0.1 V lower in ethylene glycol electrolyte than in standard electrolyte. Physical chemical and electrochemical experiments indicated that electrolyte conductivity was lower in the mixed aqueous/organic electrolytes. Generally, the transport losses were again higher and residual capacity lower in SOLF (ethylene glycol) as compared to

SOLC, the control.

Table 6.4 compares the efficiencies and losses for modified electrolytes to those for the control electrolyte. This summary shows that at both 2 and 25 % ethylene glycol the residual capacity of the battery was reduced and that as the concentration of ethylene glycol increased, the residual capacity decreased. The coulombic efficiency was relatively constant and independent of ethylene glycol concentration. Both voltaic and energy efficiencies decreased with increasing ethylene glycol concentration.

Table 6.4: Ratio of efficiencies of alternate electrolytes to that of standard electrolyte (SOLC) for ethylene glycol solutions

Solution	Efficiencies (%)			Losses (%)	
	Coulombic	Voltaic	Energy	Residual Capacity	Transport Losses
SOLH: 2 % ethylene glycol	95 ± 4	100 ± 3	98 ± 6	85 ± 14	114 ± 14
SOLF: 25 % ethylene glycol	103 ± 4	91 ± 4	93 ± 4	57 ± 20	114 ± 15

6.3 Conclusions Based on Pilot Battery Testing

In conclusion, the pilot scale testing suggested that ethylene glycol is a suitable improved low-temperature electrolyte for zinc/bromine batteries. Electrolytes containing propan-2-ol are not suitable.

Chapter 7

Conclusions and Recommendations for Future Work

This chapter presents the conclusions of the present study on electrolytes for zinc/bromine batteries. Recommendations for future work are also given.

The principal objective of this study was to obtain an understanding of the basic electrochemical behaviour of electrolytes used in the aqueous zinc bromine battery and to extend the performance of the battery to low temperatures. In this study the chemical species distribution and conductivity of actual and model battery electrolytes was determined in order to understand their effects on the mechanisms of oxidation and reduction occurring in a zinc/bromine battery. Earlier studies have been conducted in aqueous zinc bromide solutions without battery additives such as quaternary ammonium bromide salts and $ZnCl_2$. The kinetics and chemistry of both the zinc and the bromine half reactions were determined in the presence of additives to gain an understanding of the failure mechanisms in a zinc bromine battery employing a novel electrolyte. Electrochemical response, chemical species distribution, conductivity, and phase change data were obtained for battery electrolytes at low temperatures. On the more practical side, a simple method to identify electrolytes having properties that could improve low temperature operation of the zinc/bromine battery was developed based on physical and electrochemical techniques. Both fundamental and practical conclusions can be reached based on this study.

7.1 Fundamental Conclusions

It was found, as a result of molecular vibrational spectroscopic studies, that the addition of quaternary ammonium bromide complexing agents did not affect the distribution of zinc/bromine species. Further, electrochemical studies indicated that the addition of MEPBr did not influence the deposition of zinc metal onto the foreign substrate. The distribution of zinc/bromide complexes with bromine was found to be significantly affected by decreasing temperature and the state-of-charge of the battery. As temperature was increased from -10 to 25 °C, the distribution of zinc complexes with bromide shifted from higher order species ($ZnBr_4^{2-}$) to lower order species ($ZnBr_2$). This result was in agreement with studies of Yang (1988) and Marley and Gaffney (1990) in aqueous $ZnBr_2$ solutions at 25 and 350 °C.

The quaternary ammonium bromide complex was found to act on the free bromine in solution. The cyclic voltammograms obtained were characteristic of a quasi-reversible weak product adsorption mechanism. Addition of MEPBr was believed to facilitate bromine adsorption on glassy carbon. This conclusion was in agreement with earlier work of Mastragostino and Gramellini (1991) in $NaClO_4$ solutions, and Vogel and Mobius (1991) in pure polybromide solutions.

Electrochemical studies indicated that bromide oxidation/bromine reduction was quasi-reversible in electrolytes containing 2.25 M $ZnBr_2$, 0.5 M $ZnCl_2$, 0.8 M MEPBr and 25 % volume ethylene dichloride, propan-2-ol or ethylene glycol. It was found that in the presence of propan-2-ol, bromine formed from the oxidation of bromide ions, underwent an irreversible chemical reaction rather than reversibly complexing with MEPBr. The absence of molecular bromine in solutions of 25 % by volume propan-2-ol electrolytes indicated that bromine was reduced.

7.2 Practical Conclusions

Physical chemical analysis of conductivity, viscosity, specific gravity and freezing point depression of electrolytes identified ethylene glycol and propan-2-ol as potential candidates for mixed aqueous/organic low temperature electrolytes for zinc bromine flow batteries.

Propan-2-ol was selected to be tested in the single cell battery, and it was expected from fundamental considerations that battery performance would not be as good as in standard battery electrolyte. It was believed that an irreversible chemical reaction occurs in the propan-2-ol solutions, and that the battery would have low efficiency. Tests in the single cell battery confirmed this hypothesis. An electrolyte containing 25 % by volume propylene glycol, 2.25 M $ZnBr_2$, 0.5 M $ZnCl_2$ and 0.8 M MEPBr was found to have no capacity.

Ethylene glycol was also selected to be tested in the single cell battery. It was expected from basic studies that coulombic efficiency of the battery using this electrolyte would be comparable to that of a standard electrolyte battery. Due to reduced conductivity (higher solution resistance), the voltaic and energy efficiencies were expected to be lower than those of a standard electrolyte battery. Pilot scale testing confirmed these results. The single cell battery, incorporating 25 % by volume ethylene glycol, had similar coulombic efficiency as a battery using standard electrolyte, with energy and voltaic efficiencies approximately 90 % of the standard electrolyte battery efficiencies. Transport losses, associated with diffusion of bromine across the separator to the zinc electrode, were higher in the electrolyte incorporating ethylene glycol. It was concluded, that ethylene glycol was a suitable electrolyte for zinc/bromine batteries required to operate at low temperatures.

It can be concluded that cyclic voltammetry, conductivity, and freezing point depression studies can be used to identify candidate electrolytes for the zinc bromine flow battery. In addition, the hypothesis that battery performance predictions could be based on fundamental investigations of electrolytes was confirmed in pilot scale studies.

7.3 Recommendations for Future Work

Ethylene glycol was identified as a potential electrolyte for low temperature operation of a zinc/bromine battery. Optimization of the battery to maximize efficiencies and minimize pumping and stack losses must be completed with the alternate electrolyte. This process includes optimization of electrolyte composition (including $ZnBr_2$ concentration, quaternary ammonium bromide salt selection and concentration, and inorganic additive concentration), stack design (choice of separators, electrode carbons, electrode spacing, and flow channels), and system parameters (design and selection of pumps and heat exchangers, and determination of an optimum flow rate). This optimization process will improve the performance of the low temperature electrolyte.

It is also necessary to conduct cycle life testing of the zinc/bromine battery employing the alternate electrolyte. This is a long term project that would require the fabrication of several batteries, both of single cell and multi-cell sizes, and cycling over a period of years. Cycling should be performed using a variety of charge/discharge schedules to carefully characterize the batteries' performance.

Finally, it is important to determine the temperature performance characteristics of a battery using the low temperature alternate electrolytes. These tests will involve subjecting the entire battery to a controlled cold room climate, and conducting cycling tests as a function of charge and discharge rate.

At a fundamental scientific level, it was found that cyclic voltammetry, chronoamperometry, physical chemical and spectroscopic analysis characterized the electrolytes well. Spectroscopic analysis of novel electrolytes can provide an understanding of zinc species distribution. These techniques could be used to optimize the composition of alternate mixed aqueous/organic battery electrolytes.

Bibliography

[1] Adams, W.A., E. Bernard, A. Fahim, A. Hicks, D. Ladd, S. Lines, L. Nash, J.C.T. Oliveira, W. Pell and G. Song, "Design and Performance of a Photovoltaic Zinc/Bromine Battery Propulsion System for a Solar Powered Electric Racing Vehicle", Proc. 10th Electric Vehicle Symposium, Hong Kong, December (1990).

[2] Adams, W.A., personal communication based on purchase price of 40 kWh Ni/Cd system, (1994).

[3] Arnold, Charles Jr., "Durability of Polymeric Materials Used in Zinc/Bromine Flow Batteries", Proc. 26th Intersoc. Energy Conv. Eng. Conf., **3**, 440-445, (1991).

[4] Assink, R.A., C. Arnold Jr., "Preparation of Ionic Membranes for Zinc/Bromine Storage Batteries", Proc. 26th Intersoc. Energy Conv. Eng. Conf., **3**, 458-462, (1991).

[5] Asyst Software Technologies Inc., "Asystant^{TM} GPIB The Scientific Number Cruncher, (1988).

[6] Avraamides, J., "The Iodine-Propionitrile-Water System. Effects of Added Salts on Distribution Coefficient and Conductivity", Aust. J. chem., **40(1)**, 209-14 (1987).

[7] Bajpal, S.N., "Vapour Pressures of Bromine-Quaternary Ammonium Salt Complexes for Zinc-Bromine Battery Applications", J. Chem. Eng. Data, **26**, 2-4, (1981).

[8] Banwell, C.N., "Fundamentals of Molecular Spectroscopy, 3rd Edition", McGraw Hill Book Co. Ltd., 124-154, (1983).

[9] Barnartt, S., and D.A. Forejt, "Bromine-Zinc Secondary Cells", J.Electrochem. Soc., **111(11)**, 1201-1204, (1964).

[10] Bellows, R.J., D.J. Eustace, P. Grimes, J.A. Shropshire, H.C. Tsien, and A.F. Venero, "Zinc-Bromine Battery Studies", Power Sources **7**, 301-312 (1979).

[11] Bellows, R., H. Einstein, P. Grimes, E. Kantner, P. Malachesky, K. Newby and H Tsien, "Development of a Circulating Zinc-Bromine Battery Phase 1 -Final

Report, SAND82-7022, prepared by Exxon Research and Engineering Co. for Sandia National Laboratories, Albuquerque, NM, January (1983).

[12] Bellows, R., H. Einstein, E. Kantner, P. Grimes, P. Malachesky, "Zinc/Bromine Battery Scale-Up to a 30-kWh Electric Vehicle Design", Proc. 20th Intersoc. Energy Conv. Eng. Conf., **2**, Paper 859186, 2.70-2.79, (1985).

[13] Bellows, R.J., and E. Kantner, "Metal Halogen Electrochemical Cell", Eur.Pat. Appl., 11pp, EP 235444 A2, 9 Sept. (1987)

[14] Biserni, M., A. Marinangeli, and M. Mastragostino, "Bromine Doped Polydithienothiophene: A Cathode-Active Material in Aqueous Medium", Electrochim. Acta, **31(9)**, 1193-1196 (1986).

[15] Boden, D.P., V.J. Spera, R.B. Wylie, "Potential Distribution Over the Surface of Planar Zinc Electrdes During Charge and Diuscharge at Constant Current", Extended Abstracts, The Electrochem. Soc. Inc, Fall Meeting, Detroit, (1969).

[16] Bolstad, J.J., and R.C. Miles, "Development of the Zinc/Bromine Battery at Johnson Controls, Inc.", Proc. 24th Intersoc. Energy Convers. Eng. Conf.,**3**, 1311-1318 (1989).

[17] Bosco, E., and S.K. Rangarajan, "Electrochemical Phase Formation (ECPF) and Macrogrowth Part I. Hemispherical Models", J. Electroanal. Chem., **134**, 213-224, (1982).

[18] Bosco, E., and S.K. Rangarajan, "Electrochemical Phase Formation (ECPF) and Macrogrowth Part II. Two Rate Models", J. Electroanal. Chem., **134**, 225-241, (1982).

[19] Bulmer, J.T., D.E. Irish, and L. Odberg, "The Temperature Dependence of Raman Band Parameters for Aquated Mg(II) and Zn(II)", Can. J. Chem., **53**, 3806-3811, (1975).

[20] Cathro, K.J., K. Cedzynska, and D.C. Constable, "Some Properties of Zinc/Bromine Battery Electrolytes", J. Power Sources, **16**, 53-63 (1985).

[21] Cathro, K.J., K. Cedzynska, D.C. Constable, and P.M. Hoobin, "Selection of Quaternary Ammonium Bromides for Use in Zinc/Bromine Cells", J. Power Sources, **18**, 349-370 (1986).

[22] Cathro, K.J., K. Cedzynska, and D.C. Constable, "Preparation and Performance of Plastic-Bonded-Carbon Bromine Electrodes", J. Power Sources, **19**, 337-356 (1987).

[23] Cathro, K.J., D.C. Constable, and P.M. Hoobin, "Performance of Porous Plastic Separators in Zinc/Bromine Cells", J. Power Sources, **22**, 29-57 (1988a).

[24] Cathro, K.J., "Performance of Zinc/Bromine Cells Having a Propionitrile Electrolyte", J. Power Sources, **23(4)**, 365-383 (1988b).

[25] Cedzynska, K., "Some Properties of Zinc-Bromine Cell Electrolytes Containing Symmetrical Ammonium Bromides", Electrochim. Acta, **34(10)**, 1439-1442 (1989).

[26] The Chemical Rubber Company, "CRC Handbook of Chemistry and Physics, 64th Edition", CRC Press, C-287, (1985a).

[27] The Chemical Rubber Company, "CRC Handbook of Chemistry and Physics, 64th Edition", CRC Press, C-471, (1985b).

[28] The Chemical Rubber Company, "CRC Handbook of Chemistry and Physics, 64th Edition", CRC Press, C-295, (1985c).

[29] The Chemical Rubber Company, "CRC Handbook of Chemistry and Physics, 64th Edition", CRC Press, D-233 - D-253, (1985d).

[30] Chen, C., "Effect of Impinging Flow on the Morphology of Zinc Deposits", J. Electrochem. Soc., **137**, 212c-214c, (1990).

[31] Choi, K.W., D.N. Bennion, J. Newman, "Engineering Analysis of Shape Change in Zinc Secondary Electrodes i. Theoretical", J. Electrochem. Soc., **123**, 1916-1927, (1976).

[32] Choi, K.W., D. Hamby, D.N. Bennion, J. Newman, "Engineering Analysis of Shape Change in Zinc Secondary Electrodes ii. Experimental", J. Electrochem. Soc., **123**, 1628-1637, (1976b).

[33] Cournoyer, E., "Zinc/Bromine Battery Performance Evaluation as a Photovoltaic Energy Storage Unit", B.A.Sc. Thesis, Department of Chemical Engineering, University of Ottawa, (1992).

[34] Donepudi, V.S., and B.E. Conway, "Electrochemical Calorimetry of the Zinc and

Bromine Electrodes in Zinc-Bromine and Zinc-Air Batteries", J. Electrochem. Soc., **131**, 1477-1485, (1984).

[35] Donepudi, V.S., and W. Pell, "Advanced Battery Energy Storage Research for PV Applications in Cold Climates" DSS Contract No. 23440-0-9498/01-SZ, Submitted to the Energy Diversification Research Laboratory, Department of Energy Mines and Resources, December, 1992.

[36] Duffield, A., "Nickel-Zinc Batteries in Modern Battery Technology", Editor Clive D.S. Tuck, Ellis Horwood Limited, 452-458, (1991).

[37] Eidler, P.E., Y.M. Yaccarino, "Zinc/Bromine Electric Vehicle Program", US-DOE Contractors Meeting, Idaho, 253-260, (1989).

[38] Eidler, P.E., Johnson Controls, Inc., Personal Communication, June (1992).

[39] Eskra, M.D., P.A. Eidler and R.C. Miles, "Zinc Bromine Battery Development for EV Applications", 7 pages, (1991).

[40] Eustace, D.J., "Bromine Complexation in Zinc-Bromine Circulating Batteries", J. Electrochem. Soc., **127(3)**, 528-532 (1980).

[41] Evans, T.I., and R.E. White, "A Review of Mathematical Modeling of the Zinc/bromine Flow Cell and Battery", J. Electrochem. Soc., **134**, 2725-2733, (1987).

[42] Fleischmann, M., and H.R. Thirsk, "Metal Deposition and Electrocrystallization" in Advances in Electrochemistry and Electrochemical Engineering, V3, P. Delehay and C.W. Tobias Editors, Interscience Publishers, John Wiley and Sons, 123-210, (1963).

[43] Fujii, T., K. Fushimi, T. Hashimoto, Y. Kumai, A. Hirota, H. Itoh, K. Jinnai, Y. Kishimoto, M. Kanazashi, T. Hiramatsu and S. Kondoh, "80-kWh Zinc Bromide Battery for Electric Power Storage", Proc. 21st Intersoc. Energy Conv. Eng. Conf., **2**, Paper 869220, 999-1003, (1986).

[44] Fujii, T., M. Igarashi, K. Fushimi, T. Hashimoto, Y. Kumai, A. Hirota, H. Itoh, K. Jinnai, M. Kanazashi, T. Hiramatsu, and T. Nakayama, "400 kWh Zinc Bromide Battery for Electric Power Storage", Proc. 23rd Intersoc. Energy Conv. Eng. Conf., Paper 889305, 335-339, (1988).

[45] Gibbard, H.F., "Heats of Dilution of Aqueous Zinc Bromide", ECS Proceedings May 8-13, 1983, Extended Abstracts, **83-1**, 1230 (1983).

[46] Gibbard, H.F., "Physical Chemistry of Zinc-Bromine Battery: i. Activity Coefficients of Aqueous Zinc Bromide", J. Sol. Chem., **10(9)**,611-620 (1981).

[47] Gibbard, H.F., "Bromine Complexing Agents for Energy Storage Applications", ECS Proceedings (Extended Abstracts), **83-1**, 1230, (1983).

[48] Grimes, P., Proceedings of the EPRI/LBL Workshop on the Electrochemistry of Zinc/Halogen Batteries Vol II, P.C. Symons, Ed., 7-25, (1984).

[49] Grimes, P., " Circulating Electrolyte Zinc/Bromine Battery. Test Program and Procedures", J. Power Sources, **17(1-3)**, 135-141 (1986).

[50] Grimes, P.G., "Surfactants in Advanced Battery Technology", Surfactant Sci. Ser., **26**, 101-129 (1987).

[51] Gross, L., "Low-Cost ZnBr Battery Developed by Weizmann-SUNY/Syracuse Team", International Solar Energy Intelligence Report, April 5, 69-70 (1991).

[52] Goggin, P.L., G. Johansson, M. Maeda, and H. Wakita, "The Structures of Zinc Bromide Complexes in Aqueous Solution", Acta Chemica Scandinavien A,**38**, 625-639 (1984).

[53] Gunawardena, G., G. Hills, and I. Montenegro, "Electrochemical Nucleation Part II. The Electrodeposition of Silver on Vitreous Carbon", J. Electroanal. Chem., **138**, 241-254, (1982a).

[54] Gunawardena, G., G. Hills, I. Montenegro and B. Scharifker, "Electrochemical Nucleation Part III. The Electrodeposition of Mercury on Vitreous Carbon", J. Electroanal. Chem., **138**, 255-271, (1982b).

[55] Gunther, R., R.M. Bendert, "Zinc Electrode Shape Change in Cells with Controlled Current Distribution", J. Electrochem. Soc., **134**, 782-791, (1987).

[56] Hashimoto, T., "Electrolyte for Zinc-Bromine Battery", Eur. Pat. Appl., 6pp, EP 411614 A1, 6 Feb. (1991).

[57] Hills, G.J., D.J. Schiffrin, and J. Thompson, "Electrochemical Nucleation from Molten Salts I. Diffusion Controlled Electrodeposition of Silve from Alkali Molten Nitrates", Electrochim. Acta, **19**, 657-670, (1974).

[58] Hoobin, P.M., K.J. Cathro, and J.O. Niere, "Stability of Zinc/Bromine Battery Electrolytes", J. Appl. Electrochem., **19(6)**, 943-945 (1989).

[59] Hsie, W.C., and J.R. Selman, "Mass Transport in Supported Zinc Halide Solutions - II Complexation and Migration Effects", Electrochimica Acta, **30**, 1381-1392 (1985).

[60] Iacovangelo, C.D., and F.G. Will, "Parametric Study of Zinc Deposition on Porous Carbon in a Flowing Electrolyte Cell", J. Electrochem. Soc., **132**, 851-857, (1985).

[61] Irish, D.E., B. McCarroll, and T.F. Young, "Raman Study of Zinc Chloride Solutions", J. Chem. Phys., **39**, 3426-3444, (1963).

[62] Ito, H., "Automatic Cooling of Zinc/Bromine Batteries", Jpn. Patent 02098070 A2, 10 April (1990).

[63] Jinnai, K., "Electrolyte for Zinc-Bromine Battery", Jpn. Patent JP 61206180 A2, 12 Sept. (1986a).

[64] Jinnai, K., and T. Hashimoto, "Operation of Zinc-Halogen Battery, Jpn. Patent JP 61290669 A2, 20 Dec. (1986b).

[65] Jinnai, K., Meidensha Electric Mfg. Co., Ltd., "Growth Suppression of Zinc Dendrites in Batteries", Jpn. Patent JP 63034851 A2 15 Feb. (1988).

[66] Jinnai, K., "Electrolytes for Zinc/Bromine Batteries", Jpn. Patent 02142071 A2, 31 May (1990).

[67] Jorne, J., Y.J. Li, K.E. Yee, "Supression of Dendrites and Roughness During Electrodepositon by Impinging Flow", J. Electrochem. Soc., **134**, 1399-1402, (1987).

[68] Kabisch, G., E. Kalman, G. Palinkas, T. Radnai and F. Gaizer, "Complex Formation and Solvation of Zinc Bromide in n,n-dimethylformamide Soution: An Electron Diffraction and Raman Study", Chem. Phys. Let., **107**, 463-468, (1984).

[69] Kalman, E., I. Serke, G. Palinkas, G. Johansson, G. Kabisch, M. Maeda, and H. Ohtaki, "Complex Formation in an Aqueous $ZnBr_2$ Solution Based on Electron Diffraction, X-ray Scattering and Raman Spectra", Z. Naturforsch. **38a**, 225-230 (1983).

[70] Kanazashi, M., T. Fujii, H. Hashimoto, Y. Kumai, Y. Ando, A. Hirota, K. Jin-nai,

H. Ito, and H. Misaki, "80kWh Zinc Bromide Battery for Electric Power Storage", Proc. 20th Intersoc. Energy Conv. Eng. Conf., **2**, Paper 859187, 2.79-2.84 (1985).

[71] Kinoshita, K., "Carbon, Electrochemical and Physicochemical Properties", John Wiley and Sons, Toronto (1988).

[72] Kordesch, K., G. Tomazic, Ch. Fabjan, "Zinc-Bromine Batteries For Electrotraction", Extended Abstract, Meeting of the Electrochemical Society Toronto, (1992).

[73] Kumagai, T., "Ion Exchange from Nonaqueous Solutions. Zinc (II) Bromide and Iodide in Ethylene Glycol", Bull. Chem. Soc. Jpn., **57**, 2738-2740, (1984).

[74] Leo, A., and R. Bharvani, "Zinc-Bromine Storage Batteries for Utility Load Leveling", Proc. 19th Intersoc. Energy Conv. Eng. Conf., Paper 849472, 1156-1163, (1984).

[75] Leo, A., and A. Charkey, "Development of Zinc-Bromine Batteries for Stationary Energy Storage", Proc. 20th Intersoc. Energy Conv. Eng. Conf., **2**, Paper 859185, 2.63-2.69, (1985).

[76] Leo, A., G. Albert, and M. Bilhorn, "Development of Zinc-Bromine Batteries for Stationary Energy Storage Applications", Proc. 21st Intersoc. Energy Conv. Eng. Conf., **2**, Paper 869219, 992-998, (1986).

[77] Leo, A., "Zinc-Bromine Batteries in Modern Battery Technology", Editor Clive D.S. Tuck, Ellis Horwook Limited, 502-516, (1991).

[78] Lex P.J., and J.F. Mathews, "Recent Developments in Zinc/Bromine Battery Technology at J.C.I.", IEEE 35th International Power Sources Symposium (1991).

[79] Lim, H.S., A.M. Lackner, and R.C. Knechtli, "Zinc-Bromine Secondary Battery", J. Electrochem. Soc., **124(8)**, 1154-1157 (1977).

[80] Macklin, J.W., and R.A. Plane, "Raman Study of Stepwise Formation of Bromine Complexes of Zinc, Cadmium, and Mercury in Aqueous Solutions", Inorganic Chemistry, **9**, 821-827, (1970).

[81] Manassen, J., Cabasso, I., "Non-Flow zinc/Halogen Storage Cell with Thin Film Polymer Composites", Proc. 25th Intersoc. Energy Convers. Eng. Conf., **3**, 332-334 (1990).

[82] March, J., "Advanced Organic Chemistry. Reactions, Mechanisms, and Structure, 2nd Edition", McGraw-Hill Book Company, New York, 1082-1084, (1977).

[83] Marley, N.A., and J.S. Gaffney, "Laser Raman Spectral Determination of Zinc Halide Complexes in Aqueous Solutions as a Function of Temperature and Pressure", Applied Spectroscopy, **44**, 469-476, (1990).

[84] Mastragostino, M., and S. Valcher, "Polymeric Salt as Bromine Complexing Agent in a Zn-Br_2 Model Battery", Electrochim. Acta, **28(4)**, 501-505 (1983).

[85] Mastragostino, M., and C. Gramellini, "Kinetic Study of the Electrochemical Processes of the Bromine/Bromide Aqueous System on Vitreous Carbon Electrodes", Electrochim. Acta, **30(3)**, 373-380, (1985).

[86] McBreen, J., "Zinc Electrode Shape Change in Secondary Cells", J. Electrochem. Soc., **137**, 1620-1628, (1972).

[87] McBreen, J., and E. Gannon, "Electrodeposition of Zinc on Glassy Carbon from $ZnCl_2$ and $ZnBr_2$ Electrolytes", J. Electrochem. Soc., **130(8)**, 1667-1670, (1983).

[88] McBreen, J., "Zinc Electrodes: Reactions and Mechanisms", Electrochem. Soc. Cleveland Section Local Meeting, 23-24, (1993).

[89] Meidensha Electric Mfg. Co., Ltd., Jpn. Patent JP 59151768 A2, 30 Aug. (1984).

[90] Pell, W., V.S. Donepudi, W.A. Adams, R. Calinot, P.E. Eidler, "An Experimental Study of A Photovoltaic System Including a Zinc/Bromine Battery", The 11th European Photovoltaic Energy Conference and Exhibition, Paper 5.13, October, (1992).

[91] Pletcher, Derek, "A First Course in Electrode Processes", The Electrochemical Consultancy, Hants, England, (1991), p.43.

[92] Preston, C.M., and W.A. Adams, "A Laser Raman Spectroscopic Study of Aqueous Phosphoric Acid", Can. J. Spec., **22**, 125, (1979).

[93] Putt, R.A., "Assessment of Technical and Economic Feasibility of Zinc/Bromine Batteries for Load-Levelling", EPRI Report EM-1059, May (1979).

[94] Rallo, F., and P. Silvestroni, "Insoluble Polybromides of Quaternary Ammonium Salts and Their Phase-Transitions in the Presence of Aqueous Bromine-Bromide Solution", J. Electrochem. Soc., **119(11)**, (1972).

[95] Raman, C.V. and K.S. Krishnan, "A New Type of Secondary Radiation", Nature, **121**, 501 (1928).

[96] Seitz, C.W., "Volume I: Business Opportunities for Large Batteries, Part I: Global Overview and Large Battery Technology", SRI International Project No. 2771, pIV-40, SRI International, Menlo Park California, (1987).

[97] Singh, P., K. White, and A.J. Parker, "Application of Non Aqueous Solvents to Batteries. Part I. Physicochemical Properties of Propionitrile/Water Two-Phase Solvent Relevant to Zinc-Bromine Batteries", J. Power Sources, **10(4)**, 309-318 (1983).

[98] Solomons, T.W.G., "Organic Chemistry, 2nd Edition", John Wiley and Sons, New York, 609-612, (1980).

[99] Southampton Electrochemistry Group, "Instrumental Methods in Electrochemistry", Ellis Horwood Limited, 178-229, (1990a).

[100] Southampton Electrochemistry Group, "Instrumental Methods in Electrochemistry", Ellis Horwood Limited, 283-316, (1990b).

[101] Stencel, J.M., "Raman Spectroscopy for Catalysis", Van Nostrand Reinhold Publishing, (1990).

[102] Sun, H., J.L. Delplancke, R. Winand, and T.J. O'Keefe, "Nucleation and Growth of Copper Electrodeposits on Titanium Substrates", Copper '91, Hydrometallurgy and Electrometallurgy of Copper, **3**, 405-417, (1991).

[103] Tange, K., Toyota Motor Corp., "Zinc-Bromine Batteries", Jpn. Patent JP 01102863 As 20 April (1989).

[104] Tomazic, G., "Metal-Halogen Battery", Eur. Pat. Appl., 6pp, 89-890017, 25 January (1989).

[105] Tomazic, G., "Advances in Zinc Bromide Batteryies For Electric Vehicles and Energy Storage at S.E.A.", Paper presented at the Annual Battery Conference, California State University, Long Beach, CA, January 16-18, 1990.

[106] Uceda, D.A., J.D. Scott, and T.J. O'Keefe, "Electrochemical Evaluation of Gas Sparging Effects on Copper Deposition in the Presence of Additives", Copper '91, Hydrometallurgy and Electrometallurgy of Copper, **3**, 303-319, (1991).

[107] Vogel, I., and A. Mobius, "On Some Problems of the Zinc-Bromine System as an Electric Energy Storage System of Higher Efficiency - I. Kinetics of the Bromide Electrode", Electrochim. Acta, **36(9)**, 1403-1408 (1991).

[108] Vogel, I., and A. Mobius, "The Addition of Bromine to Quaternary Ammonium Compounds Basis of the Bromine Storage in Zinc-Bromine Batteries", Power Sources, **13**, 237-243 (1991).

[109] Wopschall, R.H., and I. Shain, "Effects of Adsorption of Electroactive Species in Stationary Electrode Polarography", Anal. Chem., **13**, 1514-1527, (1967).

[110] Wopschall, R.H., and I. Shain, "Adsorption Effects in Stationary Electrode Polarography with a Chemical Reaction Following Charge Transfer", Anal. Chem., **13**, 1535-1542, (1967).

[111] Yang, M.M., D.A. Crerar, and D.E. Irish, "Raman Spectral Studies of Aqueous Zinc Bromide Solutions to 300 °C at Pressures of 9 MPa", J. Sol. Chem., **17**, 751-762, (1988).

[112] Yellin, W., and R.A. Plane, "A Study of the Bromide Solutions of Zinc and Cadmium", J. Am. Chem. Soc., **83**, 2448-2452, (1961).

[113] Zagrodnik, J.P., J.J. Bolstad, R.C. Miles, "Zinc/Bromine Battery: Recent Advances for EV Applications", SAE Future Transportation Technology Conference and Exposition, Vancouver, Canada, Abstract No. 891692, 81-89, (1989).

APPENDIX: SAMPLE CALCULATION FOR PERCENT COMPLEXED SPECIES AS DETERMINED FROM RAMAN SPECTROSCOPY

Proportionality between integrated intensity and concentration was assumed (Kalman *et al.*, 1982)

$$I_i = \sigma_i \times c_i$$

where I_i is the integrated relative intensity of species i
σ_i is the molar scattering coefficient for species i
and c_i is the concentration of species i

To calculate the relative concentration:

i) determine relative integrated intensity from Raman spectra for species $ZnBr_4^{2-}$, $ZnBr_3^-$, and $ZnBr_2$

ii) calculate I_i/σ_i for each species ($ZnBr_4^{2-}$, $ZnBr_3^-$, and $ZnBr_2$) using σ_i of Macklin and Plane (1970)

iii) then set relative concentration of $ZnBr_2$ to 1, and determine concentration of other species as related to $ZnBr_2$

iv) the relative % of species $ZnBr_4^{2-}$ is the relative concentration of $ZnBr_4^{2-}$ divided by the sum of the relative concentration of species $ZnBr_4^{2-}$, $ZnBr_3^-$, and $ZnBr_2$

Table A-1: Sample calculation for 3 M $ZnBr_2$ at 25 °C using molar scattering coefficients of Macklin and Plane (1970)):

Species	Relative Integrated Intensity	Molar Scattering Coefficient	I_i/σ_i	Ratio of $[ZnBr_i^{i-2}]$ to $[ZnBr_2]$	Relative Concentration (%, 3%)
$ZnBr_4^{2-}$	26.9	1.75	15.4	1.73	31
$ZnBr_3^-$	46.5	1.8	25.8	2.90	51
$ZnBr_2$	7.6	.85	8.9	1.00	18

If the values for molar scattering coefficient determined by Yang *et al.* (1988) are used qualitatively similar results are obtained. The Yang *et al.*, (1988) values for molar intensity are: $ZnBr_2$: 0.33, $ZnBr_3^-$: 2.14 and $ZnBr_4^{2-}$: 5.05. The relative concentration of complexed species as a function of temperature and state of charge are presented in the tables below. These tables can be compared to Tables 3.6 and 3.7.

Table A-2: Relative concentration of complexed species as a function of temperature for 3 M $ZnBr_2$ solutions.

Temperature (°C)	% of total complexed species		
	$ZnBr_4^{2-}$	$ZnBr_3^-$	$ZnBr_2$
25	11	43	46
10	13	44	43
0	14	47	48

The results in Tables 3.6 and A-2 show a shift toward higher order species ($ZnBr_4^{2-}$ from $ZnBr_2$) as temperature decreases.

Table A-3: Relative concentration of complexed species as a function of state-of-charge and temperature for $ZnBr_2$ battery electrolytes including 1 M quaternary ammonium complexing agent.

State-of-charge	Anolyte % of total complexed species			Catholyte % of total complexed species		
	$ZnBr_4^{2-}$	$ZnBr_3^-$	$ZnBr_2$	$ZnBr_4^{2-}$	$ZnBr_3^-$	$ZnBr_2$
Temperature 25 °C						
0 %	11	48	41	10	40	50
50 %	8	41	52	10	35	55
100 %	7	29	65	10	35	55
Temperature 10 °C						
0 %	13	48	39	12	45	43
50 %	12	50	38	15	52	33
100 %	10	34	56	12	34	54
Temperature 0 °C						
0 %	15	50	35	13	49	37
50 %	15	51	34	17	49	34
100 %	8	44	48	17	37	46

The results in Tables 3.7 and A-3 indicated that the species distribution was dependent on both temperature and state-of-charge (or concentration). Clear trends linking state-of-charge with species distribution were not found. Generally, anolyte species distribution shifted to lower order species as the state-of-charge increased. This result was found in analysis based on the molar scattering coefficients of both Macklin and Plane (1970) and Yang *et al.*, (1988). This result was due to the competing effects of temperature, which shifted the species distribution to higher order species, and the lowering of zinc cation and bromide anion concentration, which shifted the species distribution to lower order species.